Sapienza University of Rome
PhD in Morphofunctional Sciences and Biophysics

Physiological and Pathological Modulations of Intrinsic Brain Activity assessed via Resting-State fMRI

Daniele Mascali | PhD Thesis

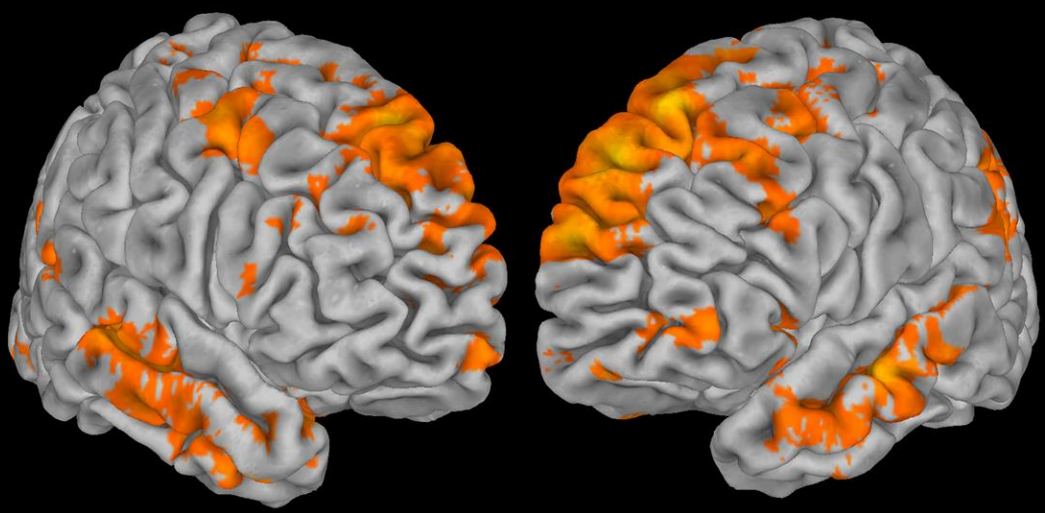

Supervisors:
Prof. Federico Giove
Prof. Bruno Maraviglia

PhD Coordinator:
Prof. Alfredo Colosimo

XXVIII cycle (2013-2015)

Physiological and Pathological Modulations of Intrinsic Brain Activity assessed via Resting-State fMRI

A dissertation submitted in partial fulfilment of the requirements for the degree doctor of philosophy.

Supervisors: Prof. Federico Giove and Prof. Bruno Maraviglia

PhD Coordinator: Prof. Alfredo Colosimo

PhD in *Morphofunctional Sciences and Biophysics*

Curriculum: *Biophysics*

XXVIII cycle (2013-2015)

Sapienza, University of Rome.

Cover images: *most globally connected regions in a healthy elderly population during a resting-state condition. Functional connectivity was assessed through wGBC metric ($p < 0.005$). Front: lateral views. Back: mixed lateral and medial views.*

Dedicated to
Tina & Ines

Introduction

Since its inception in 1992, functional magnetic resonance imaging (fMRI) has considerably boosted our knowledge of the human brain function, primarily due to its non-invasive nature, and its relative high spatial and temporal resolution. Among the available fMRI contrasts, blood-oxygenation level-dependent (BOLD) signal plays a leading role in this field. The contrast is based on the different magnetic properties of the haemoglobin which - combined with the specific relation existing between neuronal, vascular and metabolic activity - allows to ascribe variations in the measured signal to variations in the underlying neuronal activity. During BOLD acquisitions, the comparison of different cognitive states in task-based experiment (alternating rest states to sensory or cognitive stimulations) has revealed the modular organization of the human brain function, an operation that is commonly referred to as *functional brain mapping*.

> *We have to assume that the central nervous system is always, and not only during wakefulness, in a state of considerable activity. (Berger, 1929)*

Surprisingly, task-induced activity requires an increase in brain's energy consumption by less than 5 percent of the underlying baseline activity. Most of the brain's energy demand, from 60 to 80 percent, is used to sustain intrinsic, task-unrelated, neural activity (Raichle, 2006). In this light, functional brain mapping, utilizing task-based fMRI, focuses only on the tip of the iceberg, whereas most of the brain's activity remains largely uncharted.

The notion that the brain has an intrinsic or spontaneous activity is known from early electro-encephalography (EEG) measures due to Hans Berger. However, only in recent years, after the seminal work of Biswal and colleagues (Biswal et al., 1995), the study of spontaneous brain activity has overwhelmingly emerged as a primary field of research in neuroscience. In the so called resting-state condition (i.e., when the brain is not focused on the external world), Biswal reported BOLD low-frequency (< 0.1 Hz) fluctuations (LFFs) synchronized across functionally related and anatomically connected regions. Thereafter, several studies have consistently shown that specific patterns of synchronized spontaneous LFFs identify different resting-state networks, including, but not limited to, visual, motor, auditory, and attentive network. The overall picture emerging from thousands of resting-state fMRI studies depicts a never-resting brain, continuously engaged in maintaining communications within several wide-distributed networks. Such intrinsic brain activity, reflected in spontaneous BOLD LFFs, is the focus of the present thesis.

The study of LFFs in spontaneous BOLD signal can reveal much about brain's functional organization, especially considering that signal variability has been related to variability in behaviour (Fox et al., 2007). In addition, the simplicity of data acquisition – subjects just lie in the scanner refraining from falling asleep - makes the technique particularly suited for studying pathological conditions, in which subject's cooperation might not fulfil the demands of task-based studies. Indeed, several psychiatric and neurological disorders, including degenerative dementia, have shown altered patterns of LFFs, even in the absence of observable anatomical abnormalities (Barkhof et al., 2014). Thus, how the intrinsic brain's activity is modulated in response to different behavioural states and in response to pathological conditions can give insights into the brain functionality and into the mechanisms behind illnesses, respectively.

Importantly, correct result interpretation is highly influenced by the type of metrics adopted and how they are implemented. The resting-state approach to the study of the brain's function has required the development of more sophisticated processing and analysis techniques compared to those commonly applied in task-based fMRI. While seeking for task-responding regions in the brain is guided by information embedded in the experimental paradigm, in steady-state fMRI no a priori cue is provided. In such experiment the extraction of relevant information is based on (i) the temporal synchronization between spatially segregated elements of the brain, feature known as functional connectivity, and on (ii) the amplitude of the oscillation *per se*, a measure of the strength of the intrinsic brain activity. Despite such simple classification, the field of resting-state fMRI is scattered with a disparate amount of metrics, each of which highlight different facets of spontaneous LFFs. Before turning

to the study of spontaneous LFF modulations, we will provide a comprehensive and optimized mathematical framework for the extraction of relevant information from resting-state data (Chapter 2). The results of this effort is an easy-to-use matlab toolbox specifically designed for the processing and analysis of steady-state fMRI data.

In principle, the information coded in functional connectivity and in oscillation amplitude are unrelated. While the former assesses the degree of cooperation between segregated elements of the brain, the latter quantifies the neural workload of each single brain's element, independently from the activity of other regions. Nonetheless, modulations in both measurements have been reported in several pathological conditions - yet in separate studies - suggesting a possible relation between them. In this context, we sought to investigate the potential coupling between the functional connectivity and the oscillation amplitude in cohort of healthy elderly and the probable modulations induced by dementia of the Alzheimer's type (Chapter 3).

Regardless of how the brain relates the two types of measures extractable from resting-state data, their disease-induced modulations are relevant *per se* in uncovering the illness. Indeed, Alzheimer's disease is known to produce alterations in spontaneous brain activity, both at the synchronization and the amplitude level (Wang et al., 2007). Since the hallmark of the pathology is a profound deficit in episodic memory, much effort has been done in characterizing the alterations in spontaneous brain activity underlying such deficit. Contrarily, little is known about another commonly reported deficit, the language related impairment (Taler and Phillips, 2008). In the second part of Chapter 3 we sought to disclose the brain regions underpinning language deficits by looking at the alterations in functional connectivity of the relevant network.

While the study of LFFs in pathological conditions can contribute to reveal the mechanisms behind the pathology and how it spreads into the brain, the study of spontaneous brain activity in physiological conditions can disclose the intrinsic brain functionality. In healthy subjects the resting brain has been extensively characterized and its network topology has shown to be a consistent and reliable physiological feature (Damoiseaux et al., 2006). An intriguing issue is how the brain reorganizes its patterns of spontaneous BOLD LFF while it is focusing on the external world. Indeed, the intrinsic brain activity is not an exclusive feature of the resting condition, instead it is present also on the top of the task-evoked response.

In chapter 4, with peculiar experimental paradigms we separated the task-evoked response from the intrinsic brain activity during sustained cognitive stimulations. In

a first experiment we sought to characterize the spatio-temporal proprieties and the dynamic of the transition from a resting to a stimulated condition. In the second part we specifically investigated how the brain reorganizes its internal functional architecture during visuospatial attention. Indeed, besides strongly affecting the processing of visual incoming stimuli, visual spatial attention also affects brain networks. Recent studies suggest that visual attention affects functional connectivity within and between the visual network and the attention network (Spadone et al., 2015), yet modulations of attention on brain networks are still poorly understood.

Table of Contents

Acronyms

$A\beta$	β-Amyloid
ACC	Anterior Cingulate Cortex
AD	Alzheimer's Disease
ALFF	Amplitude of Low-Frequency Fluctuations
ANOVA	ANalysis Of VAriance
APP	Amyloid Precursor Protein
ATL	Anterior Temporal Lobe
BH	Breath Holding
BOLD	Blood-Oxygenation Level-Dependent
CBF	Cerebral Blood Flow
CBV	Cerebral Blood Volume
CMR0_2	Cerebral Metabolic Rate of Oxygen consumption
CoEn	COrrelation ENtropy
CSF	CerebroSpinal Fluid
DA	Dorsal Attention network
DC	Degree Centrality
DMN	Default Mode Network
EEG	Electro-EncephaloGraphy
EPI	Echo Planar Imaging
fALFF	Fractional Amplitude of Low-Frequency Fluctuations
FC	Functional Connectivity
FLAIR	Fluid Attenuated Inversion Recovery
FFT	Fast Fourier Transform
fMRI	Functional Magnetic Resonance Imaging
FOV	Field Of View

FP	FrontoParietal network
FWHM	Full Width at Half Maximum
GE	Gradient Echo
GLM	Generalized Linear Model
GM	Grey Matter
GMV	Grey Matter Volume
HC	Healthy Controls
HRF	Hemodynamic Response Function
ICA	Independent Component Analysis
ICC	Intrinsic Connectivity Contrast
LIMB	LIMBic network
LFFs	Low-Frequency Fluctuations
LFP	Local Field Potential
MCI	Mild Cognitive Impairment
MDEFT	Modified Driven Equilibrium Fourier Transform
MMSE	Mini-Mental State Examination
MNI	Montreal Neurological Institute
mPFC	Medial PreFrontal Cortex
MR	Magnetic Resonance
MRI	Magnetic Resonance Imaging
MUA	Multi-Unit Activity
NMR	Nuclear Magnetic Resonance
OEF	Oxygen Extraction Fraction
PCA	Principal Component Analysis
PCC	Posterior Cingulate Cortex
PET	Positron Emission Tomography
pMTG	Posterior Middle Temporal Gyrus
pOPE	Pars OPErcularis
PS	Power Spectrum
PSC	Percent Signal Change
ReHo	Regional Homogeneity
ROI	Region of Interest
RSFA	Resting-State Fluctuation Amplitude
SD	Semantic Dementia
SE	Spin Echo
SM	SomatoMotor network
StV	Seed-to-Voxel
TE	Echo Time
TI	Inversion Time
TOT	Tip-Of-the-Tongue
TR	Repetition Time
VA	Ventral Attention network
VIS	VISual network
wGBC	Weighted Global Brain Connectivity
WM	White Matter

CHAPTER 1

Functional magnetic resonance imaging

Functional magnetic resonance imaging allows the detection of metabolic and vascular changes that mirror the underling changes in neuronal activity. Without the use of external contrast agent or invasive cortical electrodes, it is possible to infer brain's activity tanks to the fast acquisition of T_2^* or T_2 weighted images. Comparison of different cognitive states during images acquisition allows the mapping of the brain's function (referred to as task-based fMRI).

This work is not focused on the task-based fMRI, but on the study of the low-frequency fluctuations (LFFs) that characterize the fMRI data acquired in the absence of any overt sensory or cognitive stimulation (referred to as resting-state fMRI). Such fluctuations are thought to reflect the intrinsic, ongoing, activity of the brain. A full understanding of such phenomenon requires the knowledge of the physical and physiological mechanisms underlying the blood-oxygenation level-dependent (BOLD) signal, namely, the contrast used in fMRI.

The BOLD signal

The extraordinary capability of BOLD contrast to detect brain activity is primarily based upon a series of somehow fortunate facts. First, haemoglobin presents different magnetic propriety depending on the presence of bounds with oxygen molecules, thus variations in the local content of oxygen can be detected with opportune magnetic resonance imaging (MRI) sequences. However, detecting variations in the local oxygen content in principle could not lead any information on the underlying neuronal activity. Fortunately, the brain is a highly energy demanding system, which exploits oxidative metabolism, primarily through catabolism of organic compounds derived from glucose, to sustain the complex chain of physiological processes that leads to neuronal activation. Since the brain has limited storage supplies of glucose and oxygen, it constantly depends on blood perfusion to sustain neuronal activity. Once again, the fact that brain requires oxygen to work does not imply that variation in neuronal activity leads to variation in local oxygen content. In fact, in the case of a perfect coupling between the rate of oxygen consumption and the blood perfusion, there would be no variation in local oxygen content. Fortunately, to sustain even a small increase in oxygen consumption the engaged brain area triggers a disproportional increase in blood perfusion, resulting in a local iperoxygenation. This chain of "fortunate" facts leads to regional increase of BOLD signal in activated regions of the brain and allows the study of brain function without any exogenous contrast agent and in a safe and comfortable fashion.

In the following sections, we will go deeply into the origin of the BOLD contrast by separately considering the physic principles rising signal in MRI and the vascular propriety of the brain producing local iperoxigenation during increased neuronal activity.

Physical origin

BOLD contrast refers to transverse time relaxation changes of water protons due to local changes in venous blood deoxyhemoglobin concentration. While oxyhemoglobin molecule is diamagnetic and has similar magnetic properties as tissue, deoxyhemoglobin molecule is paramagnetic (Pauling and Coryell, 1936), thus its presence leads to large susceptibility difference between compartments that contains the molecule and others that are devoid of it. Such susceptibility difference will induce a loss of coherence among water spins that will lead to a measurable

decrease in transverse relaxation times, specifically in T_2, via spin-echo weighted images, or in T_2^*, via gradient-recalled weighted images.

The difference in magnetic susceptibility between fully oxygenated and fully deoxygenated blood is estimated to be approximately 0.08 ppm (Tofts, 2005). Blood vessels containing fully oxygenated blood, such as arterial vessels, cause little or no distortion to the magnetic field in the surrounding tissue. Contrarily, capillary and venous vessels, containing blood, which is partially deoxygenated, will significantly contribute to BOLD signal changes. Of note, although the true endogenous contrast is the deoxyhemoglobin molecule, the assumption of complementarity between oxy- and deoxyhemoglobin, that is valid under physiological conditions, allows to interpret the contrast as a function of blood oxygenation.

As it will be discussed in the next section, increased neuronal activity is accompanied by a local decrease in deoxyhemoglobin concentration, this leads to a small but detectable increase in T_2 and T_2^*. However, the precise relationship between the acquired signal and the actual variation in oxygen level of a brain voxel (i.e., the unit volume element of an image) is highly complex and is influenced by several parameters including the acquisition sequence and the voxel anatomical composition. Based on previous work regarding NMR signal in the presence of contrast agent (Fisel et al., 1991), Ogawa and colleagues (Ogawa et al., 1993b) developed the following biophysical model of the BOLD signal.

Considering an infinite cylinder as an approximation for a blood vessel with magnetic susceptibility difference $\Delta\chi$, the magnetic field at any point in space will be perturbed from the applied static magnetic field B_0. Inside the cylinder (intravascular contribution), the perturbation will be given by the equation:

$$\Delta B_{IN} = 2\pi\Delta\chi(1-Y)B_0\left(cos^2\theta - \frac{1}{3}\right) \quad (1.1)$$

Whereas, in a given point outside the cylinder (extravascular contribution) the perturbation will be according to the equation:

$$\Delta B_{OUT} = 2\pi\Delta\chi(1-Y)B_0\left(\frac{r_b}{r}\right)^2 sin^2\theta cos2\varphi \quad (1.2)$$

In these equations, $\Delta\chi$ is the maximum susceptibility difference expected in the presence of fully deoxygenated blood, Y the fraction of oxygenated blood, r_b the cylinder radius and r the distance from the point of interest to the center of the cylinder (the angles are depicted in Figure 1.1). Inside the vessel, magnetic perturbation is constant and depends on the orientation of the vessel respect to the

static magnetic field as well as on the fraction of oxygenated blood. Water molecules outside the vessel experience a magnetic gradient whose spatial extension depends also on the radius of the vessel that, however, given the $1/r^2$ dependency, falls down rapidity over distance compared to the cylinder radius.

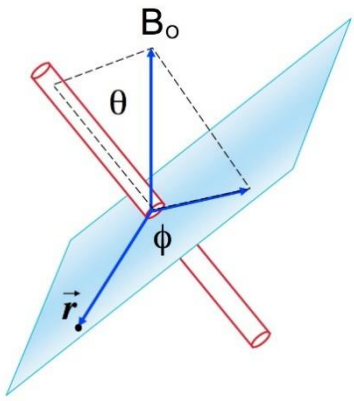

Figure 1.1 Representation of a blood vessel as an infinite cylinder. A point external to the cylinder is identified by the triad r, θ and φ.

These magnetic field perturbations influence transverse relation times in such a way that can be explained in terms of *static* and *dynamic* averaging, the latter arising as the result of the diffusive motion of water molecules. Dynamic averaging plays a critical role when water molecules experience a gradient magnetic field during their diffusive motion in the acquisition time T_E. On the contrary, when the perceived magnetic field is constant the deoxyhemoglobin-induced field inhomogeneities will be statically time-averaged. The main difference between the two regimes is that a refocusing pulse (i.e., a spin-echo sequence) cannot undo the loss of phase coherence due to the dynamic averaging (while can undo that of static averaging), since deoxyhemoglobin-induced field inohomogenities are not "perceived" as static field by diffusive waters. Because of dynamically averaging, NMR signal decay will be characterized with a decrease in T_2. A gradient-recalled sequence will be sensitive to dynamic averaging as well; however, it will be also sensitive to static averaging, since no refocusing pulse is applied in this type of sequence. Summarising, both T_2 and T_2^* changes can arise from dynamic averaging, but static averaging will only influence the T_2^* changes.

It is now important to understand in which conditions the two regimes are relevant. Since in equations (1.1) and (1.2) the induced field distortion is a function of the radius of the vessel, blood vessel size compared to the distances spanned by water molecules in the acquisition time becomes a critical parameter in the BOLD effect.

Considering a diffusion constant $D = 10^{-5}\ cm^2/s$ and a typical acquisition time of 30 ms, the mean diffusion distance of water molecules is approximately 13 μm. Essentially, the dynamic averaging regime is present when water molecules surround small blood vessels such as microvessels (i.e., capillaries) and venules; whereas, inohomogenities due to large blood vessels are perceived as static field by diffusive water molecules. In addition, dynamic averaging will also occur inside blood vessel as result of field inohomogenities due to red blood cells.

Typically, a brain voxel contains a large number of blood vessels arbitrarily oriented respect to the static magnetic field. Thus, the observed BOLD signal changes will be a volume-weighted average of signals, both from extravascular and intravascular water, over this collection of vessels.

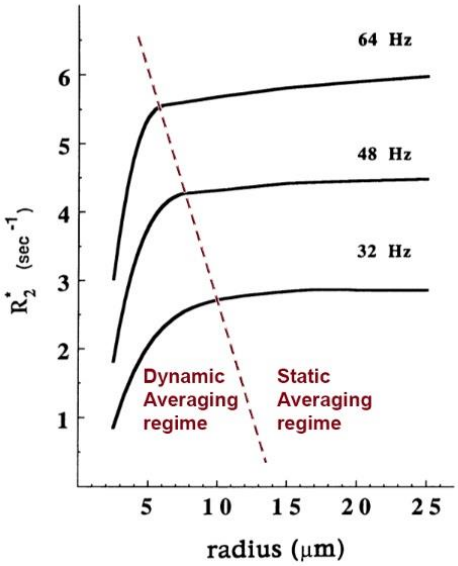

Figure 1.2. The susceptibility induced R_2^* in the presence of water diffusion plotted as a function of cylinder radius. Plots are shown at three different values of frequency shifts (32, 48, 64 Hz). T_E = 40 ms, fractional blood volume 0.02 (adapted from Ogawa et al., 1993a).

EXTRAVASCULAR SIGNAL. Let us consider only the contribution to signal changes arising from water molecules surrounding blood vessels, i.e. only eq. (1.2). Ogawa, through Monte Carlo simulations, studied the relaxation rate R_2^* (i.e. $1/T_2^*$) as a function of vessel size. Simulation results are reported in Figure 1.2 for different values of $\Delta\chi(1-Y)B_0$ (expressed in angular frequency: 32, 48 and 64 Hz). The figure clearly shows the two different averaging regimes. At radius less than ~ 5 to 10 μm, typical of capillary and venules, R_2^* steeply decreases because of dynamic averaging; above these radius lengths, R_2^* is almost independently on the vessel size as the static averaging dominates. The boundary between the two regimes is slightly dependent on the static magnetic field and on the magnetic susceptibility difference (thorough the factor $\Delta\chi(1-Y)B_0$). This imply that at very high static magnetic fields,

the radius at which the transition between static and dynamic averaging occurs will shift to values smaller than the capillary size.

Results of Odawa's modelling studies are summarised in the following empirical equations:

$$R_2^* \propto \{\Delta\chi(1-Y)B_0\}\, CBV \quad (large\ vessels) \tag{1.3}$$

$$R_2^* \propto \{\Delta\chi(1-Y)B_0\}^2 CBV \quad (small\ vessels) \tag{1.4}$$

where CBV is the cerebral blood volume. Once again, the distinction of small and large vessels reflect the distinction between static and dynamic averaging, and it primarily depends on the static magnetic field; for example, at 4 T the boundary radius is $\sim 5\ \mu m$. These equations lead to two important results. First, while for large vessels R_2^* varies linearly with the external magnetic field, for small vessels there is a quadratic dependence. This implies that high magnetic fields will emphasise the contribution of small vessels, which is highly desired since they are closer to the activation zone than large vessels are. Secondly, changes in CBV will also influence the signal arising from extravascular spins; for example, an increase in blood volume will reduce the relaxation time thus lowering the NMR signal.

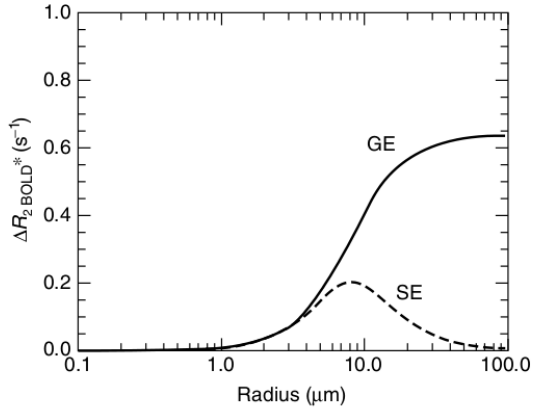

Figure 1.3. Schematic theoretical dependencies of the extravascular $\Delta R_{2\,BOLD}^*$. BOLD (gradient echo, GE) and $\Delta R_{2\,BOLD}$ (spin echo, SE) changes as a function of vessel size. A constant deoxygenation level for the blood was assumed, and a field strength of 1.5 T. The curves overlap below vessel radii of approximately 8 μm radius, and diverge significantly above approximately 8 μm radius (Tofts, 2005).

Up to this point, we have described T_2^* as a function of the vessel size and the static magnetic field, taking as fixed value the fraction of oxygenated blood, Y. However, the BOLD contrast arises from variations in this latter parameter. Therefore, let us now consider signal changes due to variations in blood oxygenation level, ΔY, assuming constant all other parameters. Figure 1.3 reports simulation results of relaxation time changes due to BOLD on extravascular water spins, separately for a spin-echo, $\Delta R_{2\,BOLD}$, and a gradient recalled echo sequence, $\Delta R_{2\,BOLD}^*$. As expected, results mirror the above reported conclusion; indeed, the boundary between static

and dynamic averaging is clearly visible around $\sim 5\ \mu m$. This simulation also evidences that a gradient recalled echo pulse, although is not able to discern between small and large vessels, produces much more signal contrast compared to a spin-echo pulse.

INTRAVASCULAR SIGNAL. Intravascular spin waters also contribute to the BOLD effect, primarily in two ways. First, the T_2 of blood itself is sensitive to deoxyhemoglobin molecules. In fact, such molecule is compartmentalized within red blood cells, which dimensions are comparable to diffusion distances of water spins during acquisition times. Thus, signal change in T_2-blood due to deoxyhemoglobin-induced fields arises as the result of dynamic averaging and, as it is expected for this regime, it quadratically depends on magnetic field strength (Thulborn Kr, 1982). Secondly, there is an addition vascular T_2^* effect resulting from different blood vessel orientations. Indeed, from equations (1.1) and (1.2) spin waters in a given vessel will experience a perturbation field dependent on the orientation of the vessel respect to the static field plus a further modulation due to the perturbation effects of neighbouring vessels.

The role of CBV in the signal arising from intravascular spin waters is more complex than that arising from the extravascular space. An increase in CBV implies a rise in the ratio between blood and tissue volume in the voxel. If the blood T_2 is higher than that of tissues, a raise in the blood-tissue ratio results in an increase in BOLD signal, and the opposite for a decrease in the ratio. At 1.5 T the estimated T_2 of tissue is $\sim 70\text{-}90\ ms$, while for venous blood is $\sim 180\ ms$ (Thulborn Kr, 1982); so, at this static field, increasing CBV will lead to a reduction in intravascular BOLD signal. Whit higher magnetic field, both relaxation times decrease, but in a quadratic fashion for blood T_2. This means that at high magnetic field the role of CBV in the intravascular BOLD will be opposite; for example, at 4 T the estimated brain-tissue T_2 is $\sim 60\ ms$, while for venous blood is $\sim 20\text{-}60\ ms$ (Barth M, 1997).

LARGE VERSUS SMALL VESSEL. The relative contribution of macro and micro vessels to BOLD signal is an important factor in estimating the ability of fMRI to localize the neuronal activation site. Indeed, large vessels might carry blood signal changes due to distant activation zones. Summarising the above reported observations:

The T_2^* BOLD signal has both an intra- and extravascular component, originating from both small and large vessels. The relative contributions depend on the magnetic field strength.

The T_2 BOLD signal has an intravascular component arising from both small and large vessels, while the extravascular component arises only form micro vessels.

Thus, the major difference between T_2 and T_2^* BOLD images is that in the former the extravascular BOLD effect can only arise from the microvasculature, while in the latter can arise from vessels of any size. Considering that in the grey matter only the 2-5% of water spins are in the intravascular space, one might think that T_2 BOLD signal is primarily due to the extravascular space, and thus from the microvasculature alone. Actually, blood has a dominant role at conventional fields. Diffusion weighted measures, using bipolar gradients, have shown that at 1.5 T about 60% of the BOLD signal is due to intravascular water (Boxerman et al., 1995). Only at very high field (> 7 T), due to the robust T_2 blood decrease, the intravascular component becomes negligible. Thus, at conventional field it is not true that the T_2 BOLD signal is more spatially localized to the neuronal activation site. In practise, the reduction in BOLD sensitivity when using a spin-echo sequence rather than a gradient-echo sequence (at 1.5 T a 0.5% signal change for the former vs a 3–5% signal change for the latter) means that few investigators adopt the spin-echo approach (Tofts, 2005).

Physiological origin

NEUROVASCULAR COUPLING. Relaxation rate in equation (1.3) and (1.4) relies on several vascular and metabolic parameters. Directly R_2^* shows a dependence on the CBV and, most importantly, on the oxygen extraction fraction, $OEF = (1 - Y)$, that is, the difference between the fraction of oxyhemoglobin in the arterial blood (which is assumed to be 1) and that of the venous blood. Indirectly, it also depends on cerebral metabolic rate of oxygen consumption ($CMRO_2$) and cerebral blood flow (CBF), since OEF is related to all these parameters through the Fick's principle of mass conservation:

$$CMRO_2 = 4[Hb] \cdot CBF \cdot OEF \tag{1.5}$$

where $[Hb]$ is the hemoglobin concentration and the factor 4 accounts for the fact that a single hemoglobin can bind four oxygen molecules. Thus $OEF \propto CMRO_2/CBF$, which means that $CMRO_2$ and CBF play an opposite role in the detection of the BOLD signal: while an increase in CBF will lead to an increase in the concentration of oxyhemoglobin in the venous blood, an increase in $CMRO_2$ will reduce it.

Physiologic processes involved in the phenomenon of neuronal activation are energy demanding and cause a sharp increase in the local glucose and oxygen consumption, accompanied by an increase in the CBF and CBV. The relative contribution of all these physiological parameters during brain activity is crucial for the interpretation of the BOLD signal. In 1986, by means of positron emission tomography (PET) measurements, it was shown that during visual stimulation the brain responds with a massive increase in CBF accompanied by only a small increase in $CMRO_2$ (Fox Pt, 1986), at the point that an uncoupling between the two measures was proposed. Such not commeasured variations in CBF and $CMRO_2$ lead to a decrease in the local OEF, that is, to a local iperoxigenation, which is the physiological basis of the BOLD signal rise during increased neuronal activity. Successive experiments showed a linear coupling between CBF and $CMRO_2$, with an estimated ratio of 2:1. This result was evident combining BOLD and perfusion [1] measures during graded visual stimulation and during CO_2 induced vasodilation as consequence of hypercapnia (CO_2 inhalation produces increase in CBF without affecting $CMRO_2$). Figure 1.4 reports the lower BOLD level during visual stimulation compared to BOLD acquired during matched hypercapnia, with the discrepancy linearly increasing with stimulation contrast.

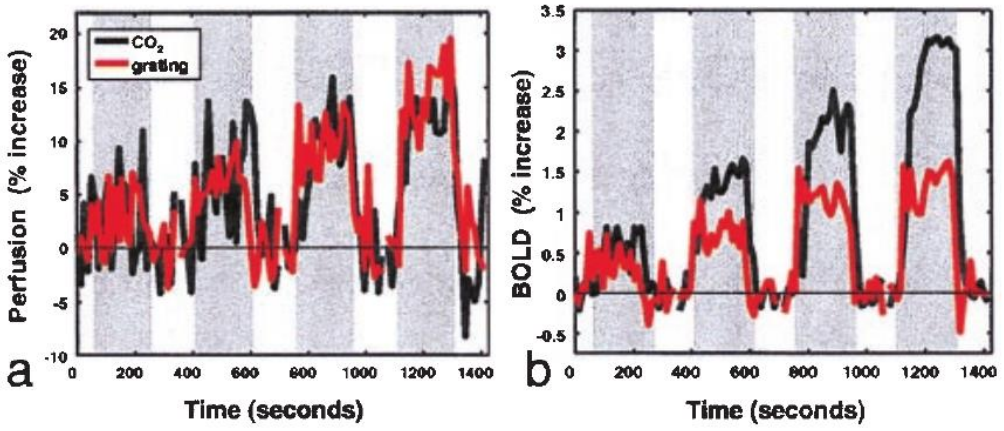

Figure 1.4 CBF (a) and BOLD (b) measures during graded stimulation (red traces) and hypercapnia (black traces). a) Stimulation contrast was set up to match perfusion levels induced by hypercapnia. **b**) Stimulation-induced BOLD attenuation is evident, moreover such attenuation is related to the perfusion level (Hoge Rd, 1999).

[1] Quantitative measures of CBF can be obtained tagging arterial blood via NMR inversion pulse, technique known as "arterial spin labelling".

The imbalance between oxygen metabolism and blood flow can be explained considering the *oxygen diffusion limitation* model (Buxton Rb, 1997). According to this model, the increase in blood flow is required to increase the oxygen concentration gradient between capillaries and mitochondria, with the latter driving the vascular response. The relationship between OEF and CBF is given by the equation:

$$OEF = 1 - (1 - OEF_0)^{CBF/CBF_0} \tag{1.6}$$

Where the 0-index indicates values at rest as opposed to those during activation. By differentiating Fick's principle and combining the result with equation (1.6), we obtain:

$$\frac{CMRO_2}{CMRO_{2|0}} = \frac{CBF}{CBF_0} \cdot \frac{1 - (1 - OEF_0)^{CBF/CBF_0}}{OEF_0} \tag{1.7}$$

This relations is reported in Figure 1.5 for different values of OEF_0. It is evident how a great increase in blood flow is needed to sustain a moderate increase in oxygen consumption.

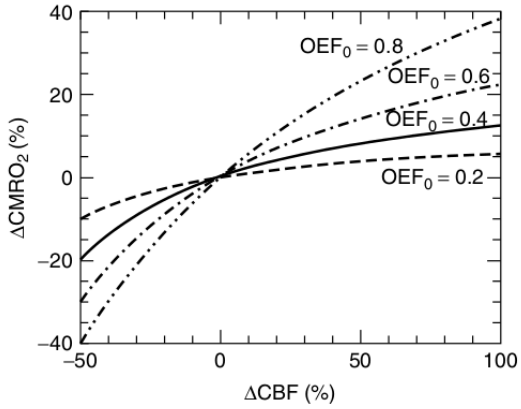

Figure 1.5 Percentage change in oxygen metabolism ($\Delta CMRO_2/CMRO_{2|0}$) versus the required percentage change in cerebral blood flow ($\Delta CBF/CBF_0$) for a variety of resting oxygen extraction fraction values, according to the oxygen diffusion limitation model. Simulation are reported for resting OEF values of 0.2, 0.4, 0.6 and 0.8 (Tofts, 2005).

BOLD NEUROPHYSIOLOGICAL CORRELATES. BOLD signal, depending on metabolic and vascular changes, does not directly measure neuronal activity. On the contrary, electrophysiological measures, especially those utilizing microelectrode implants in cerebral cortex, allow direct measure of neuronal activity. For this reason, a huge effort has been done in discovering the electrophysiological correlates of the BOLD signal.

Extracellular electrical signal can be divided into single-unit activity, representing the action potentials of well isolated neurons next to the electrode tip, multi-unit

activity (MUA), reflecting the spiking of small neural populations in a sphere of 100-300 μm radius, and local field potential (LFP), reflecting perisynaptic activity of a neural population within 0.5-3 mm of the electrode tip (Logothetis, 2008). MUA and LFPs are discriminated by their spectral proprieties, as MUA represents the high-frequency component of the electrophysiological signal (500-1000 Hz) whereas LFPs represents the low-frequency component (lower than 250 Hz). For their different origins, MUA can be interpreted as the output of a neuronal population whereas LFPs as the result of the processing and input inside the population.

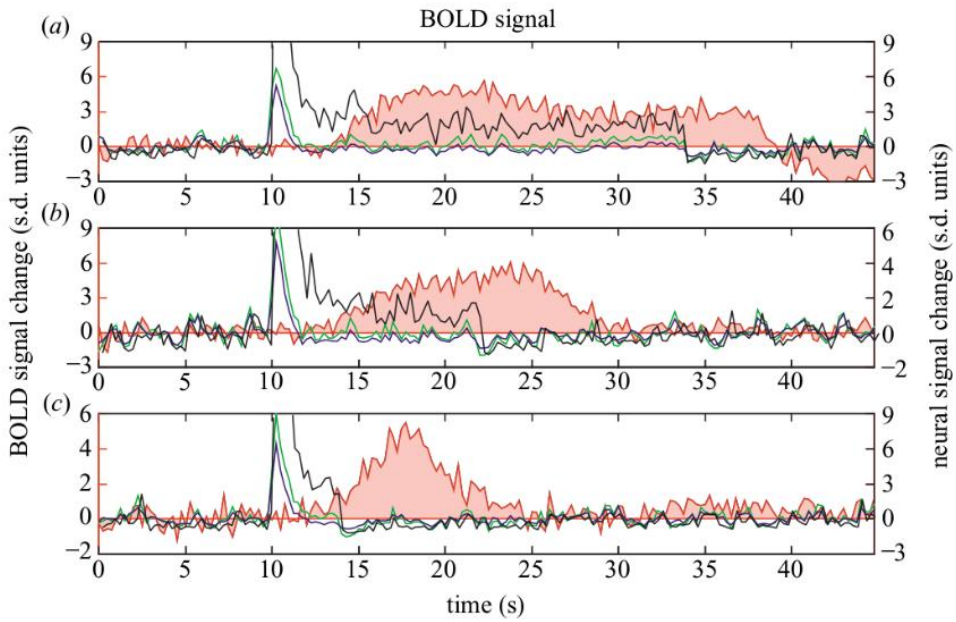

Figure 1.6 Simultaneous BOLD (red area), LFPs (black trace), and MUA (green trace) recordings from a cortical site in response to pulse stimuli of (**a**) 24, (**b**) 12 and (**c**) 4s. MUA response adapt a couple of seconds after stimulus onset, whereas LFPs remain the only signal correlated with the BOLD response (Logothetis et al., 2001).

Logothetis was the first who simultaneously recorded electrophysiological and BOLD signal during enhanced neuronal activity (Logothetis et al., 2001). The experiment, conducted in the macaque's cortex during visual stimulation, showed a roughly linear relationship between BOLD and electrophysiological responses. Nevertheless, the best correlation was found between BOLD and LFP. Indeed, while MUA quickly returned to baseline after the stimulus onset, LFP activity was maintained high during the whole stimulus duration (Figure 1.6). This result suggests that the BOLD response reflects integrative neural activity rather than spiking activity, in agreement with other experiments in which the spiking activity was found to be a poor predictor of BOLD signal (Logothetis, 2002). However, the downside of these studies is that they rely on correlation measures that can be biased by the

intrinsic correlation existing between LFP and MUA (as can be easily seen from Figure 1.6). One might argue that the BOLD-LFP correlation could be the result of MUA-LFP correlation. However, several studies, disentangling the two types of electrophysiological activity, have reported either no sensitivity of hemodynamic response to MUA changes (Lauritzen, 2001) or correlations with LFP in the absence of MUA (Viswanathan and Freeman, 2007, Lippert et al., 2010).

Further support for the crucial role of LFPs in the origin of BOLD signal comes from metabolic studies which have shown that the greatest demand of glucose is located in brain regions with high density of dendritic arborizations (Nudo and Masterton, 1986). Taken together, these results indicate that fMRI BOLD signal primarily reflects synaptic rather than spiking activity.

Brain function localization

The above dissertation leads to the conclusion that regionally increase in BOLD signal can be attributed to focal increase in neuronal activity. The experimental procedure for localizing brain function consists in the continuous acquisition of T_2^* weighted images while subjects is actively engaged in a task execution or, equivalently, is exposed to a sensory stimulation. Since the BOLD signal does not measure the absolute oxygenation content, such task state must be compared to a lower cognitive condition allowing to ascribe the variations in the recorded BOLD signal to the task execution. In Figure 1.7 is reported an example of task-based fMRI in which subjects are required to open and close their eyes at fixed intervals. Only those voxels located in the visual cortex show BOLD time courses that follow the task evolution. In general, modulations of BOLD signal attributable to the experimental functional conditions can be observed in distinct brain areas, allowing one to relate brain topography to function.

From this example it can be seen how noisy the BOLD signal is, displayng spontanous fluctuations superimosed to the task effect. To minimize the effect of such task-unrelated fluctuations, several blocks of alternated functional conditions are acquired. In this manner, noise is minimized through averaging (since it is not correlated to the task), allowing the effect of interest to be emphasized.

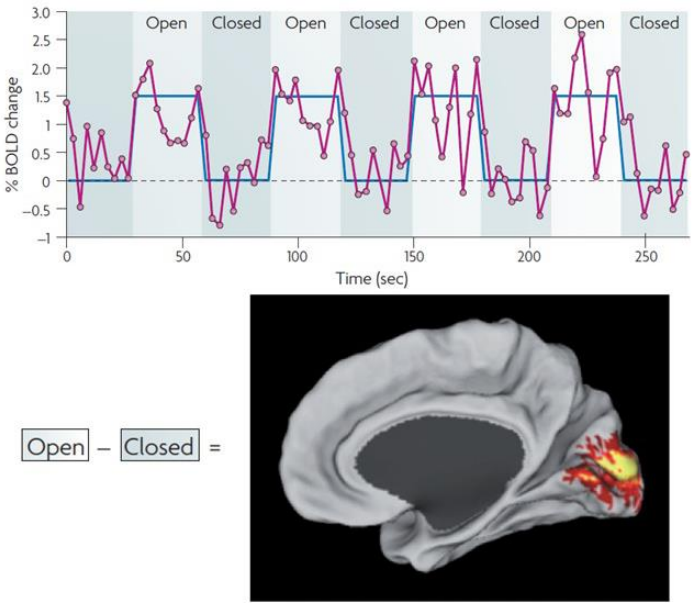

Figure 1.7 BOLD time course (magenta) from a region in the primary visual cortex during a simple task paradigm that requires subjects to open and close their eyes. The paradigm is shown in blue (delayed to account for the haemodynamic response). fMRI analysis involves correlating BOLD data with a stimulation time-course across multiple blocks. Multiple block are required in order to minimize noise effect in the BOLD signal. In this case, subtraction of the eyes-closed condition from the eyes-open condition identifies a BOLD signal intensity difference in the primary visual cortex (Fox and Raichle, 2007).

Resting-state fMRI

In task-based fMRI, spontaneous fluctuations in the BOLD signal negatively affect the ability of detecting task-related modulations. Consequently, in task-based fMRI, they are considered as noise and their effect is mitigated through several procedural expedients. However, just few years after the development of BOLD based fMRI it was proposed that signal fluctuations, not attributable to an overt task, could not be entirely tagged as noise. Biswal and colleagues, in 1995, were the first to disclose the functional relevance of spontaneous BOLD fluctuations (Biswal et al., 1995). The authors showed that spontaneous low-frequency fluctuations (LFFs; < 0.08 Hz) in the left somatomotor cortex were specifically correlated with those in the right somatomotor cortex and with medial motor areas during resting state, therefore, in the absence of any overt motor behaviour. Indeed, spontaneous LFFs have the remarkable feature of being synchronous in functionally related areas, as in this case of the sensorimotor network. As soon as Biswal's results were replicated for other well established functional networks, it was clear that a new era of fMRI had begun: the study of brain functional organization by means of BOLD measures acquired during resting state, or, more generally, during steady state.

The term "spontaneous" refers to fluctuations that cannot be ascribed to a specific task and are intrinsically generated by the brain. As such, the majority of studies focused on these fluctuations attempt to minimize any change in sensory input and

require subjects to refrain from any kind of activity. A typical experiment consists in subjects lying in the scanner with closed eyes or maintaining the gaze steady on a cross-hair.

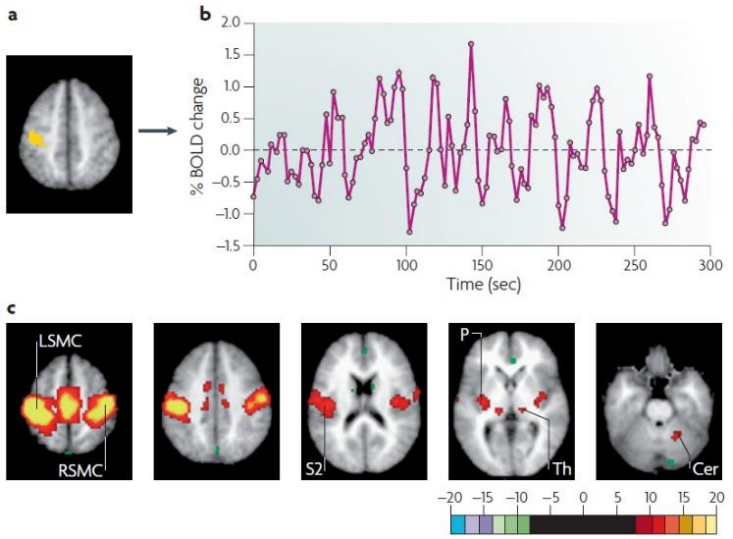

Figure 1.8 Generation of resting-state FC maps. a) Seed region in the left somatomotor cortex (LSMC) is shown in yellow. **b**) Time course of spontaneous BOLD activity recorded during resting fixation and extracted from the seed region. **c**) Statistical z-score map showing voxels that are significantly correlated with the extracted time course. In addition to correlations with the right somatomotor cortex (RSMC) and medial motor areas, correlations are observed with the secondary somatosensory association cortex (S2), the posterior nuclei of the thalamus (Th), putamen (P) and cerebellum (Cer) (Fox and Raichle, 2007).

Differently from task-based fMRI, in which prior knowledge about stimulation protocol guides the spatial search for correlated neurovascular responses, in resting-state fMRI no a priori information is provided; therefore, new analytic techniques have been developed. A very common and simple way of identifying spatial patterns of coherent spontaneous LFFs – the same used in the Biswal's original paper – is reported in Figure 1.8. Briefly, it consists in extracting a reference BOLD time-course from a region of interest, known as seed, and correlating it with all other voxels in the brain. Significant correlations underlie voxels that make up a coherent network with the chosen seed. The resulting brain map is known as *functional connectivity* (FC) map and two coherent voxels are said to be functionally connected. The term FC in general refers to any physiological process generating temporal correlations between spatially discrete brain areas (Friston et al., 1993). Several others methods have been successfully applied to study coherent spontaneous LFFs, including but not limited to, principal and impendent component analysis, graph theory, clustering and spectral-based methods (van den Heuvel and Pol, 2010, Zuo et al., 2010, and reference therein). Different approaches stress

different facets of coherent fluctuations, as the ability to discern between short- and long-range connections; given their importance in interpreting results, methodological aspects will be the focus of a dedicated chapter (Chapter 0). Regardless of the exact method, spontaneous LFFs carry two theoretically independent kinds of information. One is the FC in itself, which is a multivariate measure based on the synchronicity of spatially segregated signals, the other is the magnitude of such spontaneous fluctuations, that is, a univariate measure. Both measures have a functional relevance that is supported by the following evidence.

Functional relevance

BOLD LFF, A QUESTIONABLE SIGNAL. Soon after their first appearance as physiological measure, spontaneous BOLD fluctuations have raised doubts regarding their neuronal origin. Indeed, cardiac and respiratory fluctuations, spontaneous oscillations in carbon dioxide, and many other physiological phenomena have been identified or proposed as source of variance in BOLD signals (Wise et al., 2004, Birn et al., 2006, Birn et al., 2008, Chang et al., 2009, DiNuzzo et al., 2011, Murphy et al., 2013). The majority of fMRI protocols have a low temporal resolution (typical repetition time between acquired images of 2-3 seconds), causing high frequency respiratory and cardiac oscillations to be aliased back into the low frequencies of interest (0.01–0.1 Hz). Although these higher frequent cardiac and respiratory patterns might shape the BOLD time-series of anatomically separate brain regions, studies obtained at high sampling rates showed that resting-state networks persist when these confounds are accounted for (Cordes et al., 2001). Thus, no-neuronal sources of variance cannot entirely explain coherent BOLD patterns. Undoubtedly, such noise component must be removed from data for the correct interpretation of results. At this aim, several techniques have been developed including direct measure of physiological parameters during BOLD acquisition and subsequent removal through linear regression (Glover et al., 2000), independent component analysis (ICA) to estimate non neuronal sources (Kiviniemi et al., 2003), or regression of signal from brain regions that are likely to have a high degree of physiological artefact component, such as ventricles of white matter (Behzadi et al., 2007).

RESTING-STATE TOPOGRAPHY. Certainly, the most obvious evidence supporting the neuronal origin of spontaneous BOLD fluctuations comes from the topography of synchronized oscillation patterns. Up to 10 networks were found in functional relevant brain zones, displaying spatio-temporal patterns remarkably consistent across subjects and time (Damoiseaux et al., 2006). Anatomical boundaries of resting-state networks are consistent with the known functional organization of the

human brain (Smith et al., 2009), mostly inferred by collected evidence from task-based fMRI, PET and EEG studies.

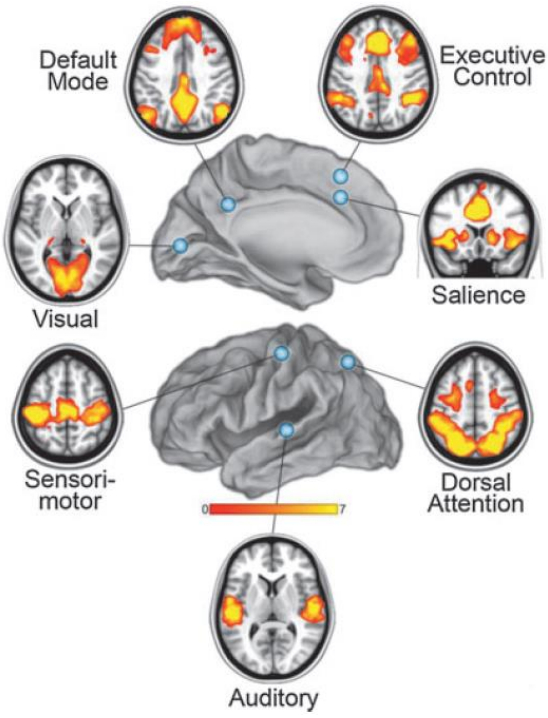

Figure 1.9 Commonly reported networks of synchronized spontaneous BOLD fluctuations during resting state. Maps were generated with a seed-to-voxel functional connectivity approach. Reference time-courses were extracted from seed location depicted with blue circles. These reference time-series were then used as regressor to search the brain for correlated time-series (Raichle, 2011). More detailed information information on the function of these networks is given in Table 1.1.

These networks include, among others, sensorimotor, visual, auditory, language and attentional systems. Perhaps the most interesting of such system is the "default mode network" (DMN). The idea of an organized default mode of the brain function, that is present as a baseline and is suspended during specific goal-directed behaviours, was suggested from PET and fMRI studies showing that during the execution of a variety of different tasks specific brain regions consistently reduced their activity. Raichle and colleagues were the first to record the spatial signature of DMN activity during rest by means of PET (Raichle et al., 2001). The ability of resting-state fMRI to reproduce this recently discovered network further corroborated this technique. For their intrinsically different features, resting-state networks are often classified as "task-positive" (sensory and cognitively systems) and "task-negative" (DMN) networks.

Table 1.1 Commonly reported resting-state network with relative compositions (Barkhof et al., 2014)

Networks	Description
Default mode	Precuneus and posterior cingulate, bilateral inferior–lateral–parietal and ventromedial frontal cortex. Involved in introspection and active episodic memory; becomes deactivated during specific goal-directed behavior
Visual processing	Striate cortex, occipital pole, and lateral visual areas. Mostly primary visual cortex, but extending to higher-order visual processing
Sensorimotor	Primary sensorimotor cortex, supplementary motor area and secondary somatosensory cortex. Detection and processing of sensory input and preparation and execution of motor functions
Executive	Mesiofrontal areas, including anterior cingulate and para-cingulate cortex. Involved in executive control and working memory function
Salience	Dorsal anterior cingulate cortex and bilateral insulae. The network responds to behaviorally salient events
Dorsal attention	Superior parietal and superior frontal areas, including intraparietal sulcus and frontal eye-fields. Involved in voluntary (top-down) orienting and selective attention
Auditory	Superior temporal gyrus, including Heschl gyrus, including primary auditory and associated areas

Resting-state networks composed of functional connected regions are supported by anatomical connections via direct monosynaptic links (Vincent et al., 2007). Strong support to such relation comes from subjects undergoing corpus callosotomy; after surgical resection interhemispheric functional connections are strikingly lost (Johnston et al., 2008). However, anatomical and FC are not perfectly coupled, since functional connections can be seen in areas lacking of direct monosynaptic connections, as in the case of left and right primary visual cortex (Vincent et al., 2007). Thus, FC, arising from both monosynaptic and polysynaptic connections, can tell more about brain functional organization than the brain anatomical structure alone can do.

PHYSIOLOGICAL MODULATIONS IN LFFS. The functional relevance of spontaneous BOLD LFFs is pushed forward by studies showing signal modulations under various physiological conditions. For example, the magnitude of LFFs increases in the visual cortex during rest with open eyes compared to the closed eye condition (Yang et al., 2007, Yan et al., 2009), while decreases in the DMN during working memory tasks compared to rest (Fransson, 2006). In this context, it is useful to report that the magnitude of LFFs has shown to be correlated with the metabolic demand (Fukunaga et al., 2008, Tomasi et al., 2013), further supporting its physiological nature. Considering the strength of LFF synchronization instead of its magnitude, a

parallel increase in FC was reported in the DMN comparing closed and open-eye resting-state conditions (Yan et al., 2009).

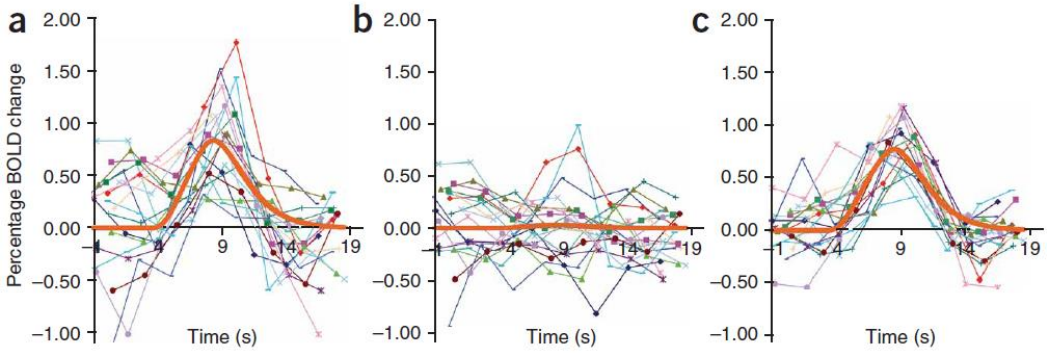

Figure 1.10 Coherent spontaneous fluctuations account for a significant fraction of the variance in measured event-related responses. (**a**) Raw event-related responses in the left motor cortex (MC) for 18 button presses from a single subject. (**b**) The corresponding activity in the right MC for each button press. (**c**) Task-related responses in the left MC after subtraction of spontaneous fluctuations measured in the right MC. The thick orange line in each graph represents the best fit gamma function to all data points (Fox et al., 2006b).

Interestingly, ongoing brain activity plays an important role in shaping behaviour performances. Effectively, spontaneous BOLD fluctuations account for a significant fraction of intertrial variability in BOLD evoked-response (Fox et al., 2006b, Fox et al., 2007) as well as for intertrial variability in behaviour (measured as spontaneous variability in button press force) (Fox et al., 2007). The former result is reported in Figure 1.10, where it can be seen how spontaneous LFFs in the right somatomotor cortex account for variability in left somatomotor cortex BOLD responses following right-handed button presses. This link between spontaneous BOLD activity and behaviour variability is further suggested by their similarity in temporal proprieties, both exhibiting a 1/f frequency distribution (Gilden et al., 1995).

Pathological modulations in LFFs. The intrinsic organization of the brain, as revealed by spontaneous BOLD LFFs, is altered under various neurological and psychiatric diseases. The list of diseases with altered FC patterns is striking extended and actually, it continues to grow on a daily basis. For example, alterations in networks strength and/or in their extensions were reported in Alzheimer's disease (Brier et al., 2012), multiple sclerosis (Zhou et al., 2013a), Parkinson's disease (Tessitore et al., 2012), bipolar disorder (Vargas et al., 2013), schizophrenia (van den Heuvel et al., 2013), autism (Monk et al., 2009) and so on (see for example, Barkhof et al., 2014). Interestingly, most of such FC alterations involve the DMN, pointing to its key role in the physiological function. Most findings regard reductions in

connectivity, but increases were reported as well, suggestive of possible compensatory mechanisms.

More recently, abnormal magnitudes of LFFs were also reported. For example, abnormal intensities were found in Alzheimer's (Liu et al., 2014b) and Parkinson's disease (Zhang et al., 2013), schizophrenia (Yu et al., 2012) and diabetes (Xia et al., 2013).

FINAL REMARKS. One might complain that the resting state, during which measures are collected, does not actually represent a rest condition for the brain, since unconstrained thoughts, mind wandering or day dreaming do happen in this state (Christoff et al., 2009). However, such uncontrollable behaviours are unlikely to explain the spatio-temporal patterns of coherence in spontaneous BOLD fluctuations. Indeed, resting-state networks have been reported in different levels of consciousness, being present under anaesthesia in humans (Greicius et al., 2008) and monkeys (Vincent et al., 2007), and also during the early stage of sleep in humans (Fukunaga et al., 2006). It is also unlikely that such uncontrolled activity could shape all functionally distinct networks at once. On the contrary, it is reasonable that unconstrained behaviours in the scanner would result in BOLD modulations that are in addition to, not the source of, spontaneous coherent BOLD fluctuations (Fox and Raichle, 2007).

All the above reported evidence suggests the existence of spatio-temporal patterns of intrinsic coherent neuronal activity that are mirrored in BOLD LFFs. The recorded BOLD signal probably reflects a linear mixture of intrinsic brain activity, unconstrained thought activity as well as non-neuronal physiological fluctuations. In addition, this ongoing activity seems to be the infrastructure upon which task-evoked response is added.

Neurophysiological correlates

The notion that the brain has an intrinsic activity is known from early EEG measures, and is further supported by metabolic studies showing high energy consumption during rest, especially if compared with the small increase in energy demand during task performance (Raichle, 2010). Thus, the brain can be thought as a never-stopping machine that is continuously at work. The question, which is still matter of debate, is whether spontaneous BOLD LFFs reflect such ongoing neuronal activity and, in case, what component represent.

Since the spectral signature of coherent BOLD fluctuations is in the low-frequency range (< 0.1Hz), neurophysiological correlates should be searched among signals

with similar time scales. Possible neurophysiological candidates with low-frequency profiles are (i) fluctuations in the power of high frequency (> 1 Hz) LFPs and (ii) raw signals from the lowest edge of LFPs (0,001-4 Hz), termed as slow-cortical potentials (SCPs). Indirect evidence for their contribution to BOLD fluctuations comes from several studies reporting synchronized activity at several spatial scales. Indeed, synchronized γ-LFP[2] power modulation has been reported in awake monkeys over a small cortical distance (Leopold and Logothetis, 2003), and on larger spatial scale (i.e., interhemispheric) in humans by means of electro-corticography (He et al., 2008, Nir et al., 2008) and depth electrodes (Nir et al., 2008). SCPs have shown similar correlation structures to that of spontaneous BOLD fluctuations (Lu et al., 2007, He et al., 2008, Weissenbacher et al., 2009). Of note, while synchronized γ-LFP power modulations were reported only in wakefulness and REM sleep, synchronized SCP fluctuations has shown to be state-invariant (He et al., 2008), suggesting that the latter could be the main responsible for BOLD fluctuations.

Simultaneous recordings of fMRI and electrophysiological signals have also been reported and provide strong support for the neuronal origin of BOLD fluctuations. Much work has focused on correlations between hemodynamic signal and LFP power. By means of implanted electrodes, direct couplings were found between the γ-band and BOLD signal in anesthetized monkeys (Shmuel and Leopold, 2008) and between the γ-band and CBV in awake monkeys (Schölvinck et al., 2010). In humans, less spatial specific measures, obtained with EEG recordings, have shown association between BOLD signal activity within the DMN and power in different frequency bands (Laufs et al., 2003, Scheeringa et al., 2008). Recently, SCPs have also showed couplings with spontaneous hemodynamic fluctuations in humans. Indeed, slow scalp potentials, a non-invasive measure of SCPs, have shown correlation patterns with spontaneous BOLD fluctuations spatially localized in different resting-state networks (Hiltunen et al., 2014).

Despite such evidence, much work is still needed to exactly quantify the contribution of different neurophysiological signals to the emergence of BOLD LFFs. Just think that, among the cited studies, the highest fraction of variance explained by the neuronal-hemodynamic coupling only reached the 25% of the total variance (Leopold and Maier, 2012).

[2] LFPs are conventionally described in terms of their band-limited frequency components (delta, 1–4 Hz; theta, 4– 8 Hz; alpha, 8–12 Hz; beta, 12–24 Hz; and, gamma, > 24 Hz). The reader should not confuse such high frequency signals with those much lower arising from modulations in their power.

CHAPTER 2

Mathematical and computational framework for analysing LFFs

The study of LFFs in spontaneous BOLD signals can reveal much about brain functional organization both in physiological and pathological conditions. However, correct result interpretation is highly influenced by the type of measures adopted and how they are implemented. Here, we will provide a mathematical framework for the extraction of relevant information from LFFs. We will discuss some methodological issues and we will provide insight in different fMRI measures. Finally, a comprehensive software for the analysing of steady-state data is presented. The toolbox, personally developed during my PhD course, encompasses all of the measures that will be now introduced.

Some of the following measures, especially amplitude-based and global FC metrics, will be successfully applied to study functional alterations in Alzheimer's disease (Chapter 3) and physiological LFF modulations induced by different cognitive states (Chapter 4). Of note, pre-processing strategies for reduction of MRI artefacts and

mitigation of no neuronal source of variance, although extremely important in steady-state data, are not the aim of the present chapter; these issues are efficiently addressed elsewhere (Smith et al., 2001, Birn et al., 2014).

Oscillation amplitude assessment

This section is dedicated to the study of univariate measures quantifying the magnitude of low-frequency (typically < 0.1 Hz) fluctuations of BOLD time series. In the last few years, several different measures of this type have been adopted to study physiological and pathological brain function in resting-state data (e.g., ALFF, RSFA, fALFF, mALFF, zALFF). Moving through this zoo of amplitude measures can be chaotic. Actually, these measures can be easily classified in two terms: the domain in which the amplitude is calculated (time versus frequency) and the type of normalization.

Time versus frequency domain

In the **frequency domain**, Zhang et al. introduced the Amplitude of Low-Frequency Fluctuation (ALFF; Zang et al., 2007), defined as the sum of the spectral amplitudes in a selected frequency range. To derive the ALFF equation, let us consider a time series $x_i = x(t_i),\ i = 1,2,\dots,N$ with N time points; this can be written in the frequency domain as:

$$x_i = \frac{1}{N}\sum_{k=1}^{N} X_k\ e^{\frac{2\pi j}{N}ki}, \qquad i = 1,2,\dots,N \tag{2.1}$$

where the spectral amplitude terms, $X_k = x(f_k)$, with $k = 1,2,\dots,N$, are the discrete Fourier transformed coefficients. The power spectrum (PS), in the frequency range $f_1 \le f \le f_2$, is defined as:

$$PS(f_1, f_2) = \frac{1}{N}\sum_{k=f_1}^{f_2} |X_k|^2 \tag{2.2}$$

Since, each term in the above summation is proportional to the square of the amplitude of a given frequency k present in the original time series x_i, ALFF can be easily computed by summing the square root of the PS at each frequency component (i.e., the square root of the PS density):

$$ALFF(f_1, f_2) = \frac{1}{\sqrt{N}}\sum_{k=f_1}^{f_2} |X_k| \tag{2.3}$$

In the **time domain**, Kannurppatti et al. defined the Resting-State Fluctuation Amplitude (RSFA; Kannurpatti and Biswal, 2008) as the standard deviation of a filtered time series:

$$RSFA = x_{std} = \sqrt{\frac{1}{N}\sum_{i=1}^{N}(x_i - \bar{x})^2} \tag{2.4}$$

RSFA is usually calculated starting from a filtered time series with zero mean; in this situation, the standard deviation is equal to the root mean square (rms) of the signal, namely $RSFA = x_{rms} = \sqrt{\frac{1}{N}\sum_{i=1}^{N} x_i^2}$.

These two measures of oscillation amplitude, ALFF and RSFA, are related by the Parseval's theorem:

$$\sum_{i=1}^{N}|x_i|^2 = \sum_{k=1}^{N}\frac{|X_k|^2}{N} \tag{2.5}$$

The right side equation is the PS, indeed, $\frac{|X_k|^2}{N}$ is the power spectral density (PSD) at the given frequency k. It follows from x_{rms} definition that $x_{rms} = \frac{1}{\sqrt{N}}\sqrt{PS}$. Thus, considering a zero-mean signal, $RSFA = x_{std} = x_{rms} = \frac{1}{\sqrt{N}}\sqrt{PS}$, and both measures, ALFF and RSFA, can be written as a function of the spectral amplitude:

$$\begin{cases} RSFA = \dfrac{1}{\sqrt{N}}\sqrt{\displaystyle\sum_{k=1}^{N}\frac{|X_k|^2}{N}} \\ ALFF = \displaystyle\sum_{k=1}^{N}\frac{|X_k|}{\sqrt{N}} \end{cases} \tag{2.6}$$

The above comparison shows that RSFA and ALFF are two different ways of summarising the spectral amplitude. Indeed, aside for a constant factor, ALFF and RSFC are the L^1- and L^2-norm of the spectral amplitude, respectively.

In Figure 2.1 is reported a test comparison among different measure types of oscillation amplitude. The test was performed on preliminary data acquired at the aim of studying how visual attention modulates the ongoing brain activity. Regarding our current concerns, these results show a striking similarity between ALFF and RSFA. Of note, the mean of $|x_i|$ has a qualitatively similar trend as well. In fact, once again, the mean is the L^1-norm of $|x_i|$, while the standard deviation of a zero-mean signal is the L^2-norm.

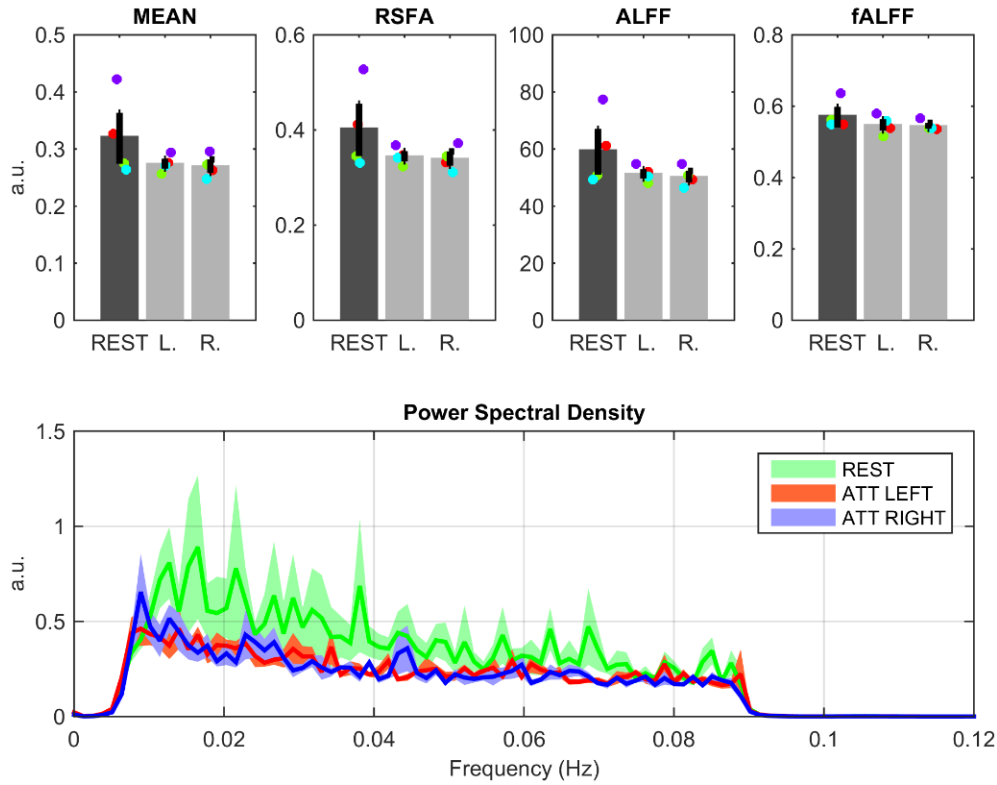

Figure 2.1 ALFF and RSFA comparison. In this test, steady-state fMRI scans were acquired in five subjects. Each subject was scanned under three conditions: 1) resting-state with closed eyes (REST), 2) visual attention on the left hemi-field (ATT LEFT), 3) and to the right hemi-field (ATT RIGHT). In the upper panels are reported several measures of oscillation amplitude (see text for details) averaged over the whole brain. In the bottom panel is reported the corresponding power spectral density.

Normalization strategies

To compare the oscillation amplitude of different subjects (i.e., to perform a second-level analysis) it is mandatory to apply a normalization. The reason for this is that the mean value of the BOLD signal depends on several parameters that are out of the control of the researcher (such as the static field, field inhomogeneities, the hematocrit content and many others); only variations around the mean can be related to variations in the oxygenation content.

Even though a normalization could be applied directly on time series, it is typically carried out by dividing the ALFF (or RSFA) map by the mean value of the measure across the entire brain (or, to improve sensitivity, in the grey matter). An *m-* prefix usually indicates this type of normalization:

$$mALFF = \frac{ALFF}{mean(ALFF)} \tag{2.7}$$

In this way, the oscillation amplitude are normalized respect to the subject mean oscillation (maps are centred around one).

A similar approach commonly applied is to transform the ALFF (or RSFA) map in z-score, subtracting the mean and dividing by the standard deviation of the measure computed across the entire brain (or across the gray matter). A *z-* prefix usually indicates this type of normalization:

$$zALFF = \frac{ALFF - mean(ALFF)}{std(ALFF)} \tag{2.8}$$

Each voxel in the map indicates the number of z-score above or below the subject mean oscillation (maps are centred around zero). This approach has the advantage of improving the normality of the data.

A completely different method was introduce by Zou et al. (Zou et al., 2008). They defined the fractional ALFF (fALFF) as the ratio of the oscillation amplitude in the frequency range of interest to the amplitude in the entire spectrum:

$$fALFF(f_1, f_2) = \frac{ALFF(f_1, f_2)}{ALFF(0, f_n)} \tag{2.9}$$

where f_n indicates the Nyquist frequency. Similarly, fRSFA is defined as the ratio of the standard deviations of the two differently filtered time series. fALFF measure, which is mathematically equivalent to ALFF computed starting from a normalized PSD, has been shown to be less prone to physiological noise (Küblböck et al., 2014) and to be more localized in grey matter than ALFF (Zou et al., 2008, Zuo et al., 2010).

Despite fALFF is, by definition, comparable among subjects, different studies have applied the m- or z- transformation – eq. (2.7) and (2.8), respectively – to improve the normality (Zuo et al., 2010, Han et al., 2011, Zhou et al., 2013b). Actually, normality tests carried out on data from our laboratory suggest that it is not the case. In Figure 2.2 is reported the percentage of voxel in the brain that follows a normal distribution ($p < 0.05$) for ALFF and fALFF and relative standardized measures. Our results showed that z- or m- transformation only minimally influence the normality of data, on the contrary fALFF *per se* was characterized by more than 90% of voxels normally distributed.

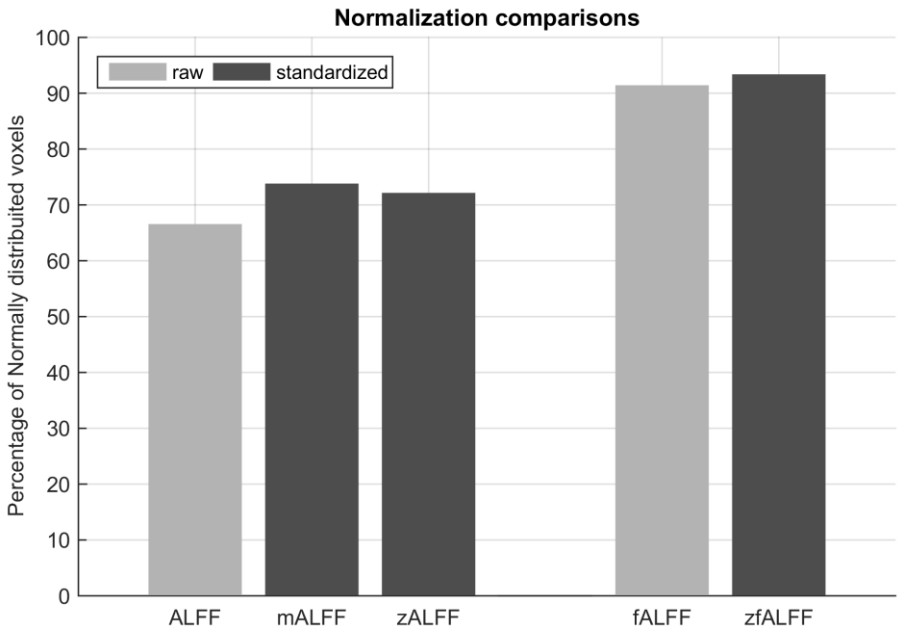

Figure 2.2 Comparison of different standardization strategy for ALFF and fALFF. Assessment of normalization goodness was carried out counting the number of Gaussian distributed voxel via Jarque-Bera normality test ($p < 0.05$). For each voxel the test was performed on 10 data points (i.e., 10 healthy subjects).

Functional connectivity assessment

In fMRI, "functional connectivity" (FC) has been defined as the temporal correlation of physiological processes between spatially discrete brain areas (Friston et al., 1993). From this definition, it results that two ingredients are required: 1) a mathematical function to assess the temporal correlation and 2) the definition of spatially discrete brain areas from which the time series should be extracted.

The temporal correlation is commonly assessed by means of Pearson correlation coefficient computed between two different BOLD time-series. Although this method is the most widely used in fMRI, it has the disadvantage to be sensitive to phase lags. Indeed, two brain regions might have the same underlying neuronal activity but out-of-phase BOLD-time courses because of different vascular reactivity. However, this is a minor concern compared to the thorniest issue regarding the choice of the brain regions from which the time-series should be extracted to be compared. Historically, the first method of FC assessment was presented by Biswal et al. (Biswal et al., 1995) and can be defined as seed-based approach. In this method, either a single region of interest (ROI) is chosen and the connectivity between that ROI and the rest of the brain is calculated, or multiple

ROIs are chosen and connectivities between different couples of ROIs are assessed. The main weakness of this method is that the average time course extracted from the ROI might not represent any of the independent time courses within the region, especially if the ROI is a wide area. Thus, the definition of the ROI is crucial. There are two ways of defining ROIs: 1) anatomically or 2) from task-based fMRI. The former method is not always suitable, especially when the anatomic landmarks of chosen regions are not well defined. Instead, the latter has the advantage of being highly specific, but requires different tasks to localize multiple areas and it is not always possible to selectively activate a specific region.

In this section, we introduce several other FC metrics aiming to overcome some of the limitations of ROI-based FC. Specifically, the ROI limitation will be handled with different voxel-based metrics (Global FC and Regional Homogeneity), while the phase lag issues will be handled by the coherency method.

Voxel-wise global connectivity

Here we will introduce a set of measures that quantifies the global connection of a brain network at a voxel-wise spatial resolution. In this kind of measures, the connectivity value stored at each voxel in the brain quantifies the degree of connection of that voxel with all other voxels. The main advantage of these approaches is to produce a single connectivity map in a data-driven fashion and, not less importantly, to be independent on the choice of any ROI. On the other hand, the downside is that long- and short-range connections are equally weighted and thus, they cannot be discriminated.

A prerequisite of any voxel-wise global FC metric is the definition of an adjacency matrix. In a voxel-wise network, each voxel is a node and the edge between two nodes is defined by Pearson correlation. To produce a single value measure, the so defined weighted, undirected adjacency matrix must be collapsed in one dimension according to a given criterion. The collapse of the matrix is generally accomplished summing the adjacent links with a weighting function, $w(x)$. Different weightings produce different voxel-wise FC metrics each of which highlights different aspects of global connection.

One possible strategy to summarize the global FC propriety of a given node consists in counting the number of strongly connected links arising from that node. This metric is defined as *degree centrality* (DC) in graph theory (sometimes simply referred to as *degree),* and it is practically achieved binarizing the adjacency matrix, considering only significant correlations above an arbitrary threshold th, and

counting, for each node, the surviving number of connections. For a given node i, DC can be written as

$$DC_{+}(i) = \sum_{i \neq j} w\big(r(i,j)\big) \qquad w(x) = \begin{cases} 1 & x \geq th \\ 0 & x < th \end{cases} \tag{2.10}$$

where $r(i,j)$ is the Pearson's correlation coefficient and $w(x)$ is a step function. This metric has been successfully applied to characterize both the healthy and the diseased brain (Buckner et al., 2009, Cole et al., 2010). Of note, in this definition of DC_{+}, negative correlations are excluded, mainly due to their controversial origin (see, for example, Murphy et al., 2009); however, some researchers have also used the absolute value of correlation as threshold:

$$DC_{+/-}(i) = \sum_{i \neq j} w\big(r(i,j)\big) \qquad w(x) = \begin{cases} 1 & |x| \geq th \\ 0 & |x| < th \end{cases} \tag{2.11}$$

This measure has been termed by Martuzzi et al. as intrinsic connectivity contrast (ICC-d; Martuzzi et al., 2011); however, in this review of global connectivity metrics, we prefer the more pertinent term $DC_{+/-}$. The main issue about DC measures is the choice of the threshold. These are frequently chosen to be large enough to prevent false positive results but small enough to maintain the important connections. However, the choice is usually arbitrary and it is often justified by presenting results produced by a range of thresholds highlighting the robustness of the results to the chosen threshold (Buckner et al., 2009). Alternatively, the threshold could be selected based on significance level. However, this approach has several complications such as issues related to the pertinent multiple comparison correction (each voxel is correlated with several thousands of other voxels and this procedure is repeated for the same number of voxels) and the estimation of the number of degree of freedom (which is influenced not only by acquisition protocols but also by several preprocessing steps).

Alternatively, two weighting functions that do not require the definition of a threshold term have been proposed. Cole and colleagues defined weighted global brain connectivity (wGBC) as the average of the Fisher-trasformed correlation coefficients (Cole et al., 2010):

$$\mathrm{wGBC(i)} = \frac{1}{N} \sum_{i \neq j} w\big(r(i,j)\big) \qquad w(x) = \frac{1}{2}\ln\left(\frac{1+x}{1-x}\right) \tag{2.12}$$

Martuzzi and colleagues introduced the ICC-power, ICC_p (Martuzzi et al., 2011), as the sum of the squared correlation coefficients (differently from the original paper,

(i) we consider only positive correlations and, (ii) we use an average value instead of the sum):

$$\mathrm{ICC}_p(\mathrm{i}) = \frac{1}{N_+}\sum_{i\neq j} w\big(r(i,j)\big) \qquad w(x) = \begin{cases} x^2 & x \geq 0 \\ 0 & x < 0 \end{cases} \tag{2.13}$$

Where, N_+ is the number of voxels with positive correlations. The weightings in both ICC_p and wGBC are designed to minimize the contribution of weak correlations, either by suppressing them ($w(x) = x^2$), or empathising the strong connections ($w(x) = \frac{1}{2}\ln\left(\frac{1+x}{1-x}\right)$).

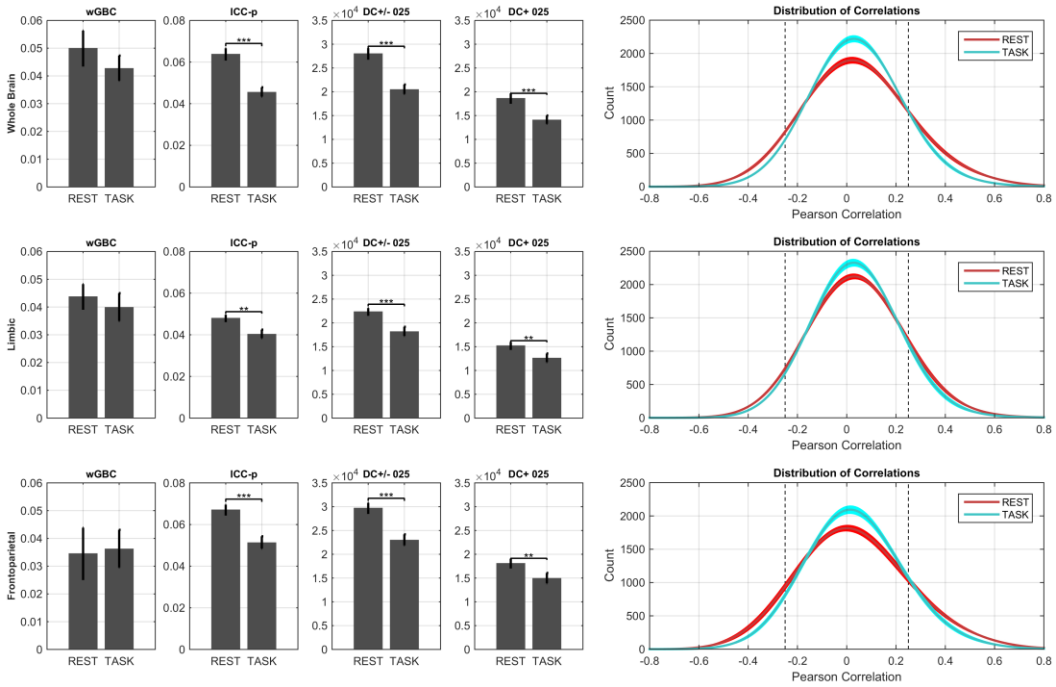

Figure 2.3 Comparison of global FC metrics. wGBC, ICC_p, $DC_{+/-}$ and DC_+ measured in different cognitive states (rest vs task) and averaged in three representative regions. Each row is a different ROI from which the measure was averaged; from top to bottom: whole brain mask, limbic and frontoparietal cortex. The last two ROIs are part of the 7-brain regions from Yeo et. al parcellation (Yeo et al., 2011). Last column is the distribution of correlations averaged in the same ROIs. Dashed lines indicate thresholds for $DC_{+/-}$ and DC_+ calculation.

For comparison purpose, we applied the above-defined metrics to data acquired at our laboratory at the aim of studying the brain FC under different cognitive conditions. Ten subjects participated at the experiment that consisted in the acquisition of two different steady-state scans: one in resting-state with open eyes and another one during a working memory task. In Figure 2.3 the different metrics,

averaged in representative brain regions, are reported along with the relative *distributions of correlations* [3]. The first two columns in the figure report the threshold independent measures, wGBC and ICC_p; of the two measures only the ICC_p is able to significantly discriminate between the two types of conditions. wGBC fails to report any difference because it measures the average value of correlation (both positive and negative values) that, as it is clear from the distribution of correlations, is centred around zero for both conditions. In fact, the task state seems to not alter the mean distribution of correlations but to modify how low and high correlations are distributed; thus, in this particularly case, wGBC is not useful. On the contrary, ICC_p is able to discriminate the two conditions because it considers only one side of the distribution. Further, it is remarkable the effect of the weighting function $w(x) = x^2$; considering for example the first ROI (i.e., the whole brain), there is a clear opposite behaviour for low and high correlation values: the former are more copious in the task condition and the opposite for the latter. Although the area difference between the two conditions is in favour of the task state (task has around 1150 counts more than rest[4]), the ICC_p result is striking higher in the rest condition. This is due to the suppression of low correlation values by the r^2 function.

Considering the threshold based metrics $DC_{+/-}$ and DC_{+} (third and fourth column of Figure 2.3, respectively), they are both able to discriminate between the two cognitive states. The former measure appears to be more sensitive in this duty because the task state produces a reduction in the number of both positive and negative correlations.

In Figure 2.4, we report the effect of different thresholds on DC_{+} (thr = 0.25, 0.35 and 0.45) in two representative brain regions. Our data appear to be stable under the three different thresholds, although, depending on the experiment, this could not be always the case.

The above comparison is only illustrative of the potential capacity of these metrics; it should be consider that, depending on the situation, one metric could be more suitable than another one.

[3] The distribution of correlations contains the whole information of a given voxel relatively to its brain connections, prior to any type of collapse of the unweighted adjacency matrix. This huge amount of information is unmanageable at the single voxel level (that is why we need to collapse the adjacency matrix); however, the distribution of correlation averaged in a ROI is remarkably useful to understand the behaviour of the different metrics.

[4] Counting only positive correlations. Indeed, the total area under the distribution curve is equal for each condition, corresponding to the number of voxels in the brain.

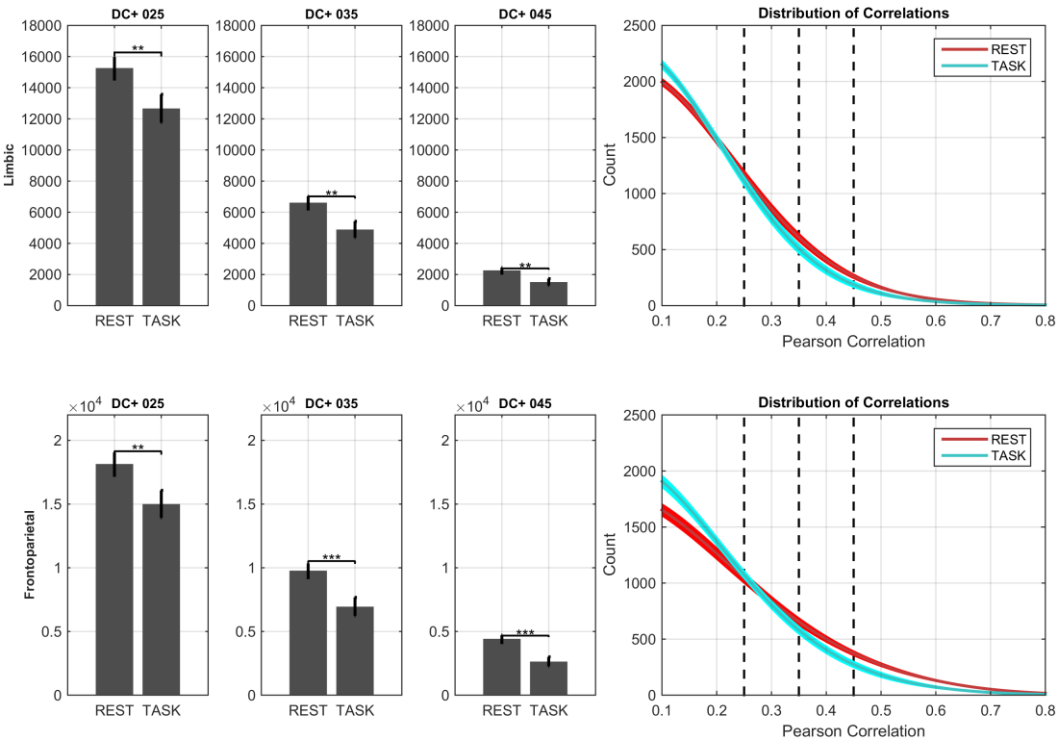

Figure 2.4 Comparison of different threshold terms on DC_+. DC_+ is measured in different cognitive states (rest vs task) and averaged in two representative regions. Each row is a different ROI from which the measure was averaged; from top to bottom: limbic and frontoparietal cortex. ROIs are part of the 7 brain regions from Yeo et. al parcellation (Yeo et al., 2011). Last column is the distribution of correlations averaged in the same ROIs. Dashed lines indicate thresholds for DC_+ calculation, thr = 0.25, 0.35 and 0.45.

Finally, an important issue regards the normalization of these metrics. Threshold-based metrics are usually converted to z-score, i.e., subtracting the mean across the brain and dividing by the standard deviation (Buckner et al., 2009, Scheinost et al., 2012, Liu and Tian, 2014). The motivation for such approach is that maps are equally scaled and can be compared across subjects (Buckner et al., 2009). Actually, differently from BOLD amplitude-based measures, such as ALFF, the absolute value of global FC metrics is meaningful per se and can be compared across subjects; furthermore, transforming to z-score costs the loss of mean whole-brain information. In fact, once the map is converted to z-score the information is now relative to the brain average behaviour; for example, positive values of a z-score converted DC measure indicate that voxels are more globally connected relative to the mean behaviour of all other voxels. When comparing different populations of subjects, or different condition states as in the above reported comparison, the raw and z-score values can have even opposite behaviour if the average whole-brain values are different in the two populations/conditions. Our data clearly illustrate this point. In

Figure 2.5 are reported raw and z-score DC_+ values averaged in the whole-brain ROI and in a representative brain region. The transition from rest to task produces a remarkable whole-brain reduction in DC_+ (raw) that is also present in almost all other ROIs in the brain (here only the frontoparietal is reported). Converting DC_+ to z-score, this striking feature of the rest-task transition is lost but another information regarding the internal organization of the brain emerges. Indeed, the frontaparietal network, for example, although less connected in absolute value, has a greater relative connection (respect to the whole-brain mean) compared to rest. In conclusion, the conversion to z-score is an useful way to study how the brain rearranges its internal connectivity, however, the study of the absolute values cannot be overlooked, otherwise important information might get lost.

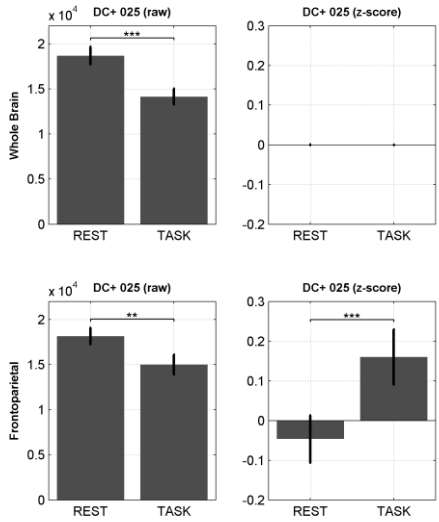

Figure 2.5 Comparison of raw and z-score DC_+ values. Converting raw values in z-score the information on the whole-brain behaviour is lost. Z-score transformed images give information relative to the whole-brain mean behaviour.

Correlation entropy

Here we propose an entropy-based method to convert the distribution of correlations in a descriptive single-value measure, in a completely data-driven fashion. It is reasonable to assume that voxels with widespread connections should also have a highly complex distribution profile of correlations, which corresponds to a high information content.

Information content can be calculated according to the standard Shannon formula:

$$\mathrm{H} = -\sum_{r} p_r \log p_r \tag{2.14}$$

where p_r denotes the probability of the voxel to have a discretized correlation r. p_r satisfies the normalization condition:

$$\text{Tot voxels} = \sum_{r}^{N} n_r \rightarrow 1 = \sum_{r}^{N} p_r \tag{2.15}$$

with n_r being the number of occurrences of the r correlation value and N being the total number of discrete correlation states.

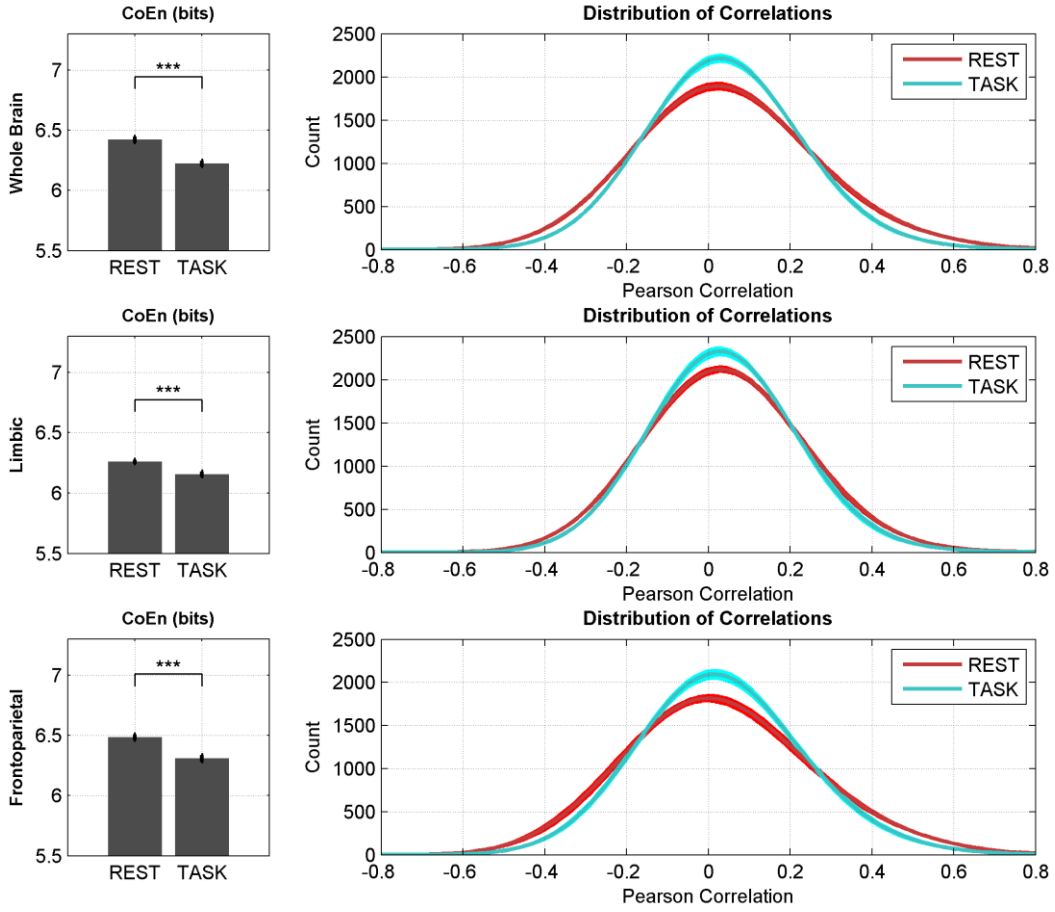

Figure 2.6 Correlation Entropy. $CoEn$ is measured in different cognitive states (rest vs task) and averaged in representative regions. Each row is a different ROI from which the measure was averaged; from top to bottom: limbic and frontoparietal cortex. Last column is the distribution of correlations averaged in the same ROIs.

We define Correlation Entropy (CoEn) the Shannon entropy applied to the distribution of correlations. The only parameters that must be defined is N, i.e., the

bin size for the extraction of the probability distribution function. We adopted N = 200 bins to cover the range of correlations: $r \in [-1,1]$. However, our first preliminary analysis showed no significant effect for the choice of N under a wide range of values (data not shown).

Application of CoEn to the above-described data revealed that the measure is significantly able to discriminate between the two different cognitive conditions (Figure 2.6). In agreement with our hypothesis, the information content (i.e., entropy value) decreases in the task condition, paralleling a decrease in the number of high connections.

Before any further conclusion about this novel metric, further test should be done. In particular, the stability of the measure should be tested in prolonged resting-state conditions and the ability to discriminate more subtle changes of state must be further investigated.

Regional Homogeneity

Global FC metrics assess local (i.e., at voxel level) synchronization properties at a global scale (i.e., taking into account all – or a great portion of – brain's voxels), irrespectively of any distinction between short- and long-range connections. One possible question, that it is not answered by the measures introduced until now, is how BOLD low frequency fluctuations are synchronized locally, at a short-range scale. To answer this question, Zang and colleagues introduced a voxel-based measure that assesses the similarity of time series among nearest neighbouring voxels (Zang et al., 2004). The measure, named regional homogeneity (ReHo), is just a renaming of the rank based Kendall's coefficient of concordance (KCC; Kendall and Smith, 1939) for a set of time series:

$$ReHo \equiv W = \frac{\sum(R_i)^2 - n(\bar{R})^2}{\frac{1}{12}K^2(n^3 - n)} \tag{2.16}$$

Where W is the KCC among given voxels, ranged from 0 to 1, with 0 representing no concordance at all and 1 complete agreement among time courses; R_i is the sum rank of the i-th time point; $\bar{R} = (n+1)K/2$ is the mean of the R_i's; K is the number of time series within a measured cluster; n is the number of ranks (i.e., time points). The number of time series K (or equivalently, the number of voxels) that makes up a cluster can be liberally chosen; however, typically values are $K = 7$, 19 and 27 voxels, which correspond to choose only voxels that share a face, a face or an edge, a face or an edge or a node, respectively.

It has been shown that regions of DMN have higher ReHo than other brain regions during resting state (Long et al., 2008). In addition, ReHo method has been applied to the detection of local abnormalities in several brain disorders (Yuan et al., 2008, Wu et al., 2009, Paakki et al., 2010), including AD (He et al., 2007).

Of note, KKC is not the only measure that has been proposed to assess the regional homogeneity of BOLD time series, for example, a measure based on coherency has been recently introduced (Liu et al., 2010; see next section for coherency introduction). The main disadvantage of KCC is that rank is sensitive to phase lags in time series; thus, random noise that induce phase delay could possible lower the measure of ReHo. However, further investigation is still needed to elucidate the sensitivity and specificity of KCC and Coherency based methods (Liu et al., 2010).

Coherency

The above-defined measures of FC have the common feature to be sensitive to the relative phase lags between compared time series. Such sensitivity is a weakness of this type of measures; indeed, even if two brain regions share the same underlying neuronal activity they could present slightly different time courses due to different regional hemodynamic response functions (HRF; Miezin et al., 2000, Saad et al., 2001). These vascular differences (characterized by HRF parameters such as onset-delay, time-to-peak and width), can result in decreases in interregional FC. In contrast, the magnitude of coherency, the spectral analogue to cross-correlation, is insensitive to phase variability (Wiener, 1949) and hence, to interregional differences in the shape of the HRF.

Coherence, $Coh_{xy}(k)$, estimates the linear time-invariant relationship between two time series, x and y, at the frequency component k. It is defined as:

$$Coh_{xy}(k) = \left|R_{xy}(k)\right|^2 = \frac{\left|f_{xy}(k)\right|^2}{f_{xx}(k)f_{yy}(k)} \tag{2.17}$$

where $R_{xy}(k)$ is the complex-valued coherency of x and y, $f_{xy}(k)$ is the cross-spectrum of x and y, and $f_{xx}(k)$ is the power spectrum of x. Coherence is a positive function, symmetric to x and y (e.g., $Coh_{xy} = Coh_{yx}$), and bounded by 0 and 1, where 0 indicates that x and y have no linear relationship, and 1 indicates that x can perfectly predict y in a linear fashion (Sun et al., 2004). Roughly speaking, coherence could be considered as a correlation coefficient in the frequency domain.

An estimate of the cross-spectrum, $f_{xy}(k)$, can be obtained multiplying the Fourier transform of x by the Fourier transform of y. The variance of such estimate is not dependent on the number of time points in the time series, but can be reduced applying a modified periodogram approach such as the Welch's method (Welch, 1967). Therefore, the time series is usually divided into N segments of length T, where each segment is assumed to approximate stationarity. Each segment is mean-centered and windowed by a Hanning filter of length T to reduce spectral leakage resulting from segmenting the time series. The reduced-variance estimate of the cross-spectrum is:

$$\hat{f}_{xy}^{(T)}(k) = \frac{1}{N}\sum_{n=1}^{N} X_n^{(T)}(k) Y_n^{*(T)}(k) \tag{2.18}$$

where $X_n^{(T)}(k)$ is the T-point discrete Fourier transform of the windowed and mean-centered n-th segment of x. Likewise, the power-spectrum estimate is:

$$\hat{f}_{xx}^{(T)}(k) = \frac{1}{N}\sum_{n=1}^{N} \left|X_n^{(T)}(k)\right|^2 \tag{2.19}$$

Combining the estimated cross-spectrum and power-spectrum as described in equation (2.17), is possible to calculate coherence as a function of frequency. However, to generate a single-value measure of coherence-based FC (i.e., a brain map of FC) the coherence magnitude is typically band-averaged in the frequency range of interest:

$$\widehat{Coh}_{xy}(\bar{k}) = \frac{\left|\sum_k \hat{f}_{xy}^{(T)}(k)\right|^2}{\sum_k \hat{f}_{xx}^{(T)}(k) \sum_k \hat{f}_{yy}^{(T)}(k)} \tag{2.20}$$

Since the coherence magnitude is restricted between 0 and 1, it is not normally distributed. Thus, to allow for statistical comparisons a z-fisher transformation is first applied.

From coherency is also possible to extract information on the temporal lag between time series (Sun et al., 2005). In fact, the phase component of coherency is the phase-spectrum $\varphi(k)$:

$$\varphi(k) = \arg\{R_{xy}(k)\} = \arg\{f_{xy}(k)\} \tag{2.21}$$

The group delay, $\tau(k)$, which is a measure of the linear delay between two time-series is defined to be proportional to the derivative of the phase-spectrum:

$$\tau(k) = -\frac{1}{2\pi}\frac{d}{dk}\varphi(k) \tag{2.22}$$

Thus, for a frequency range of interest, we can estimate a linear phase-delay as the average slope of the phase-spectrum within the band:

$$\hat{\tau}(k) = -\frac{\sum_k \varphi(k)}{2\pi \sum_k k} \tag{2.23}$$

In summary, from the complex-valued coherency it is possible to extract two real-valued functions, its magnitude and its phase component, that carry different information. The former measures how well one time-series predicts another irrespectively of any delay between them while the latter estimates their temporal lead or lag.

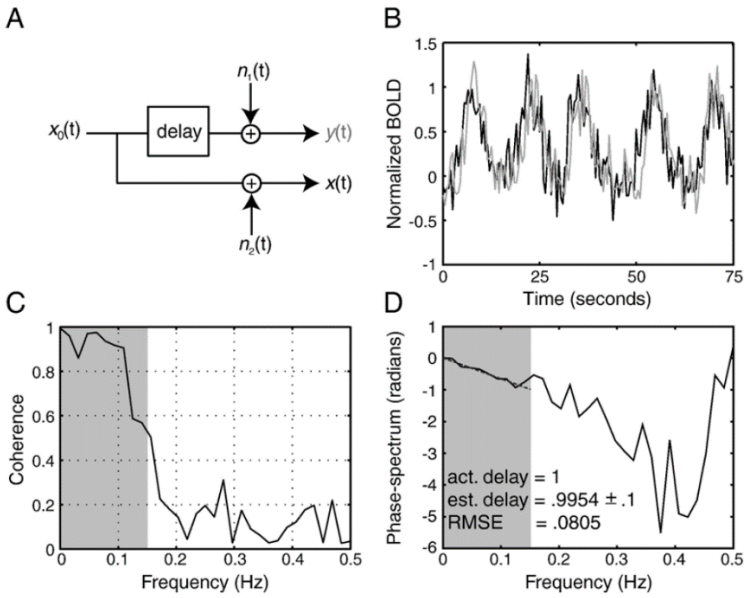

Figure 2.7 Illustration of coherence and phase-spectra as a measure of the linear time-invariant relationship and delay between two time-series. In this simulation, a time-series representative of the hemodynamic response, x0(t), is passed through a linear delay of 1 s (A). Both x(t) and y(t) (the original signal and the delayed signal, respectively) are corrupted with independent sources of noise to result in the time-series shown in panel (B). (C) The coherence of x and y is near 1 within the 0 –0.15 Hz band and near zero elsewhere. (D) The phase-spectrum reveals a linear relationship between the frequency and phase within the same band (Sun et al., 2005).

As final remarks, note that the choice of the N and T values follows two contrasting trends. A great number of segments will produce low-variance estimates of power spectrum, but, on the other hand, will decrease the number of available time points and thus lower the frequency resolution. In typical situations, we focus on the low-

frequency (e.g., 0.01–0.08 Hz) components, and the segment should not be less than 100 s (0.01 Hz) to make the frequency resolution of power spectrum high enough.

Moreover, it is important to stress the concept that coherency's measure requires a steady-state time series because it captures time-invariant information. Therefore, non-periodic functional modulations (i.e., tasks or stimuli) are not allowed in such measurement.

EASYREST

Processing and analysis of fMRI data are time-consuming procedures requiring several parameters to be set step-by-step and subject-by-subject with additional multiple check steps to ensure the correctness of the procedure. Moreover, with large amount of data, the possibility of inadvertent mistakes substantially rises. In addition, unsuitable choice of setup parameters or processing steps can mislead result interpretation. For such reasons we developed *EASYREST*, an open source easy-to-use Matlab toolbox for the processing and the analysis of resting/steady-state fMRI data. All the above defined fMRI measures and many others are easily accessible in EASYREST. The toolbox is mainly based on freely available routines of AFNI (Cox, 1996) and SPM (http://www.fi l.ion.ucl.ac.uk/spm). The former, being written in *C* / *C++* language, are extremely time efficient and thus are implemented to compute computationally heavy fMRI measures, while the latter are used to make statistical inference, being particularly suitable for voxel-wise statistics.

EASYREST is composed of four main functions foldable in three major steps:

- **easyrest**.m for the initialization and processing of data, and the computation of several fMRI measures.
- **easyrest_analysis**.m for second-level analysis at voxel-wise level.
- **easyrest_rois_extraction**.m and **easyrest_rois_plot**.m for second-level analysis at ROI-wise level.

EASYREST runs in *batch* mode only, this means that there is no graphic interface but call of main functions requires a matlab batch structure, named *ER*, which must contain all the appropriate fields to run the function. In the following, we will not discuss the required fields, which are extensively explained in the header of each function, but we will describe the operating principles and major features of the toolbox.

EASYREST can be downloaded at *http://lab-g1.phys.uniroma1.it*

Processing

easyrest.m is the core function of the whole toolbox. The first call of the function produces the initialization of the work project, the processing of the data and the computation of selected measures. Subsequent calls of this function, applied to an already existing work project, allow re-computing or adding of measures.

Project Initialization. The first fields required in ER batch define the project (such as name folders and path) and data location and subdivision. Functional data are classified in two level: (i) group (e.g., healthy subjects, patients...), (ii) session/condition (e.g., resting-state, task steady-state...). Data from each group must be located in separate folders, while in the same group-folder different sessions/conditions can coexist providing that each session/condition shares a common prefix (e.g., rest_*.nii, task_*.nii) that can be selected. Depending on the selected processing, additional files can be required including tissue probability maps of each subject, subject specific brainmask and estimated head-motion parameters.

Brainmask definition. A very important step is the definition of a common (for all subjects and all groups) brainmask. The most essential reason for the need of a common mask is that most output measures are normalized dividing by the average map value (for example, m- or z- standardizations), so it is imperative that each subject is defined on the same voxels. Moreover, this definition should be carefully chosen, in fact, restricting the analysis only to voxels of interest can (i) improve the sensitivity of results (especially for global FC measures), (ii) decrease computational burden. EASYREST allows five different methods of common brainmask definition:

1. From subject-specific tissue probability maps (grey matter (GM) plus white matter plus cerebral spinal fluid) applying different thresholds.
2. From subject-specific GM probability maps, applying a specific threshold.
3. From an a priori brainmask (deprecated).
4. From externally defined single-subject mask files.
5. From an automatic single-subject masking procedure.

Methods 4 and 5 generate the common brainmask by intersecting subject-specific brainmasks. Although it might depend on situations, the most recommended method is the number 2; selecting only GM voxels reduce the possibility of partial-volume errors and increases the specificity of results. We will spend a few more words on this method. Once you select the GM threshold, you can compute the common GM brainmask in two slight different modality:

- "hard" method: single subject GM maps are thresholded and then a common brainmask is defined by means of their intersection.
- "soft" method: single subject GM maps are averaged together and then this final map is thresholded to produce the common brainmask.

Although the two modalities could appear similar, the "soft" method is much more permissive than the "hard" one. In addition, you can perform this procedure on all subjects or you can restrict the computation only for a selected group. This can be useful, for example, if you desire to define the common mask starting from only the GM of healthy subjects. The output brainmask from the two modalities is not really the final mask. Indeed, it is very common to have echo-planar imaging[5] (EPI) volumes which field of view does not cover the whole brain. For this reason, it is mandatory to remove GM voxels that are not covered by EPI. This is accomplished by intersecting the obtained GM common brainmask with masks obtained from an automasking procedure applied to each EPI volume.

Of note, the final definition of the common brainmask might be automatically redefined if the percent signal change (PSC) option is selected in the processing step (see next section). Indeed, the automask procedure above mentioned usually does a reasonable good job in eliminating voxels with very low signal, and possible errors are generally well tolerated. However, this is not the case if PSC option is turned on; indeed, even a single not removed voxel with very low intensity when transformed in PSC can produce an undesired explosion in magnitude. For this reason, in PSC modality, an internal automatic check is performed to remove voxels that would produce abnormal PSC values.

SETUP PROCESSING. Once data have been selected and brainmask method designed, the processing fields must be defined. These include selection of volumes (this can be used to exclude first volumes in which magnetization has not yet reached a steady-state), band-pass filtering, regression of head-motion parameters and transformation of data in PSC (highly recommended if interested in amplitude measures). All this processing steps are performed via AFNI function 3dRSFC; additional steps allowed by such function can be added with a specific ER field that manages char strings which are directly passed to 3dRSFC (for example, adding the string *'-blur 6'* will perform 6 mm smoothing *inside* the brainmask).

MEASURE SELECTIONS. Here is the list of all possible measures that EASYREST can compute (most of which have been described in this chapter). Of note, most of these

[5] EPI is a gradient recalled MRI sequence, the most commonly used in fMRI.

measures require some configuration fields, all explained in the header of the function.

Oscillation-amplitude based measures include ALFF, RSFA (all possible standardization variations) and power spectral density that can be estimated with periodogram, Welch or multitapers method. It is also available a spectral correlation entropy measure (SpEn), which is the equivalent for amplitude measures of the already discussed correlation entropy measure.

Functional connectivity measures can be grouped in voxel-wise and seed-based measures. The former category includes: several global FC metrics[6] (wGBC, ICC_p, $DC_{+/-}$ and DC_+), correlation entropy (CoEn) and REHO. In the latter category there are: seed-based FC (StV, which stands for seed-to-voxel), coherency measures (COH, both in magnitude and in phase). It is also available another estimate of delays between time-series (named DEL) that is computed via AFNI function 3ddelay; it is based on Hilbert transform (Saad et al., 2001).

Second-level analysis

Test for significant differences among functional conditions and/or among groups can be assessed at the voxel level (voxel-wise approach) or at ROI level.

Easyrest_analysis.m allows specifying and testing different model designs. Available models include one-sample, two-sample t-test (both paired and unpaired) and ANOVA. More flexible models, such as full factorial, are not available at the moment but are the purpose of future releases. The function allows the easy inclusion of covariates in models, the specification of any type of contrast to be tested and the exclusion of bad subjects.

Easyrest_rois_extraction.m and **easyrest_rois_plot**.m allow for ROI level analysis. The first function extracts measure values in specified ROIs and store data in a matlab file. This file can then be passed to the second function which performs plots and statistical analysis. The division of the ROI level analysis in two steps permits to plot the extracted data without the need of the relative project folder. Easyrest_rois_plot.m has several features including different plotting modalities, detection of outliners (via Peirce's criterion, Ross, 2003), selection of the best subjects, full and partial correlations with behavioural data, the possibility of building sample combining conditions and/or group and many other functions.

[6] Names can slightly differ from those in the toolbox.

CHAPTER 3

Pathological modulations of LFFs

Bold-Oxygenation-level-dependent LFFs are modulated in different pathological conditions, including Alzheimer's disease (AD). In this pathology, modulations are reported in both amplitude-based (ALFF) and functional connectivity (FC) measurements (page 30 and 34, respectively), implying that both the synchronization between areas and the local activity might be compromised in the pathology. In spite of the increasing use of these measures, whether and how they are related to each other remains to be elucidated. This point is particularly relevant considering that synchrony-based measures (i.e., FC) are mathematically independent from the magnitude (i.e., ALFF) of the compared signals, thus, potential coupling between FC and ALFF would indicate an intrinsic propriety of the brain functionality (Figure 3.1).

In the first experiment reported in this chapter, we sought to investigate the relationship between FC and ALFF in a cohort of healthy elderly and the probable related modulations induced by the neurodegerative pathology. The latter point is

crucial, considering that concurrent investigation of FC and ALFF is lacking but it is required to assess the origin of the LFF modulation reported in the pathology. For example, previously reported reductions of FC in AD might simply reflect a reduction of oscillation amplitude towards the noise level rather than a specific desynchronization induced by the illness.

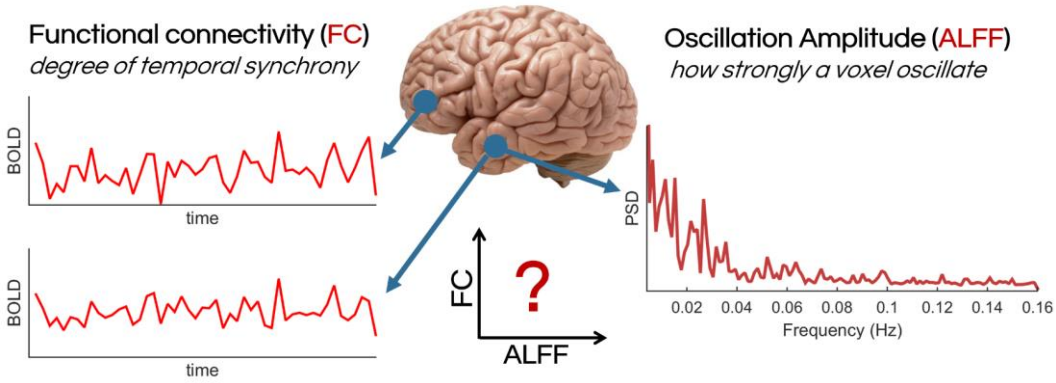

Figure 3.1 Different information coded in FC and ALFF. Functional connectivity quantifies the degree of temporal synchrony between two different elements of the brain (multivariate measure), whereas oscillation amplitude quantifies the activity of a single element of the brain (univariate measure). Whether and how they are related to each other in the brain is unknown.

In the second experiment, we applied the acquired knowledge to answer to a specific question related to the pathology, that is, whether LFF modulations can disclose brain regions underpinning language dysfunction in AD. Indeed, while the neural substrates underlying episodic memory impairment in AD have been extensively studied, those subserving language deficits remain largely unknown.

Before focusing on the two experiments, we will first briefly introduce the pathology of interest, the Alzheimer's disease, the most common cause of dementia.

Alzheimer's disease

Alzheimer's disease is a neurodegenerative disorder characterized by a slowly deterioration of memory and other cognitive functions that eventually leads to death within 3 to 9 years after diagnosis. AD affects 5.3 million of Americans and is the sixth cause of death in the United States. It is the most common cause of dementia, accounting for an estimated 60% to 80% of all dementia cases (Association, 2014).

Aging is the principal risk factor for developing AD, the incidence rate increases almost exponentially with increasing age (Figure 3.2). Nonetheless, as data on centenaries show, AD is not the natural outcome of aging. It is striking the case of a

115-year-old woman with cognitive performance above average of healthy adults of 60-75 year, and almost no signs of disease in the brain (den Dunnen et al., 2008). Other risk factors are genetic mutations, which account for a small percent of AD cases (nearly 1%) and generally lead to an *early-onset* form of the disease, family history, co-morbidities (such as, obesity, cardiovascular disease or diabetes) and educational and social engagement (Association, 2014).

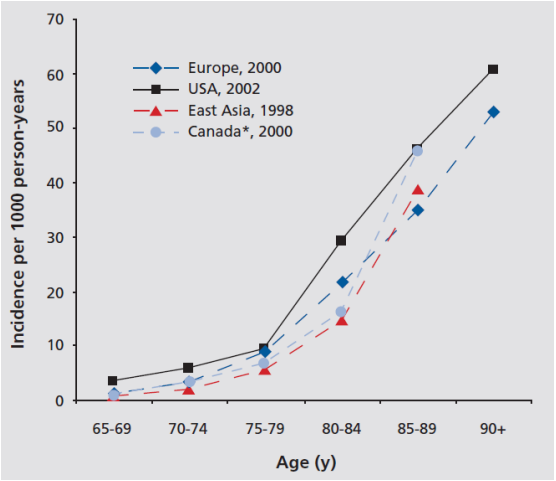

Figure 3.2 Age-specific incidence of Alzheimer's disease (per 1000 personyears)

The number of affected people is doomed to rise due to population aging. By 2050 the number of AD patients in the United States is projected to increase to 13.2 million (Qiu et al., 2009), with an estimated new case every 33 seconds (Association, 2014). Despite the tremendous social and economic impact of the disease, neither a cure nor an effective prevention strategy yet exists.

Brief History. In 1907, Alois Alzheimer, a German physician, reported the case of a 51-year-old female patient, named Auguste Deter, who exhibited severe cognitive disorders. The woman initially manifested a profound memory loss, unfounded suspicions about her husband and disorientation. She showed worsening psychological changes, including, reduced comprehension, aphasia, paranoia, auditory hallucinations and psychosocial impairment:

> *The first symptom the 51-year-old woman showed was the idea that she was jealous of her husband. Soon she developed a rapid loss of memory. She was disoriented in her home, carried things from one place to another and hid them, sometimes she thought somebody was trying to kill her and started to cry loudly. [...] She is completely disoriented in time and space. Sometimes she says that she does not understand anything and that everything is strange to her. [...] Her memory is seriously impaired. If objects are shown to her, she names them correctly, but almost immediately afterwards she has forgotten everything. When reading a test, she skips from line to line or reads by spelling the words individually, or by making them meaningless through her pronunciation. In writing, she repeats separate syllables many times, omits others, and quickly breaks down completely. In speaking, she uses gap-fills and a few paraphrased expressions ("milk-pourer" instead of cup); sometimes it is obvious that she cannot go on. Plainly, she does not*

> *understand certain questions. She does no longer remember the use of some objects (Alzheimer et al., 1995).*

As time went by, she became completely demented and after four and half year of illness she died. Following her death, Alzheimer performed autopsy and found a dramatic shrinkage of her cerebral cortex. Further, using a newly-developed staining method, he found unexpected formations, today known as neurofibrillary tangles:

> *Inside of a cell which appears to be quite normal, one or several fibrils can be distinguished by their unique thickness and capacity for impregnation. Further examination shows many fibrils located next to each other which have been changed in the same way. Next, combined in thick bundles, they appear one by one at the surface of the cell. Finally, the nucleus and the cell itself disintegrate and only a tangle of fibrils indicates the place where a neuron was previously located (Alzheimer et al., 1995).*

In addition, he described what are nowadays known as senile plaques:

> *Distributed all over the cortex, but especially numerous in the upper layers, there are minute miliary foci which are caused by the deposition of a special substance in the cortex (Alzheimer et al., 1995).*

These histopathological findings are the hallmark of the disease and are currently the definitive indicators for a diagnosis of AD.

Alzheimer reported the case as an "*unusual* illness of the cerebral cortex". Actually, the symptomatology was anything but new, indeed, it was very common in elderly population and the pathology, known as senile dementia, was believed to be the naturally outcome of aging[7]. What made the Alzheimer's case *unusual* was the young age of the patient. The term Alzheimer's disease was reserved to dementia with an early onset till the end of XX century, when it was realized that senile dementia and Alzheimer's disease were indeed the same pathology.

PATHOGENESIS. The precise etiology of AD is currently unknown, however the microscopic neuropathological hallmark is the accumulation of two misfolded proteins: β-amyloid ($A\beta$) and hyperphosphorylated tau, generating the extracellular senile plaques and intracellular neurofibrillary tangles reported by Dr. Alzheimer. Such abnormalities result in oxidative and inflammatory damage, which in turn leads to energy failure and synaptic dysfunction (Querfurth and LaFerla, 2010).

[7] To enforce this belief was the common practice at the time to apply the laws of thermodynamics (especially the second law) to organic phenomena.

Senile plaques are mainly composed of $A\beta$ peptides, a natural product of metabolism composed of 36 to 43 amino acids. Monomers of $A\beta_{40}$ are much more prevalent than the aggregation-prone and damaging $A\beta_{42}$ species. β -amyloid peptides originate from proteolysis of a larger precursor protein (Amyloid Precursor Protein, APP) by the sequential enzymatic action of β-secretase and γ-secretase, whereas the APP proteolysis by α -secretase results in the nonamyloidogenic pathway. An imbalance between production and clearance causes Aβ to accumulate, and this excess may be the initiating factor in AD. This notion is mainly based on the observation that overexpression of APP, like in the Down's syndrome[8], often results in developing the illness.

$A\beta$ spontaneously self-aggregates into multiple coexisting physical forms, soluble oligomers (2 to 6 peptides), intermediate assemblies and insoluble fibers of advanced amyloid plaques. Soluble oligomers and intermediate amyloids are the most neurotoxic forms of Aβ. The severity of the cognitive defect in AD correlates with levels of oligomers in the brain, not the total Aβ burden (Lue et al., 1999).

Neurofibrillary tangles comprise mainly of the protein tau which binds microtubules, thereby facilitating the neuronal transport system. Uncoupling of tau from microtubules and aggregation into tangles inhibit transport and result in microtubule disassembly. The number of neurofibrillary tangles is a pathologic marker of the severity of AD. Like Aβ oligomers, intermediate aggregates of abnormal tau molecules are cytotoxic and impair cognition (Santacruz et al., 2005).

Mild Cognitive Impairment. Most people undergo a gradual cognitive decline over their life span, typically with regard to memory; the decline is usually minor, and although it may be a nuisance, it does not compromise the ability to function. A minority of people, perhaps 1 in 100, go through life with virtually no cognitive decline and are regarded as aging successfully. However, another trajectory of aging is characterized by a decline in cognitive function beyond that associated with typical aging; the decline is often recognized by those experiencing it and occasionally by those around them. Known as Mild Cognitive Impairment (MCI), this entity represents an intermediate state of cognitive function between the changes seen in aging and those fulfilling the criteria for dementia and often AD (Petersen, 2011).

The term MCI was initially used for describing individuals with a Global Deterioration Scale (Reisberg et al., 1982) rating of 3 (Flicker et al., 1991). Later, in 1997, Petersen

[8] APP is coded on chromosome 21, which is overexpressed in Down's syndrome.

et al. formalized precise criteria for the identification of those patients who falls in the gap between healthy aging individuals and those with dementia (Petersen et al., 1997). The criteria, now known as Petersen's MCI criteria, were as follows:

(a) subjective complaint of defective memory
(b) objective abnormal memory function for age
(c) normal activities of daily living
(d) normal general cognitive function
(e) individual does not fulfil criteria for dementia.

Petersen's criteria put a great emphasis on memory functionality; however, clinical practise has shown preclinical dementia cases with subtle complaints in other cognitive domains and virtually no memory impairment. To encompass the large spectrum of possible clinical MCI manifestations, the criteria have been revisited (Winblad et al., 2004):

(a) the person is neither normal nor demented
(b) there is evidence of cognitive deterioration shown by either objectively measured decline over time and/or subjective report of decline by self and/or informant in conjunction with objective cognitive deficits
(c) activities of daily living are preserved and complex instrumental functions are either intact or minimally impaired.

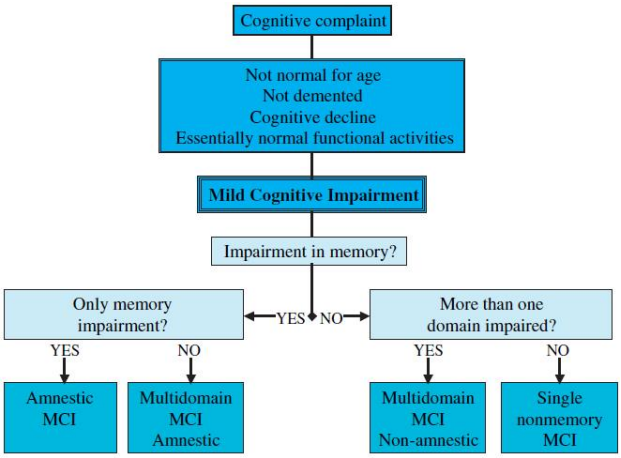

Figure 3.3 MCI classification scheme (Winblad et al., 2004)

Petersen's criteria are nowadays indicating of *amnestic*-MCI, otherwise, when there is no memory impairment, the syndrome is known as *nonamnestic* MCI. A further classification regards the number of cognitive domains affected, *single*- or *multiple*-domain (Figure 3.3).

Since, MCI is often a prodromal stage of several mental disorders, it is considered as a risk factor for developing dementia. The wide gamut of possible pathological targets for conversion reflects the heterogeneity in the clinical manifestation. Indeed, the nonamnestic MCI may be the forerunner of dementias that are not related to AD, such as frontotemporal lobar degeneration, dementia with Lewy bodies, primary progressive aphasia or vascular dementia, while multiple-domain MCI may be the forerunner of AD as well as vascular dementia. On the contrary, the etiology of the amnestic type seems to be more closely related to AD, so that it is considered as a risk factor for developing the disease. Indeed, in clinical trials involving amnestic MCI, more than 90% of those with progression to dementia had clinical signs of AD (Petersen, 2011); moreover, the conversion rate to AD has been estimated to be 14% per year compared to 1-2% in the general population (Petersen et al., 2001).

Relationship between FC and ALFF in dementia

FC and ALFF have been increasingly used to investigate the brain at rest, although the qualitative and quantitative relationship between them still needs to be fully understood. To the best of our knowledge, one single work examined systematically the relationship between FC and ALFF. Di and colleagues showed a widespread pattern of both positive and negative local correlations between network strength (i.e., ICA-based FC) and ALFF in a healthy elderly population (Di et al., 2013b). Moreover, ALFF values from a number of brain regions, such as the medial prefrontal cortex (mPFC), anterior cingulate cortex (ACC), precuneus, basal ganglia, thalamus and insula, were found to be correlated with FC in several independent resting-state networks. This latter evidence suggests that the coupling between FC and ALFF could be a global feature of the brain, which is relevant because the coupling between FC and ALFF likely depends on the way FC is defined. Indeed, while ALFF is a univariate measure univocally defined for each voxel, FC requires the definition of a relation (e.g. Pearson correlation) between features of different voxels or areas. Therefore, a global, voxel-wise measure of FC is perhaps the most appropriate to best match the nature of ALFF and to further investigate the properties of FC vs ALFF coupling.

In principle, temporal correlation should be independent from the amplitude of compared signals. However, the fact that several pathological states are characterized by partially co-localized changes in FC and ALFF suggests the existence of a specific relationship between them. For example, AD and MCI patients

show altered patterns of FC in specific DMN areas, i.e. posterior cingulate cortex (PCC)/precuneus, lateral temporal, parietal and medial frontal cortex, as well as hippocampus (Greicius et al., 2004, Wang et al., 2006, He et al., 2007, Sorg et al., 2007, Zhang et al., 2010, Gili et al., 2011). Similarly, widespread alterations of ALFF have been reported in AD (He et al., 2007, Wang et al., 2011, Xi et al., 2012) and MCI (Wang et al., 2011, Xi et al., 2013, Zhao et al., 2014) patients. Although a growing body of evidence exists to support impaired LFFs in dementias, there is no systematic study exploring the concomitant changes of FC and ALFF as an effect of neurodegeneration. Indeed, the observed FC reduction in dementia could be related to (i) a concomitant reduction of ALFF towards the noise level or (ii) a loss of synchronization between areas showing unaltered, or possibly increased, fluctuation amplitude.

Although the majority of resting state studies have focused on a relative wide range of frequency (e.g., 0.01-0.1Hz), converging evidence suggests that a finer band subdivision might provide some additional information. Zuo and colleagues, extending the Buzaski framework on neuronal oscillator classes (Buzsáki and Draguhn, 2004) to BOLD LFFs, divided the BOLD power spectrum into four distinct frequency ranges, namely slow-5 (0.01-0.027 Hz), slow-4 (0.027-0.073 Hz), slow-3 (0.073-0.198) and slow-2 (0.198-0.25 Hz) (Zuo et al., 2010). While slow-3 and slow-2 mainly reflect cardiac- and respiratory-related effects, slow-5 and slow-4 appear as stable parameters across scans (Zuo et al., 2010) with preferential spatial patterns of oscillation (Zuo et al., 2010, Baria et al., 2011). Moreover, frequency-dependent changes in ALFF have been reported in MCI (Han et al., 2011, Han et al., 2012) and in AD (Liu et al., 2014a) as well as in other neurological or psychiatric disorders, such as Parkinson's disease (Zhang et al., 2013) and schizophrenia (Yu et al., 2014). Frequency-specific patterns of BOLD fluctuations were also found to be associated with specific personality traits (Wei et al., 2014). In addition to ALFF, FC has also been characterized using a finer band analysis. Indeed, the topological properties of functional brain networks have shown frequency-dependent features, with slow-4 band displaying higher small-world metrics and test-retest reliability as compared to slow-5 (Liang et al., 2012). Band-subdivision has also significantly improved the MCI classification accuracy using graph-theory-based FC (Wee et al., 2012). The origin and the specific physiological function of each frequency band is presently still unknown. Yet, from the spectral properties of FC and ALFF taken separately, we hypothesize that the relationship between ALFF and FC could be frequency-dependent.

We sought to investigate the relationship between ALFF and global FC with a voxel-based approach in the healthy and diseased brain. The main aim of the experiment

was to assess whether the coupling between ALFF and FC depends on anatomical brain localization, frequency band, and pathological conditions. For this purpose, we performed rs-fMRI employing degenerative dementia as a pathological model, and enrolling patients with both AD and MCI. Assuming the existence of a connection between ALFF and the average FC in each voxel with the whole brain, we used a generalized linear model (GLM) to systematically assess to what extent the voxel-wise variance of FC across subjects is explained by the amplitude of the underlying oscillations.

Methods

SUBJECTS. Ten patients with a diagnosis of probable AD by NINCDS-ADRDA consensus criteria (McKhann et al., 1984), 10 amnestic MCI patients and 10 healthy elderly subjects (HC) were recruited for this study. A general cognitive evaluation was obtained using the Mini-Mental State Examination (MMSE).

Age, education and MMSE score distributions were compared among groups via one-way analysis of variance (ANOVA), while a chi-square test was applied to compare gender distribution. Where indicated, two-sample, two-tailed t-tests were performed as post-hoc analyses.

The study was approved by the ethics committee of Santa Lucia Foundation. Every recruited subject (or his/her responsible guardians if incapable) gave written consent before MR study initiation.

DATA ACQUISITION. Data were acquired on a 3T MRI system (Magnetom Allegra, Siemens, Erlangen, Germany). All subjects underwent a resting state fMRI scan using a echo planar imaging (EPI) sequence with the following parameters: TR = 2080 ms, TE = 30 ms, 32 axial slices parallel to AC-PC plane, matrix = 64 x 64, in plane resolution = 3x3 mm^2, slice thickness = 2.5 mm, 50% skip, flip angle = 70°. Resting scans lasted for 7 minutes and 20 seconds for a total of 220 volumes during which subjects were instructed to keep their eyes closed, to not think of anything in particular and to refrain from falling asleep. A T1-weighted three-dimensional modified driven equilibrium Fourier transform scan (MDEFT, Deichmann et al., 2004) was acquired for each subject for anatomical localization purposes and for grey matter (GM) volumetry; the parameters were as follows: TR = 1338 ms, TE = 2.4 ms, TI = 910 ms, flip angle = 15°,matrix = 256 x 224 x 176, FOV = 256 x 224 mm^2, slice thickness = 1 mm, total scan time = 12 min. Fluid attenuated inversion recovery (FLAIR) images (TR = 8170 ms, TE = 96 ms, TI = 2100 ms) were also acquired from all subjects to exclude the presence of remarkable signs suggestive for cerebro-vascular disease, as previously described (Serra et al., 2013).

DATA PREPROCESSING. Functional images were preprocessed using Connectivity toolbox (CONN: functional connectivity toolbox, Whitfield-Gabrieli and Nieto-Castanon, 2012). The first four volumes were discarded to allow signal and scanner stabilization. Images were slice-time corrected and realigned to the first image. For each subject, the mean EPI image, obtained from the realignment step, was used as source image to estimate the transformation parameters to match the functional images with the high resolution T1 volume. Then, all coregistered volumes were normalized into Montreal Neurological Institute (MNI) space coordinates (voxel size: 2x2x2 mm^3). Normalized images were then smoothed using an 8x8x8 mm^3 full width at half maximum (FWHM) Gaussian kernel.

Before statistical analyses, data from each subject underwent physiological noise mitigation. The six parameters of realignment and the first five eigenvectors of the PCA decomposition of the EPI time course averaged over cerebrospinal fluid (CSF) and white matter (WM) were regressed out, following aCompCor approach for physiological noise removal (Behzadi et al., 2007). Data were then entered in the EASYREST pipeline for detrending, filtering and for the computation of FC and ALFF measures. Three different frequency ranges were selected: 1) full-band: 0.01-0.073 Hz. 2) Slow-5: 0.01-0.027 Hz. 3) Slow-4: 0.027-0.073 Hz (Zuo et al., 2010).

GREY MATTER VOLUMETRY. The T1-weighted MDEFT images were processed using the VBM protocol (Ashburner and Friston, 2005) implemented in SPM8 (http://www.fil.ion.ucl.ac.uk/spm/), which consists of an iterative combination of segmentations and normalizations to produce a GM probability map (Ashburner and Friston, 2005) in MNI standard space for every subject. In order to compensate for compression or expansion which might occur during warping of images to match the template, GM maps were "modulated" by multiplying the intensity of each voxel in the final images by the Jacobian determinant of the transformation, corresponding to its relative volume before and after warping (Ashburner and Friston, 2001). All data were then smoothed using a 12x12x12 mm^3 FWHM Gaussian kernel, and finally the GM volume (GMV) was computed by summing the relevant modulated partition, multiplied by the voxel volume.

FUNCTIONAL CONNECTIVITY. As voxel-wise connectivity we adopted the $wGBC$ metric, equation (2.12), implemented in EASYREST. Briefly, Pearson correlation coefficients between each voxel and all other voxels of the brain were computed; then, after a z-Fisher transformation, these coefficients were averaged. The mean value thus obtained expresses the strength of connectivity between each voxel and the rest of the brain (i.e., a measure of global connectivity). Map of global connectivity were produced for each of the three frequency ranges.

Voxel-wise based FC computation is less sensitive than FC obtained by using a seed-based approach, which has been adopted among the others by Di and colleagues (Di et al., 2013b). Nonetheless, the former computation has a higher intrinsic spatial resolution, and it is independent from the arbitrary choice of ROIs. Thus, we adopted a voxel-wise computation of FC as it is closer to the nature of ALFF, being inherently able to map the average value of FC in each single voxel.

ALFF. For each voxel in the brain the filtered time series (0.01-0.073 Hz) was transformed into the frequency domain using a Fast Fourier Transform (FFT) algorithm. The obtained power spectral density was square rooted and averaged in the three frequency bands of interest: full-band, Slow-5 and Slow-4. ALFF maps of each subject were transformed into z-scores (Zuo et al., 2010). The computation was performed with EASYREST.

STATISTICAL ANALYSIS. For each subject group, the mean effects of ALFF and FC were assessed via one-sample, two-tailed t-tests ($p < 0.05$ corrected for multiple comparisons; see below). Distribution of abnormal ALFF and FC values across groups were evaluated via one-way ANOVA ($p < 0.05$, corr.).

Z-transformed correlation and ALFF maps from each subject were entered in a second level analysis to assess whether the amplitude of oscillations affects the correlation strength. GLM was applied voxel-wise, considering the FC and ALFF z-scores as dependent and independent variables respectively. Age, gender, education and GM volume were standardized and entered in the model as nuisance covariates. The statistical significance of the regression FC vs ALFF was assessed in each group by one sample, two-tailed t-tests. Within the areas where the regression returned significant coupling in HC, group differences in the strength of correlation were assessed between all experimental groups (i.e., HC, AD and MCI patients) by two-sample, two-tailed t-tests. Model estimation and t-contrasts were replicated for each frequency range. The calculation was carried out with custom software implemented in Matlab R2012a (The Mathworks Inc, Natick, Massachusetts, USA).

Statistical threshold was set to $p < 0.05$ after correction for multiple comparison, performed by Monte Carlo simulations (AlphaSim; AFNI package, Cox, 1996). The corrected threshold of $p < 0.05$ corresponds to a single voxel threshold of $p < 0.005$ with a minimum cluster size of 157 voxels for whole-brain inference. For mask based inferences the minimum cluster size was set around 40 voxels, depending on the mask size.

Results

Principal demographic, clinical data and GMV estimation are reported in Table 3.1. Patients and controls were matched for age (ANOVA, f = 1.5, p > 0.2) and gender (chi-square test: x2 = 1.9, p > 0.3), although patients were less educated than controls (t-tests: AD vs HC, t = -4.0, p < 0.001; MCI vs HC, t = -2.3, p < 0.05). As expected, MMSE scores were significantly different between all groups (t-tests: AD vs HC, t = -6.5, p < 0.001; MCI vs HC, t = -4.6, p < 0.001; MCI vs AD: t = 3.1 p < 0.05). AD patients showed a significant reduction of GMV when compared to both HC and MCI patients (t-tests: AD vs HC, t = -3.9, p < 0.001; AD vs MCI, t = -3.6, p < 0.05). Conversely, despite the presence of a reduction trend in GMV, volumes were not significantly different between MCI patients and HC (t-test: MCI vs HC, t = -1.4, p > 0.1).

Table 3.1 Principal characteristics of studied subjects

	AD	MCI	HC	P-value
N	10	10	10	
Gender (M/F)	4/6	6/4	7/3	0.387[a]
Age (years)	72.3 ± 8.3	70.7 ± 7.1	66.0 ± 9.6	0.235[b]
Education (years)	8.6 ± 3.6**	11.1 ± 3.5*	14.5 ± 3.0	0.002[b]
MMSE score	21.5 ± 3.7**†	25.8 ± 2.3**	29.30 ± 0.67	<0.001[b]
Grey matter volume (dl)	5.20 ± 0.51**†	6.10 ± 0.61	6.6 ± 1.0	<0.001[b]

Data presented as mean ± SD. AD and MCI data were tested against HC data (two-sample two-tailed t-test; * p < 0.05; ** p < 0.001); as well as against each other († p < 0.05). AD, Alzheimer's disease; MCI, mild cognitive impairment; HC, healthy control; MMSE, Mini mental State Examination.
[a] The p-value was obtained by chi-square test.
[b] The p-value was obtained by one-way ANOVA test.

FC and ALFF maps in the full-band range are shown for each studied group in Figure 3.4. Voxel-wise FC analysis reproduced patterns of connectivity in agreement with those reported by others using similar measures of global FC (Buckner et al., 2009, Cole et al., 2010). In particular, our results showed strongly connected regions belonging to the DMN, such as the precuneus/PCC, mPFC/ ventral ACC, and the inferior temporal/parietal cortex. These patterns are more overtly appreciated using a higher statistical threshold (Figure 3.5). No negative FC was found in any of the studied groups. Similarly to FC, high ALFF values were found in the GM, primarily in the precuneus/PCC and in the mPFC.

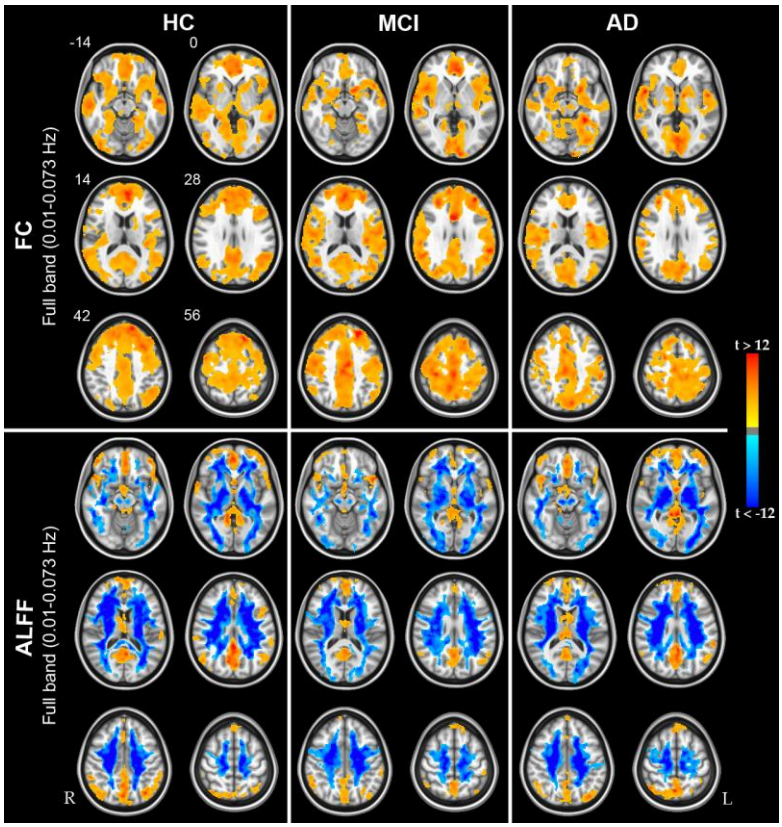

Figure 3.4 Functional connectivity and amplitude of low frequency fluctuations group results. Group-level t-statistic maps showing significantly detectable FC (upper panel) and ALFF (lower panel) in the full-band frequency range. The three groups of subjects, HC, MCI and AD patients, are reported from left to right. Hot and cold colors encode for positive and negative group effect, respectively. Results were obtained via one-sample, two-tailed, t-tests ($|t| > 3.7$; $p<0.05$, corrected). Of note, despite it is expected to find negative ALFF values in white matter (Zuo et al., 2010), this effect was striking in our results and it is primarily caused by the CompCor approach for noise mitigation (Behzadi et al., 2007). The numbers next to the images refers to z coordinates in the MNI space. R, right; L, left.

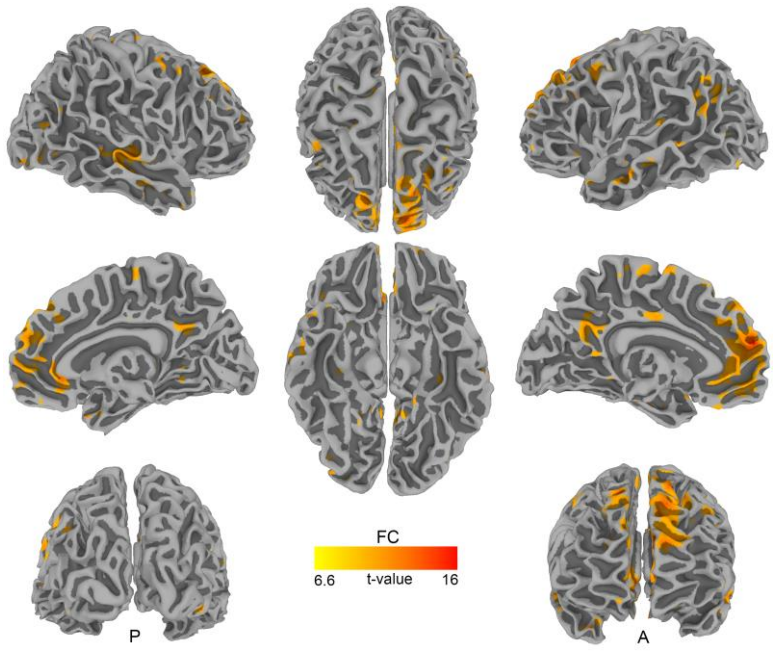

Figure 3.5 Functional connectivity of HC at high threshold level. Group-level t-statistic map showing significant FC on HC in the full-band frequency range. Map result is the same reported in Figure 3.4, but here is showed at higher threshold level (one sample t-test: $t > 6.59$, $p < 5*10\text{-}5$) for easier identification of most globally connected regions.

Group averages of FC z-score in the GM (Figure 3.6, A) showed a significantly reduced connectivity in both AD and MCI patients compared to HC (two-sample, two-tailed t-tests: HC vs AD, $t = 2.8$, $p < 0.05$; HC vs MCI, $t = 2.2$, $p < 0.05$; MCI vs AD, $t = 1.0$, $p > 0.3$). On the contrary, group averages of ALFF z-scores in the GM mask (Figure 3.6, B) revealed no significant differences among groups (one-way ANOVA test: $f = 0.04$, $p > 0.9$). Voxel-wise one-way ANOVA and relative post-hoc analyses of FC and ALFF corroborated these whole-brain trends among groups (Figure 3.7).

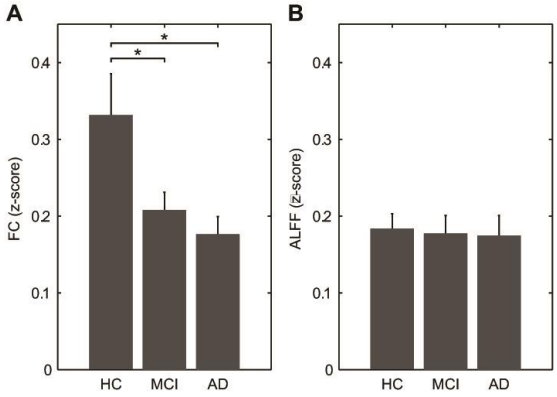

Figure 3.6 Average grey matter functional connectivity and amplitude of low frequency fluctuations. Both measures were extracted from a common grey matter mask. This mask was obtained averaging grey matter probability maps (from the segmentation step) across all subjects and thresholding the resulting map at 0.75. A) Group average FC z-score. Diseased groups show significant reduction compared to HC. B) Group average ALFF z-score. No significant difference among groups were found. In particular, MCI and AD are indistinguishable from healthy subjects ($p > 0.8$ and $p > 0.7$, respectively). * $p < 0.05$ (two-sample, two-tailed *t*-test).

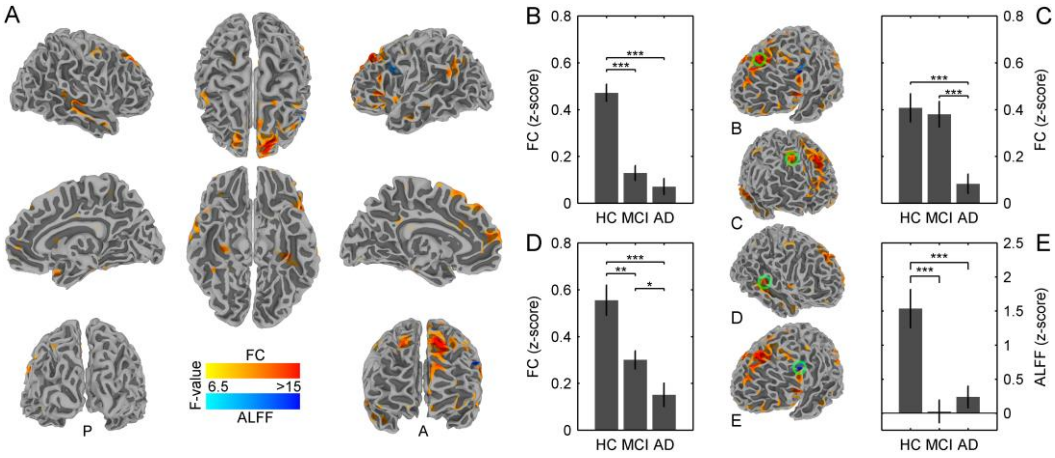

Figure 3.7 Pathology-induced changes in functional connectivity and in amplitude of low frequency fluctuations. (A) f-statistic maps showing significant detectable changes of FC (hot colors) and ALFF values (cold colors) among the three groups of subjects (HC, MCI and AD). Of note, only one lateralized frontal region showed a significant change in ALFF among groups. Results were obtained via one-way ANOVA, separately accomplished for FC and ALFF data. The statistical threshold was set at $f > 6.48$ ($p < 0.05$, corrected). (B-E) Post-hoc analyses of the most relevant clusters belonging to FC (B-D) and ALFF (E) changes. For each cluster, group comparisons were performed via two-sample, two-tailed t-tests on the voxel showing the local maximum of f-values. *, $p < 0.05$; **, $p < 0.01$; ***, $p < 0.001$; A, anterior; P, posterior.

Having confirmed previous results on the overall spatial distribution of FC and ALFF in healthy controls and patients, we next examined the results of the linear regression between FC and ALFF within each group.

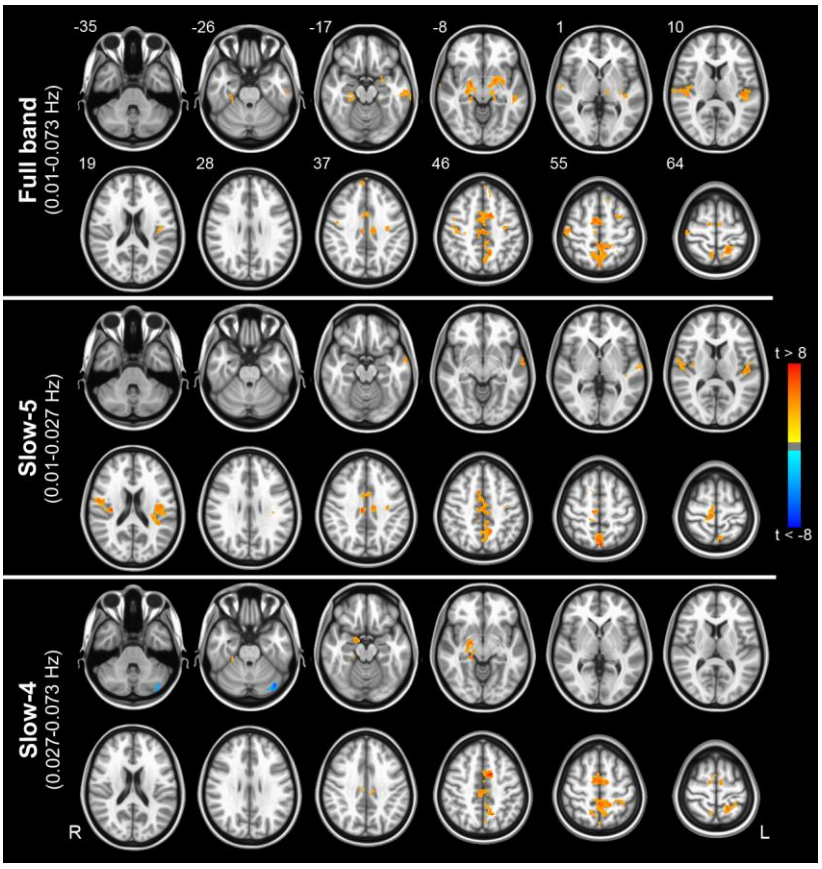

Figure 3.8 Voxel-wise correlation between functional connectivity and amplitude of low frequency fluctuations in the healthy brain. Color-coded t-statistic maps showing significantly detectable correlation between FC and ALFF for the full-band (upper panel), slow-5 (middle panel) and slow-4 (bottom panel) frequency range, considering only the HC group. Hot and cold colors encode for positive and negative correlations, respectively. Results were obtained via a t-contrast (HC > 0) in the "FC vs. ALFF" model ($|t| > 3.2$; $p < 0.05$, corrected). The numbers next to the images refer to z coordinates in the MNI space. R, right; L, left.

Brain regions in which the correlation strength was significantly explained by the amplitude of oscillations in HC are shown in Figure 3.8 for each considered frequency band. For the full-band range, these areas included the cingulate cortex and precuneus, the superior temporal cortex/insula, the medial frontal cortex, the thalamus, the lentiform nucleus and the parahippocampal cortex (Figure 3.8, top). Common patterns for the slow-5 and slow-4 bands (Figure 3.8, middle and bottom, respectively) were found in the cingulate cortex and precuneus. The slow-5 band showed also additional FC vs ALFF correlation patterns in the superior temporal cortex/insula, while the slow-4 band showed some lateralized (right) subcortical effect (thalamus, lentiform nucleus). All the regions reported above showed a positive relationship between FC and ALFF. One region only, located in left cerebellum, showed a negative association between FC and ALFF, which was isolated to the slow-4 band. However, since the cerebellum barely fell in the bottom

edge of EPI field, the area showed a lower signal to noise ratio and suboptimal normalization when compared to the cerebrum. Therefore, this negative correlation is likely due to artifacts. Remarkably, in contrast to HC, neither AD nor MCI did show any area with significant regression between FC and ALFF ($p > 0.05$ cor.).

We then investigated the specific effect of disease in those areas showing significant FC vs ALFF correlation in healthy subjects (i.e., between-group comparisons in areas shown in Figure 3.8). This analysis demonstrated the local effect of disease on the strength of the FC vs ALFF coupling (Figure 3.9 left, AD patients; Figure 3.9 right, MCI patients). Specific cluster locations resulting from t-test HC vs AD and HC vs MCI are reported in Table 3.2 and Table 3.3, respectively. No significant patterns resulted from the comparison of AD vs MCI ($p > 0.05$ cor.).

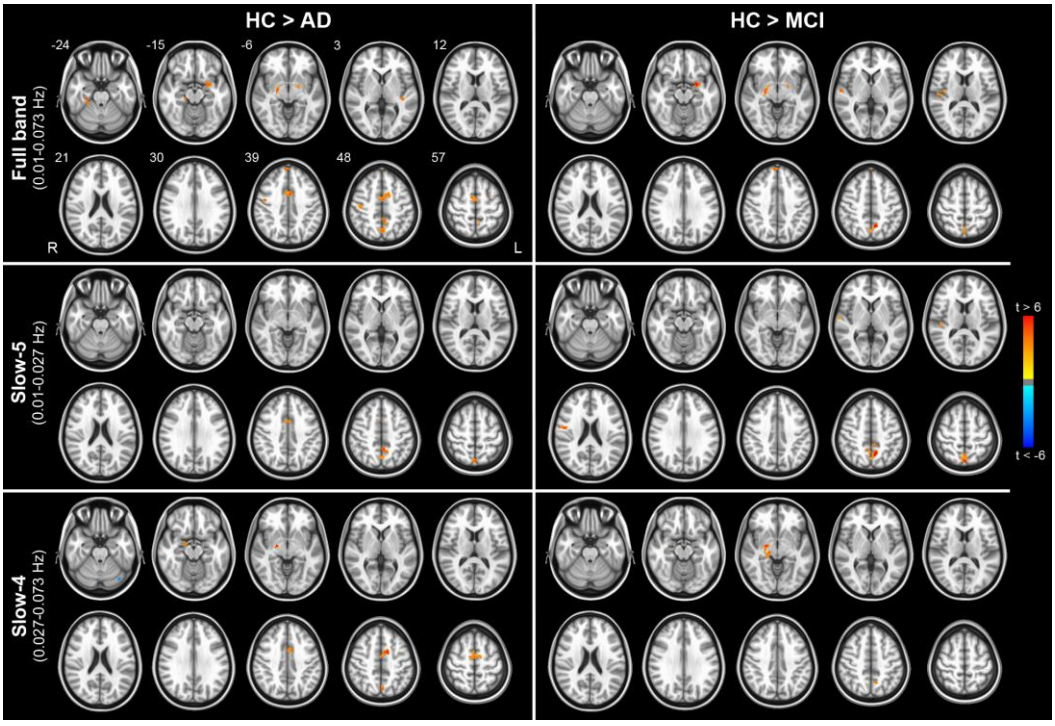

Figure 3.9 Pathology-induced changes in the coupling between functional connectivity and the amplitude of low frequency fluctuations. Color-coded t-statistic maps showing significantly detectable changes in the correlation between FC and ALFF comparing HC to AD patients (left) and MCI patients (right). Comparing AD to MCI lead no significant cluster. Tests were separately carried out for the full-band (upper panel), slow-5 (middle panel) and slow-4 (bottom panel) frequency range. Only the brain areas in which was found a statistically significant relationship in HC were considered in these tests (i.e., t-maps masked with patterns in Figure 3.8). Results were obtained via t-contrasts (HC > AD and HC > MCI) in the "FC vs ALFF" model ($|t| > 2.8$; $p < 0.05$, corrected). Hot and cold colors encode for HC > AD/MCI and HC < AD/MCI, respectively. For the details of the involved regions, see Table 3.2 and Table 3.3. The numbers next to the images refer to z coordinates in the MNI space. R, right; L, left.

To assess the origin of the reduced correlation between FC and ALFF, their values were averaged over each of the ROIs reported in Table 3.2 and Table 3.3. We found several ROIs showing a significant reduction of FC in patients as compared to HC; on the contrary, no ROIs showed either a significant reduction in ALFF or any other clear trend (Figure 3.10). Finally, according to their location the voxels included in all the ROIs were classified as cortical or subcortical, and ALFF and FC values were averaged subject by subject in these two macro-areas. In both macro-areas, and for the full-band frequency range, there was a disruption of the correlation between FC and ALFF in AD compared to HC (Figure 3.11, left plots). In both, cortical (Figure 3.11 A) and subcortical (Figure 3.11 B) regions, a significant reduction in FC, but not in ALFF, was proportional to the drop in correlation between these two measures. All other tests (i.e., in other frequency bands and including the MCI group) showed a similar trend towards reduction of FC, although they did not reach the full statistical significance.

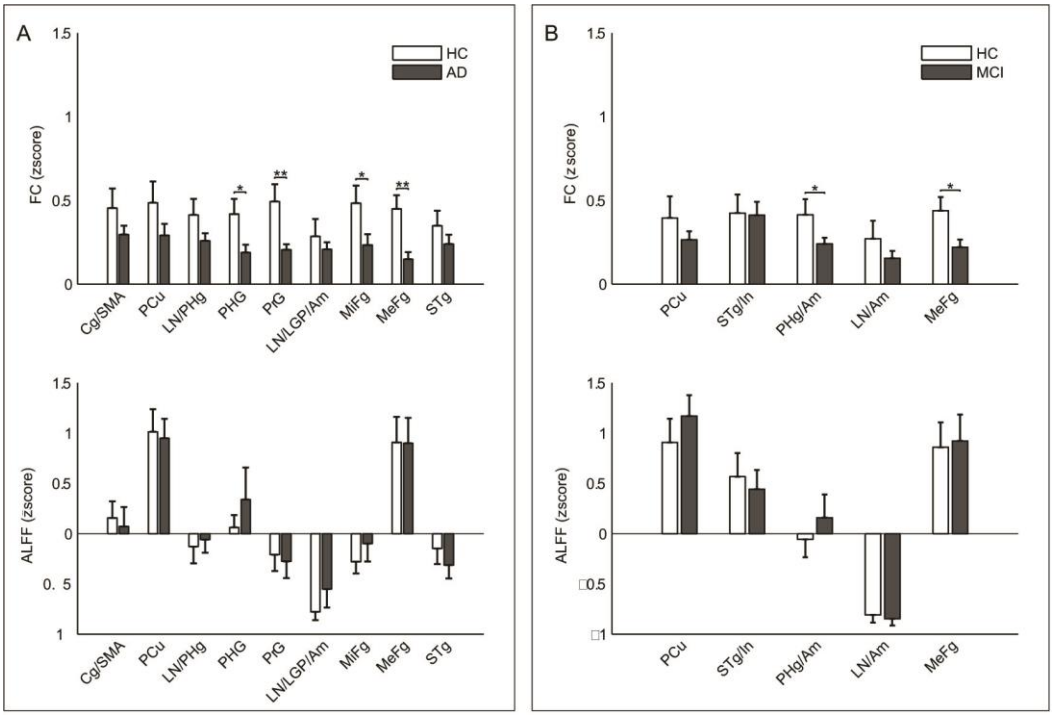

Figure 3.10 FC and ALFF mean values in brain regions showing pathology-induced FC-ALFF uncoupling. FC and ALFF values were averaged in the significant clusters resulting from t-contrasts HC vs AD (A) and HC vs MCI (B) both computed in the FC vs ALFF full-band model (see Figure 3.9). For the details of the regions, see Table 3.2 and Table 3.3. *, $p < 0.05$; **, $p < 0.01$ (two-sample, one-tailed t-test); Cg, cingulate gyrus; SMA, supplementary motor area; PCu, precuneus; LN, lentiform nucleus; PHg, parahippocampal gyrus; PrG, precentral gyrus; LGP, lateral globus pallidus; Am, amygdala; MiFg, middle frontal gyrus; MeFg, medial frontal gyrus; STg, superior temporal gyrus; In, Insula.

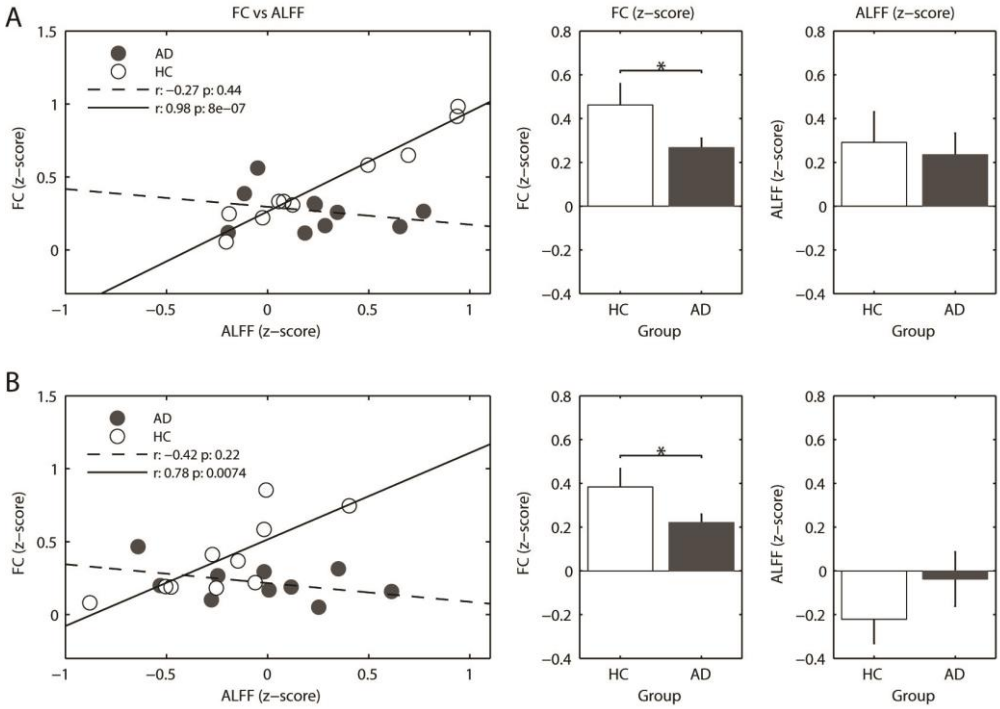

Figure 3.11 Trend of functional connectivity vs amplitude of low frequency fluctuations along with respective averaged values. FC and ALFF values were averaged in the significant clusters resulting from t-contrast HC vs AD in the full-band analysis (i.e., Figure 3.9, top row, left column). The significant clusters were grouped in cortical (A) and subcortical (B) regions. For the details of the regions, see Table 3.2. * $p < 0.05$ (two-sample, one-tailed t-test).

Table 3.2 Regional differences in the FC vs ALFF coupling comparing HC to AD

Frequency range	Brain Region	Side	Vol (voxels)	MNI coordinates			Peak t-value
				x	y	z	
Full-band	Cingulate gyrus / Supplementary motor area	B	360	0	-6	52	5.97
	Precuneus	B	171	-2	-46	50	5.38
	Lentiform Nucleus/ Parahippocampal gyrus	L	113	-20	0	-10	5.26
	Parahippocampal gyrus	R	106	30	-28	-20	5.71
	Precentral Gyrus	R	96	46	-8	42	5.66
	Lentiform Nucleus/Lateral Globus Pallidus / Amygdala	R	73	20	-6	-8	6.80
	Middle Frontal Gyrus	L	66	-32	6	54	6.79
	Medial Frontal Gyrus	B	50	4	54	42	5.33
	Superior Temporal Gyrus	L	47	-40	-28	2	4.79
Slow-5	Precuneus	B	93	-4	-46	48	5.73
	Precuneus	B	92	0	-70	58	4.85
	Precentral Gyrus	R	86	16	-38	70	4.83
	Cingulate gyrus	B	75	8	10	46	6.31
Slow-4	Cingulate gyrus / Supplementary motor area	B	424	-10	4	46	8.27
	Globus pallidus / Amygdala	R	92	22	-10	-6	7.96
	Cerebellum	L	85	-42	-72	-30	-5.89
	Precuneus	B	85	-2	-70	48	5.04

Regions showing significant pathology-induced (Alzheimer's disease) changes in the coupling between functional connectivity and the amplitude of low-frequency fluctuations (t-test: HC > AD). B, bilateral; L, left; R, right.

Table 3.3 Regional differences in the FC vs ALFF coupling comparing HC to MCI

Frequency range	Brain Region	Side	Vol (voxels)	MNI coordinates			Peak t-value
				x	y	z	
Full-band	Precuneus	B	278	-8	-54	50	7.37
	Superior Temporal Gyrus / Insula	R	139	44	-26	8	5.77
	Parahippocampal gyrus / Amygdala	L	99	-22	2	-12	7.49
	Lentiform Nucleus / Amygdala	R	99	20	-8	-10	5.77
	Medial Frontal Gyrus	R	46	4	54	42	5.70
Slow-5	Precuneus	B	375	-8	-56	48	6.89
	Insula / Precentral Gyrus	R	66	46	-2	18	5.89
	Superior Temporal Gyrus	R	54	64	-12	6	4.89
	Cingulate gyrus	L	45	-4	-40	42	4.97
	Postcentral Gyrus / Insula	R	41	50	-22	18	4.74
Slow-4	Globus Pallidus / Amygdala / Hippocampus	R	164	22	-10	-6	7.99
	Cerebellum (Declive)	L	69	-42	-72	-30	-6.29
	Precuneus	L	65	-12	-58	46	5.87
	Precuneus	R	62	6	-66	50	4.76

Regions showing significant pathology-induced (mild cognitive impairment) changes in the coupling between functional connectivity and the amplitude of low-frequency fluctuations (t-test: HC > MCI). B, bilateral; L, left; R, right.

Discussion

FC vs ALFF in healthy population. In this study we revealed specific spatial and frequency-dependent patterns of positive regression coefficients between global FC and ALFF in healthy subjects (Figure 3.8). Involved regions can be assembled in three main groups, namely temporal, parietal and subcortical areas. Results demonstrated that these brain areas are characterized by voxels whose levels of oscillation amplitude are directly associated to the strength of their global connection. Interestingly, many of these areas are known to belong to the most globally connected regions of the brain. For example, the cingulate cortex belongs to the DMN, which is characterized by a high degree of functional (Cole et al., 2010) and anatomical (Hagmann et al., 2008) connections. Similarly, the insula, thalamus and basal ganglia are implicated in several long range connections (Di Martino et al., 2008, Cole et al., 2010, Cauda et al., 2011). These results suggest therefore that highly connected regions in the brain are also regions whose connectivity is more sensitive to variations of the underlying fluctuation amplitude.

Our results in the full frequency band are broadly consistent with those obtained by Di and colleagues, even though we did not find any negative correlation pattern (with the exception of the cerebellum, as discussed in the results section) (Di et al., 2013b). However, while Di and colleagues adopted the ICA and seed-based analysis to compute FC, we privileged a voxel-wise global measure of connectivity which is independent from a specific network decided a priori. This means that FC can be directly and unequivocally compared with ALFF in each voxel. Accordingly, our results demonstrate that FC vs ALFF coupling is network independent and may be regarded as global characteristic of each single voxel.

The separation of LFFs in two distinct frequency ranges (slow-5 and slow-4) demonstrated that the relationship between ALFF and FC is sensitive to the frequency range, and specific patterns of correlation could be identified for slow-5 and slow-4 bands. Although the full-band analysis returned essentially the same areas highlighted by the sub-band analysis, the slow-5 band was clearly more sensitive for couplings in temporal lobe regions. Moreover, slow-5 primarily identified cortical regions, while slow-4 included both cortical and subcortical regions. These results are in agreement with recent studies, which reported that the fluctuations at the higher bound of LFFs are mainly localized in subcortical areas (Zuo et al., 2010, Baria et al., 2011). The different patterns are likely due to the different oscillatory mechanisms underlying these two frequency bands. Previous works suggested that the limited speed of signal propagation, primarily due to synaptic delay and axonal conduction, along with physical constraints (i.e., the size) of the engaged neuronal

network may account for the different periods of oscillation. Under this assumption, large neuronal assemblies may result in a larger period of electrophysiological oscillation if compared to small neuronal space (Penttonen and Buzsáki, 2003, Buzsáki and Draguhn, 2004). Thus, according to this view the relative large size of cortical as compared to subcortical structures might explain the different patterns observed at different bands. Alternatively, the different coupling in slow-4 and slow-5 bands could arise from different synaptic, functional or cytoarchitectonic features of the different areas (Baria et al., 2011, Song et al., 2014). Nonetheless, it still remains largely unclear how the BOLD signal depends on the spontaneous neuronal activity observed at different spatiotemporal scales. Moreover, the frequency window of BOLD signal for the slow-5 and slow-4 components is seemingly too narrow for discriminating between different frequency/size features of neuronal assemblies.

A higher fluctuation amplitude in slow-4 as compared to slow-5 has been observed with a symmetrical pattern in the basal ganglia (Zuo et al., 2010). In contrast, we found here a lateralization of the FC vs ALFF coupling in slow-4 band of subcortical areas. Since the coupling in those regions was symmetrically preserved in the full-band analysis, slow-4 lateralization pattern might be due to a suboptimal spectral division (Song et al., 2014). Indeed, the use of poorer information (nearly half of the spectrum) as well as the higher amount of noise which is present at lower frequencies, may result in a reduced statistical power.

Both the spatial specificity and the frequency dependence of the coupling between FC and ALFF suggest that the latter measure plays an active role in the generation of synchronization patterns and it is not a simple prerequisite for the emergence of FC. Indeed, the amplitude of BOLD low frequency fluctuations is of physiological relevance, as indicated by many works reporting a coupling between electrophysiological signals and spontaneous BOLD LFFs (Laufs et al., 2003, Scheeringa et al., 2008, Schölvinck et al., 2010, Hiltunen et al., 2014). ALFF was also found to be linearly related to the metabolic consumption of glucose (Tomasi et al., 2013). Moreover, the reduction of low-frequency EEG power from childhood to adulthood, a well-known feature of brain maturation, is accompanied by concurrent reductions in spontaneous BOLD power (Lüchinger et al., 2012). Spontaneous BOLD fluctuations were also reported to account for inter-trial variability in behavior (Fox et al., 2007) and to be more capable than FC in discriminating between different resting conditions (e.g., eyes-open vs eyes-closed) (Yan et al., 2009). This evidence suggests that the magnitude of fluctuations provides information on the neuronal workload of the underlying brain area. In this context, the FC vs ALFF correlation

pattern we reported here is likely to have a physiological meaning, by expressing local neuronal activity and local strength of global connectivity together.

On the other hand, a non-neuronal origin of the FC vs ALFF pattern cannot be excluded a priori. In principle, a common source of physiological noise could also account for their positive correlation pattern. Cardiac and respiratory fluctuations, spontaneous oscillation in carbon dioxide, and many other physiological phenomena have been identified or proposed as source of BOLD fluctuations (Wise et al., 2004, Birn et al., 2006, Birn et al., 2008, Chang et al., 2009, DiNuzzo et al., 2011, Murphy et al., 2013). For example, ALFF has been shown to correlate with BOLD response in breath holding (BH) task, suggesting that the spectral amplitude of LFFs might be used to scale task-related BOLD signal to account for variability in vascular reactivity (Biswal et al., 2007, Di et al., 2013a). However, previously reported regions of high correlation between ALFF and BH-BOLD response (e.g., cerebellum, midbrain, inferior occipital gyrus, PCC and precuneus) are only minimally overlapped to the correlation pattern that we observed in the current work. This suggests phenomena like vascular reactivity may have only marginally contributed to our results (Di et al., 2013a).

FC vs ALFF in Degenerative Dementia. The comparison between patients and healthy controls revealed a widespread reduction of the FC vs ALFF coupling, at all frequency bands and in both patient groups, AD and MCI (Figure 3.9). Additionally, such a disruption of correlation patterns was primarily due to a reduction in FC, i.e. loss of fluctuation synchronization rather than to a change in ALFF, in both cortical and subcortical areas (Figure 3.11).

Different works have reported decreased FC in AD and MCI patients with both seed-based and data driven-analyses (Auer, 2008), especially in the hippocampus, PCC and ACC (Gili et al., 2011). These findings are consistent with the reduction trend across groups we reported here in the average GM FC (Figure 3.6, A), as well as shown in voxel-level analysis (Figure 3.7). Conversely, we did not observe any significant trend of ALFF values either in the GM (Figure 3.6, B) or in the voxel-level analysis (Figure S2), except for a small lateralized frontal region with reduced ALFF in both AD and MCI patients. Several works have reported a heterogeneous set of brain regions with abnormal, either increased or decreased, ALFF values in dementia (Han et al., 2011, Wang et al., 2011, Xi et al., 2012, Zhao et al., 2014), which may reflect the progression of the pathology (Liang et al., 2014). Altogether, our and other results support the existence of a complex relationship between AD pathology, neuronal excitability and the underlying vascular and metabolic variables, possibly in a region-dependent manner (Putcha et al., 2011, and references therein).

We observed that the normal pattern of correlations between FC and ALFF (Figure 3.8) is disrupted in patients with MCI and AD. Strikingly, in those regions where the correlation FC vs ALFF is altered in patients compared to controls, this phenomenon is related to a loss of synchrony of the oscillations in the presence of preserved oscillation amplitude (Figure 3.11). This finding indicates that changes of ALFF and FC induced by pathology are partially disentangled, possibly reflecting distinct pathophysiological phenomena. Moreover, our results suggest that the dementia-related changes primarily affect the synchronization of LFFs rather than the oscillation amplitude.

The anatomical pattern of significant FC vs ALFF coupling observed in HC was found to be disrupted as an effect of AD pathology, as shown by group comparisons. Moreover, when considering the overall FC vs ALFF uncoupling, such a disruption was already detectable at the stage of MCI, indicating such a parameter to be sensitive to early pathophysiological aspects of the disease. Further studies on larger populations are needed to clarify the potential diagnostic value of this biomarker. It is possible that the involved regions could have a key role for the maintenance of the ongoing activity (as it is suggested by their partially overlap with the DMN). In the pathological brain, these key regions could be forced to maintain a normal level of activity that, due to the disease, does not produce a comparable degree of synchronization with other brain regions.

CONCLUSION. We revealed that ALFF is linearly related to FC in spatially segregated patterns that are consistent in a healthy elderly population. This relationship is dependent on the specific range of frequencies within the low-frequency band explored in FC studies. The relationship between FC and ALFF is disrupted in AD as well as MCI, in all the studied frequency bands. According to our findings, this is likely due to a loss of fluctuation synchrony among the involved brain areas rather than to altered local activity.

To conclude, this study suggests that the correlation patterns between ALFF and FC have a neurophysiological correlate, but that ALFF and FC convey partially distinct information, especially as far as the development of changes induced by pathology is involved.

FC alterations underpinning language dysfunction in AD

Among the results reported in the previous study there is also evidence that AD is primarily a disconnection syndrome. This is particularly noticeable by comparing the pathology-induced changes in FC with those of ALFF (Figure 3.6 and Figure 3.7). This is even more relevant considering that results were obtained with a voxel-wise based FC metric (i.e., wGBC), which is intrinsically less sensitive than the more common seed-based FC.

Consistently with the notion of a disconnection syndrome, aberrant FC patterns in specific networks might highlight corresponding cognitive impairments, elucidating both the origin of specific deficits and possibly how the disease spreads into the brain. In this section we will study the FC alterations underpinning language impairment in AD, a well-documented deficit reported early in the course of the illness.

Language dysfunction in AD

As in the original Alzheimer's case of study, language dysfunctions are commonly observed in AD (Cummings et al., 1985, Kempler, 1995, Taler and Phillips, 2008). The typical pattern of language deterioration can be roughly divided in three phases, accordingly to the development of the illness (Figure 3.12).

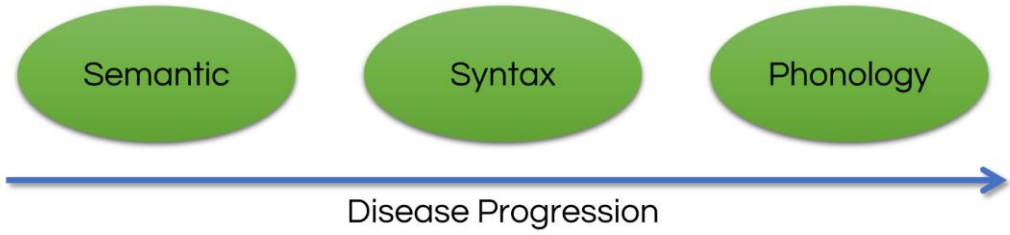

Figure 3.12. Pattern of language deterioration during the course of the pathology.

Early on semantics are affected; word-finding difficulty (anomia) is the most common and evident symptom. The deficit is noticeable both in standardized language tasks (Henry et al., 2004) and in spontaneous conversation (Nicholas et al., 1985). The use of semantically empty words (such as "thing" for a tool, or "animal" for a specific species) makes the speech fluent but sacrifices informational content. Language comprehension and knowledge of the meaning of the word is generally preserved at least for single words, while for complex abstract sentences, irony,

metaphor and other complex language aspects is poor (Critchley, 1984, Kempler et al., 1988). Language functionality in this stage of the disease is sufficient for most social situations, although patients may not be able to follow complex conversations and may tend to digress or repeat themselves (Kempler, 1995).

As disease progress, the word-finding deficit worsens and the utterances become hardly comprehensible due to frequent paraphasias and pragmatic deficits, such as topic maintenance and poor use of pronouns (Appell et al., 1982). Despite these pronounced discourse deficits, the mechanism of speech, such phoneme production, repetition and reading aloud are preserved. Language comprehension is also affected, both in auditory-spoken language and in reading. Meaningful communication is greatly reduced and patients may withdraw slightly from social situations in which communication demands may occur (Kempler, 1995).

In the latest stage of AD, even articulation begins to fail and the lexicon appears composed of only few words of biological needs (Bayles et al., 2000). At this point, comprehension is impaired in all modalities, even for single words, and the patients are no longer successfully participating in social interactions through language or any other communicative modality (Kempler, 1995).

This pattern of language deterioration during the course of AD progression is surprisingly quite specific: in linguistic terms, semantic fail first, then syntax, and, finally, phonology (Kirshner, 2012). Excluding the very latest stage of AD in which patients could resemble global aphasia, some facets of language are surprisingly unaffected. Indeed, there are no articulation problems and patients can repeat fluently; there are no reports of agrammatism, as that usually seen in Broca's aphasia, as well as phonological disturbance. For example, patients do not violate the phonotactic constraints of their native language nor make prosodic errors (Kempler, 1995). This picture of language deficits suggests that, while the late-stage linguistic deficit are probably the result of the spread of the disease in virtually all cognitive area, the early semantic deficits could reflect a *focal* deterioration rather than a simple overall decline. Such view is further supported by evidence that these deficits appear several years before clinical diagnosis (Auriacombe et al., 2006, Mickes et al., 2007, Taler and Phillips, 2008, Clark et al., 2009). For this reason, we will focus our attention on the earliest symptom, the word-finding difficulty.

The Origin of the Word Finding Difficulty. Choosing the most context-appropriate word is a complex task that requires the integration of different cognitive domains, depending on the modality. For example, picture naming requires at least the processing of the visual information that allows for a visual representation of the object, semantic processes that search for the most similar

stored concept, phonological processes that associate the selected name to its phonological form and finally, motor processes that enable the articulation of the selected name. Where in this complex process rises the anomia deficit in AD patients has been a matter of discussion. Excluding phonological and articulation breakdown, which are extremely rare in the first stage of the disease, visual perceptual deficit could play a role in the anomia since such kind of difficulties have been reported in AD (Kirshner et al., 1984). However, visual perceptual deficit cannot be the main cause of anomia, since AD patients have also word-finding difficulty in spontaneous conversations where there is no need for visual perceptual skills; furthermore, paraphasias in AD generally replaces semantic-related, and not visual-related, names. Similarly, attention deficit in AD has been reported (Parasuraman and Haxby, 1993), but this cannot explain why AD patients are selectively impaired in word-finding tasks.

Research has pointed to a semantic-related deficit at the origin of word-finding problems in AD. The most striking evidence supporting such hypothesis comes from AD performances on standardized verbal fluency tests. In these tests subjects have to retrieve and orally produce as many words as possible in a specified period of time - usually one minute - that conform to a given criterion. The main criterions are phonemic-based (letter or phonemic fluency) and category-based (semantic or category fluency) retrieval. In phonemic fluency, subjects must generate as many words as possible begging with a given letter of the alphabet (e.g., F, A or S). In category fluency, the criterion is a specified superordinate category (e.g., animals, supermarket items). Both fluency measures, phonemic and category, are considered to impose comparable demands upon executive functions; indeed, fluency measures require efficient organization of verbal retrieval and recall, effortful self-initiation, monitor responses to avoid repetitions and inhibition of inappropriate words (Henry et al., 2004). However, phonemic and category fluency differ for the required search strategy; whilst the former relies on search strategy based on lexical representations, the latter requires searching for semantic extensions of a superordinate term (i.e., the specified category), thus requiring the integrity of semantic associations within the lexicon for the successful performance of the test (Rohrer et al., 1999, Henry et al., 2004).

AD patients perform poorly in both phonemic and category fluency tests, but the latter performance is more impaired than the former (Monsch et al., 1992, Cerhan et al., 2002, Henry et al., 2004, Mickes et al., 2007, Taler and Phillips, 2008, Clark et al., 2009); especially when mild AD patients (Monsch et al., 1992), MCI (Ahmed et al., 2008, Taler and Phillips, 2008) or pre-diagnostic subjects (Mickes et al., 2007, Clark et al., 2009) are considered. Since both fluency measures engage equally the

executive functions, the difference in the performances can be attributed to the different degree of engagement of the semantic network, being this more elicited in category than in phonemic fluency. Further support for the semantic-related deficit comes from a meta-analysis of 153 studies with 15990 participants (8356 AD patients and 7634 healthy control) focused on standardized language tests (Henry et al., 2004). Comparison of fluency measures and picture naming revealed that both the latter and category fluency performances were worse than phonemic fluency, supporting the view that language performances in AD are particularly impaired when tasks require to access to semantic representation of concepts (as in the case of picture naming and category fluency). Moreover, the authors reported that picture naming was less impaired than category fluency; they suggested that the difference could arise because the former provides more support to the lexical search process through supplying information from the visual stimulus to guide the research (Henry et al., 2004).

Thus, it appears clear that word-finding difficulties in AD are primarily originated from a deregulated semantic cognition.

Neural Basis of Semantic Cognition. Semantic memory is a major constituent of declarative memory[9], sometimes referred as explicit memory[10]. Semantic memory allows the individual to construct mental models of the world, both the concrete and abstract. It makes possible the cognitive representation of objects, situations, facts, and events, and the utilization of information thus represented in the absence of the original stimulus events and complexes. Unlike episodic-memory information, semantic-memory information about a particular object, situation, or event can be shared by different individuals, and much of it is indeed widely shared (Tulving, 1987).

There is considerable agreement that semantic memory is supported by a wide-distributed neuronal system composed of sensorimotor and verbal-related areas that store object-specific features and lexical information (Damasio et al., 2004, Martin, 2007), along with some heteromodal association cortices acting as convergence zones (Damasio, 1989). Recently, the need of multiple convergence zones supporting the emergence of integrated semantic representations has been challenged by evidence from pathological conditions (Patterson et al., 2007). Patients with a subtype of frontotemporal dementia, named semantic dementia (SD), have a bilateral focal damage to the anterior temporal lobe (ATL) accompanied

[9] The other major component is episodic memory.
[10] Opposed to explicit memory is implicit memory, a type of memory that does not require conscious executive control. A major subset of implicit memory is procedural memory, which stores information on how to perform certain procedures such as walking, talking or riding a bicycle.

by a pattern of semantic deficits indicative of degraded semantic representation with relative preservation of other language functions. The focal atrophy in SD and the relative specific semantic impairment has suggested that the ATL could serve as an amodal hub for the integration of object-specific features from sensorimotor/verbal-related areas and the relative emergence of semantic knowledge. Opposed to SD, patients with stroke in the left hemisphere, specifically in frontal-temporal and parietal cortex but excluding the ATL, that being served by two different arteries is unlikely affected by this pathology, have semantic deficits characterized by almost spared semantic knowledge but difficulty in retrieve, select and manipulate semantic information in a context appropriate fashion (Jefferies and Ralph, 2006, Patterson et al., 2007, Noonan et al., 2010).

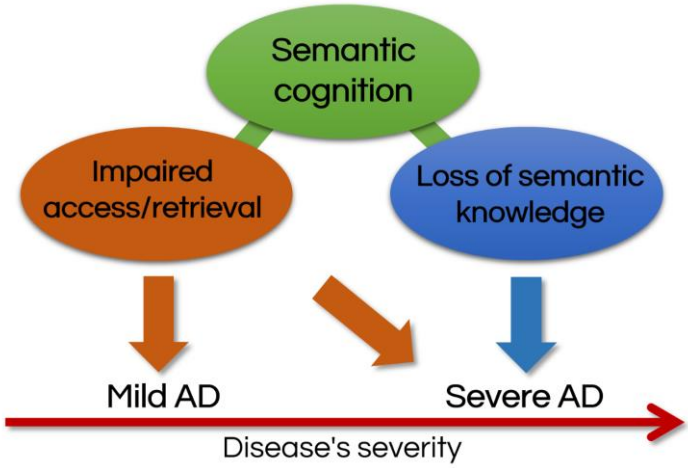

Figure 3.13 Origin of semantic impairments in AD. A recent study showed how different stages of pathology affect different components of semantic cognition. The first component to be affected is the semantic control system, followed by loss of concept knowledge.

In this framework the semantic system is composed of two distinct but interactive neuronal systems: one located in the ATL responsible for the storage of knowledge, and a fronto-temporal, and possible parietal, system for the control of semantic knowledge (Whitney et al., 2011a, Jefferies, 2013). Which component is impaired in AD has been a matter of debate. Deregulated semantic control implies that the knowledge of concepts is preserved but can be hardly retrieved; thus, it is in principle possible to facilitate the retrieval using additional modalities (such as combining visual cues or tactile information) or supplying cues (such as the first phoneme of the name). On the other hand, no strategy can facilitate the retrieval of lost information. There is evidence supporting either a degraded conceptual knowledge (Hodges et al., 1992, Garrard et al., 2005, Lin et al., 2014) or a deregulate access/control to this information (Bayles et al., 1991, Nebes and Halligan, 1996) in AD. The apparent inconsistency of neurophysiological outcomes could be related to disease severity (Bayles et al., 1991, Duong et al., 2006), a view that is supported by a recent study showing how different stages of pathology affect different

components of semantic cognition (Corbett et al., 2012). Specifically, in the mild stage (mean mini-mental state examination, MMSE = 21.3) patients showed impairments distinctive of deregulated semantic control, whereas in the severe stage (mean MMSE = 10.1) this problem, besides getting worse, became compounded by degradation of semantic representations (Figure 3.13).

Despite the remarkable nature of language-semantic deficits in AD, no study has focused on the inspection of the relevant network via resting-state functional magnetic resonance imaging (fMRI). This technique is particularly suited to the purpose of identify brain regions involved in such language-semantic impairment. Indeed, while task-based fMRI might reveal functional alterations specific of the chosen task but possibly biased by uncontrolled factors such attention level and familiarity of stimulus concepts, resting-state fMRI can reveal neuronal underlying structure independently of any task, thus possibly contributing to elucidate the origin of the semantic deficit in AD. Consistently with the specific pattern of semantic impairment reported in the early stage of the disease (Corbett et al., 2012), we focused on the semantic control network in a cohort of mild AD patients.

Methods

SUBJECTS. Thirty-eight patients with a diagnosis of probable AD by NINCDS-ADRDA consensus criteria (McKhann et al., 1984) and 19 healthy elderly subjects (HC) were recruited for this study. A general cognitive evaluation was obtained using the Mini-Mental State Examination (MMSE). All recruited patients had a MMSE score above 15, indicative of mild AD. Age and MMSE score distributions were compared among groups via two-sample t-tests, while a chi-square test was applied to compare gender distribution.

The current study was approved by the ethics committee of Santa Lucia Foundation. Every recruited subject (or his/her responsible guardians if incapable) gave written consent before MR study initiation.

DATA ACQUISITION. Subjects were scanned with the same protocol adopted in the previous experiment (see page 59).

DATA PREPROCESSING. Functional and structural MRI data were preprocessed using CONN 15.b: functional connectivity toolbox (Whitfield-Gabrieli and Nieto-Castanon, 2012; http://www.nitrc.org/projects/conn). For each subject, the first four volumes of the EPI time series were discarded to allow for signal and scanner stabilization. Realignment and slice-time correction were implemented to compensate for head movements and slice-dependent time shifts, respectively.

Additionally, to reduce the movement-related residual variance induced by the susceptibility-by-movements interaction effect, the unwarp algorithm was applied as well (Andersson et al., 2001). Then, functional volumes were spatially normalized into Montreal Neurological Institute (MNI) coordinates (voxel size: 2x2x2 mm^3) using as source image the EPI mean volume obtained from the realignment step. Normalized images were smoothed applying an 8x8x8 mm^3 full width at half maximum (FWHM) Gaussian Kernel. Separately, the T1 weighted high resolution volume was segmented and normalized to MNI space to obtain Grey Matter (GM), White Matter (WM) and Cerebral Spinal Fluid (CSF) tissue probability maps.

Additional preprocessing steps were applied to the smoothed functional data for mitigating the effect of various spurious source of variance. These included a despiking and an 0.008-0.09 Hz band-pass temporal filter applied simultaneously to the regression out, via a general linear model (GLM), of the following confounds: (1) a linear trend; (2) the six parameters of realignment and their first derivatives; (3) the first five eigenvectors of the PCA decomposition of the EPI time series separately averaged over WM and CSF, following the aCompCor noise removal approach (Behzadi et al., 2007); (4) the outliers volumes detected using the Artifact Detection Tools (ART: www.nitrc.org/projects/artifact_detect/). The simultaneous filter/regression was achieved by band-pass filtering both the fMRI time series and the confounds, prior to the regression in the GLM. This approach slightly outperforms the more common regression followed by filter (Hallquist et al., 2013).

GREY MATTER VOLUME. For each subject the GM volume (GMV) was computed from the GM probability map obtained in the segmentation step. In order to compensate for compression or expansion which might occur during warping of images to match the template, GM map was "modulated" by multiplying the intensity of each voxel in the final images by the Jacobian determinant of the transformation, corresponding to its relative volume before and after warping (Ashburner and Friston, 2001). GMV was obtained by summing the relevant modulated partition, multiplied by the voxel volume.

FUNCTIONAL CONNECTIVITY. The residual BOLD time series surviving the preprocessing were used to compute two different kinds of FC metrics that were differently used according to circumstances. The computation of both measurements was performed using EASYREST.

First, the constrained $wGBC$, equation (2.12), was applied to investigate the voxel-wise connectivity of the semantic control network. The area in which the constrained $wGBC$ was computed was composed of a set of a priori anatomically based regions

of interest (ROI) from the Harvard-Oxford probabilistic atlas (Desikan et al., 2006), including relevant regions of the semantic control network (Jefferies, 2013): the left inferior frontal gyrus (defined as pars opercularis and triangularis) and the left posterior middle temporal gyrus (defined as posterior and temporoccipital parts of the middle temporal gyrus). Other regions have been implicated in semantic control as well, including the dorsal angular gyrus (Noonan et al., 2013) and the posterior cingulate cortex (Binder et al., 2009). However, while the role of these regions still need to be further validated, there is strong neurophysiological evidence for the involvement of the left inferior-frontal and posterior-temporal regions (Indefrey and Levelt, 2004, Whitney et al., 2011a, Whitney et al., 2011b, Krieger-Redwood and Jefferies, 2014). For example, transcranial magnetic stimulation applied separately to both regions has shown to disrupt executively demanding semantic judgments (Whitney et al., 2011b). Further support for their role in control process comes from studies focusing on lexical access and selection in word production, through the investigation of the semantic interference effect (Maess et al., 2002, Schnur et al., 2009).

wGBC computation was restricted within key regions of the semantic control network because wGBC applied to the whole brain has an intrinsically poor sensitivity if the effect is localized, and it is also prone to include the effects of possible compensatory mechanisms. To avoid partial volume errors, the spatial smoothing was restrained into the relevant mask using the smooth in mask function of EASYREST, with a FWHM Gaussian kernel of 4x4x4 mm^3.

The seed-based whole-brain FC metric was adopted as well using as seed regions the clusters resulting from the wGBC analysis. As for wGBC, a z-fisher transformation was applied to seed-based FC to improve normality.

Between-group comparisons for each FC measure were performed via two-sample two-tailed t-tests. Age, sex and GMV were always used as nuisance covariates. Statistical threshold was set to $p < 0.05$ after correction for multiple comparisons via Monte Carlo simulations (AlphaSim, AFNI package, Cox, 1996). The correct threshold corresponds to a single voxel level of $p < 0.001$ with a minimum cluster size of 7 voxels, for wGBC inference, and around 70 voxels, for seed-based FC, depending on the smoothness of residuals.

Results

Principal demographic, clinical data and GMV estimation are reported in Table 3.4. Patients and controls were matched for age (t-test, $t = 1.7$, $p > 0.08$) but not for

gender (chi-square test: $x^2 = 9.3$, $p = 0.002$). As expected, MMSE scores were significantly different between the two groups (t-test, $t = -10.3$, $p < 0.001$). AD patients showed a significant reduction in GMV (t-test: $t = -5.4$, $p < 0.001$).

Table 3.4 Principal characteristics of studied subjects

	AD	HC	P-value
N	38	19	
Gender (M/F)	10/28	13/6	0.002[a]
Age (years)	72.2 ± 7.8	68.5 ± 6.8	0.089[b]
MMSE score	20.7 ± 3.7	28.8 ± 1.2	<0.001[b]
Grey matter volume (dl)	5.39 ± 0.53	6.30 ± 0.73	<0.001[b]

Data presented as mean ± SD. AD, Alzheimer's disease; HC, healthy control; MMSE, Mini mental State Examination.
[a] The p-value was obtained by chi-square test.
[b] The p-value was obtained by t-test.

Figure 3.14 reports pathology-induced changes of wGBC. We identified two significant clusters in which the FC in the selected area is reduced in AD ($p < 0.05$, corr.). One cluster is located in the superior edge of the posterior middle temporal gyrus (pMTG; MNI coordinate = [-56, -30,-2] mm; $t = 4.96$; volume = 17 voxels) while the other is located in the pars opercularis (pOPE; MNI coordinate = [-56, 10, 8] mm; $t = 4.64$; volume = 31 voxels).

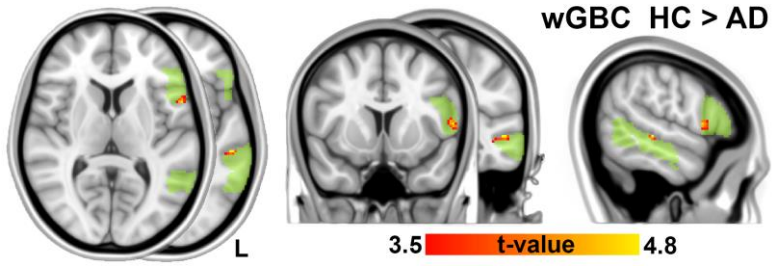

Figure 3.14 Pathology-induced changes in constrained wGBC. Color-coded t-statistic map showing significant detectable pathology-induced reductions in the internal functional connectivity of the semantic control network (reported in green) assessed by constrained wGBC. The result was obtained via a two-sample, two-tailed t-test, HC > AD ($|t|>3.5$, $p < 0.05$, corrected).

The origin of the FC reductions in semantic control network was further investigated by seed-based whole-brain FC using as seed the two clusters of reduced wGBC. The group-level patterns of FC for each seed are reported in Figure 3.15 ($p < 0.05$, corr.). Among the two seeds, the pMTG showed the most dissimilar pattern of connectivity in the two groups. Indeed, while HC subjects showed connections in frontal, parietal and anterior temporal regions, the connectivity of the mild AD patients was restricted in the middle section of the temporal lobe.

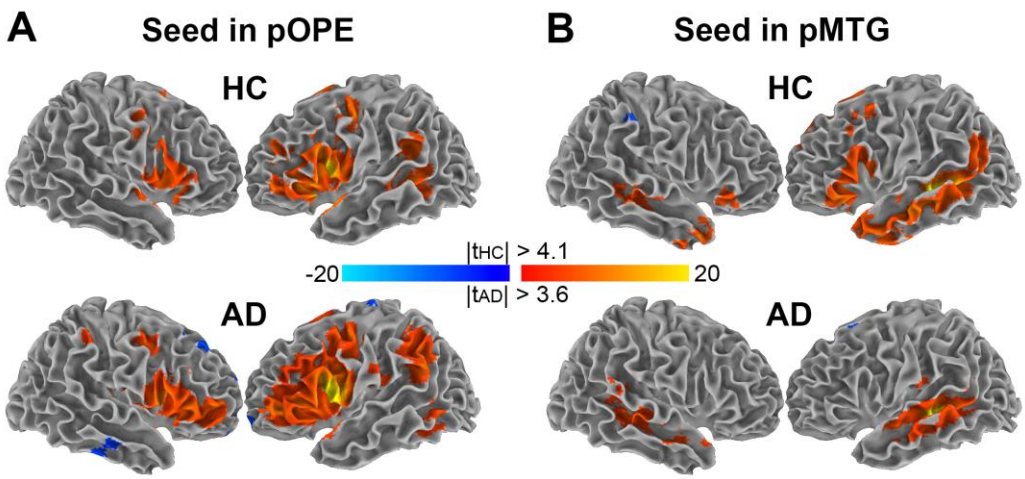

Figure 3.15 Group-level FC with the pOPE and pMTG clusters. Color-coded t-static maps showing significant group-level functional connectivity with **A**) seed in the pOPE cluster and **B**) seed in the pMTG cluster. Result were obtained via one-sample, two-tailed t-test (|tHC|>4.1 and |tAD|>3.6, $p < 0.05$, corrected).

Specific regions of altered FC with the pOPE and pMTG clusters induced by pathology are shown in Figure 3.16A and Figure 3.16B, respectively ($p < 0.05$, corr.).

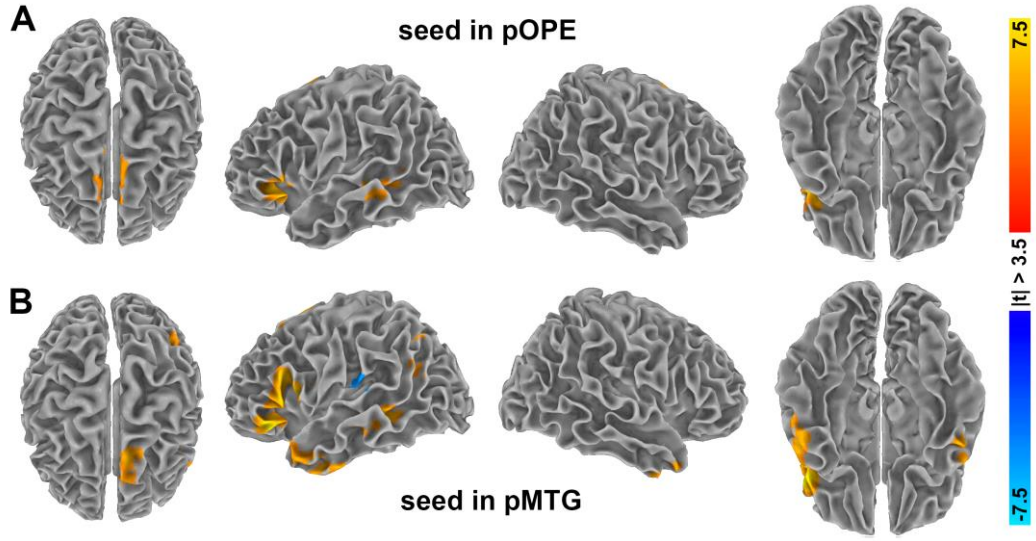

Figure 3.16 Pathology-induced changes in FC with the pOPE and pMTG clusters. Color-coded t-static maps showing significant pathology-induced functional connectivity alterations with A) seed in the OPE cluster and B) seed in the pMTG cluster. Result were obtained via two-sample, two-tailed t-test (|t|>3.5, $p < 0.05$, corrected).

Regions disconnected from the cluster in the pOPE are mainly localized within the core of the semantic control network used for wGBC computation, with the only exception of the bilateral superior frontal gyrus. On the contrary, the pathology-

induced disconnection from the cluster in the pMTG identified a network spreading several left-lateralized brain regions, including inferior frontal and anterior temporal regions, the superior frontal gyrus and the angular gyrus. The pMTG cluster was also disconnected from the right hemisphere in the temporal pole. In addition we reported an opposite trend, namely a pathology-induce increase in functional connectivity, in the left planum temporale, regions belonging to Wernicke's territory. Detailed cluster information is reported in Table 3.5.

Table 3.5 Pathological-induced changes in seed-based functional connectivity

Seed	Brain Regions	Side	Vol (voxels)	MNI coordinates			Peak t-value
				x	y	z	
	AD patients < HC						
	Frontal Orbital cortex, Temporal Pole, Pars Triangularis and Opercularis, Frontal Operculum cortex	L	962	-50	8	-6	6.26
pOPE	Superior Frontal gyrus, Supplementary motor cortex	B	613	0	12	66	4.74
	Posterior Middle and Superior Temporal gyrus, Temporooccipital Middle temporal gyrus	L	322	-62	-34	-2	4.86
	AD patients < HC						
	Pars Opercularis, Temporal Pole, Pars Triangularis, Frontal Orbital cortex, anterior Inferior and Middle Temporal gyrus	L	2310	-48	26	-12	7.56
	Superior Frontal gyrus, Supplementary Motor cortex	L	583	-12	14	66	5.89
	Posterior and temporoocipital Middle Temporal gyrus	L	493	-54	-42	-6	5.43
pMTG	Temporal Pole, anterior Inferior Temporal gyrus	R	216	50	16	-36	5.15
	Superior Lateral Occipital cortex, Angular gyrus, Supramarginal gyrus	L	188	-38	-62	44	4.62
	Angular gyrus, superior Lateral Occipital cortex	L	107	-50	-60	28	4.09
	AD patients > HC						
	Planum temporale, Parietal Operculum Cortex, Heschl's Gyrus, central Operculum cortex	L	162	-52	-24	10	-4.23

Regions showing significant pathology-induced changes in seed-based functional connectivity with seed in pars opercularis and posterior middle temporal gyrus clusters (two-sample t-tests). B, bilateral; L, left; R, right.

Discussion

Language dysfunction in the early stage of AD can heavily burden the patient's every daily life activity, especially considering that subjects aware of the impairments tend to withdraw from social situations exacerbating language symptom over time (Farrell et al., 2014). Despite such relevance, the neural substrates of language dysfunction in AD patients remain largely unknown. We contributed to elucidate the neural origin reporting functional alterations in semantic-language related areas during the mild stage of the illness.

We reported pathology-induced constrained wGBC reductions in the semantic control network (Figure 3.14). Aberrant connectivity in this network supports the specific pattern of semantic impairments previously reported in the early stage of the disease. Indeed, the poor performance of mild AD patients in semantic tasks has been related to a failure to control or shape semantic knowledge in a task-appropriate fashion, as it is proven, for example, by the significant effect of cue and miscue in confrontation naming (Corbett et al., 2012). The wGBC reduction in the semantic control network was circumscribed to two small but highly significant clusters, one located in the pars opercularis (referred to as pOPE cluster) and another in the posterior middle temporal gyrus (referred to as pMTG cluster). The wGBC reductions were primarily due to a specific fronto-temporal disconnection rather than an overall weakening of the internal connectivity of the semantic control network. This conclusion is supported by the common pattern of disconnection obtained using as seed the clusters in pOPE and pMTG. Indeed, while the connectivity with the pOPE cluster showed a disconnection in the posterior middle temporal gyrus (Figure 3.16A), the FC with the pMTG cluster showed a disconnection in Broca's area, including pars opercularis (Figure 3.16B).

A further analysis of the frontal versus temporal network revealed an uneven pattern of disconnections for the latter compared to the former. The pMTG cluster was found to be disconnected not only in the Broca's territory but also in several other language-related areas including the anterior temporal lobe, the angular gyrus and the superior frontal gyrus. The disproportion between frontal and temporal disconnections reflects the well documented difference in performance between phonemic and category fluency (Henry and Crawford, 2004). Indeed, the integrity of frontal regions was associated with great performance in phonemic fluency, while successfully category fluency to the integrity of temporal regions (Baldo et al., 2006). The comparison between frontal and temporal FC also suggests that the fronto-temporal disconnection might be the result of a specific alteration in the structure of posterior middle temporal regions and not to a primary alteration in inferior frontal regions. Consistent with this notion, AD patients are characterized by fluent speech, not compatible with the fragmented speech distinctive of the dissolution of Broca's regions (Kempler, 1995). Moreover, inferior frontal regions were found almost free of atrophy even in the late stage of the disease (Harasty et al., 1999).

Functional Role of pMTG. The pMTG and its FC patterns have shown to be a backbone for language comprehension and to have a critical role in semantic processing. In a lesion analysis, Dronkers and colleagues have highlighted the importance of the left pMTG (composed of the posterior part of Brodmann's area

(BA) 21 and the superior portion of BA37) in language comprehension (Dronkers et al., 2004). Lesions in this region produced language comprehension impairments even for the most simple sentence that, combined with a comparable deficit in confrontation naming, suggested that the impairment was at the word-level processing. The authors supported the idea that pMTG holds up the function to *tie concepts to their corresponding lexical representations*.

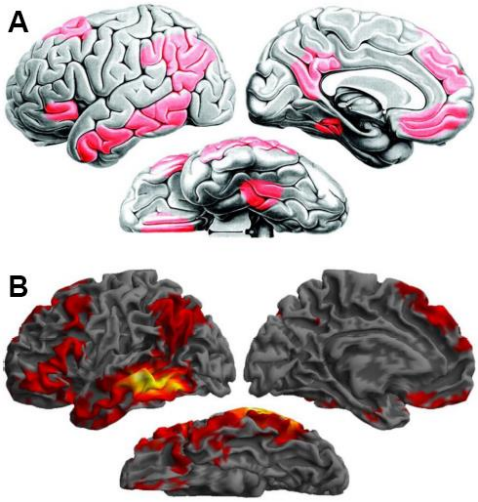

Figure 3.17 (**A**) A large-scale network for verbal semantic processing identified by a meta-analysis of 120 functional neuroimaging studies, and the underlying structural connections inferred from tracing studies of the homologous regions in the macaque (from Binder et al., 2009). (**B**) Resting FC pattern for the left posterior MTG (region from lesion analysis in Dronkers et al., 2004), assessed in a cohort of healthy subjects. The pattern is largely consistent with the meta-analysis findings (Turken and Dronkers, 2011) .

The critical role of this region in the language system was further assessed by a later study that found the region to have particularly extensive structural and functional connectivity patterns in the healthy brain (Turken and Dronkers, 2011). Indeed, tractography analysis revealed up to five major fiber pathways passing beneath the pMTG. Functional connectivity analysis, reported in Figure 3.17B, revealed widespread connections in frontal and temporal cortices, particularly in perisylvian and neighbouring areas, as well as connections in parietal cortices mostly consistent with our pattern of connections in the HC subjects (Figure 3.15B). In addition, this functional connectivity pattern shares most of its areas with the verbal semantic network resulting from a meta-analysis of 120 neuroimaging studies (Binder et al., 2009), in which the MTG, including the posterior portion, was one of the most consistently activated area across studies (Figure 3.17).

The basic role in language comprehension of the pMTG suggested by these studies is further supported by current models of lexical access in word production (Indefrey and Levelt, 2000, Indefrey, 2011).

pMTG and Lexical Access. Lexical access, sometimes referred as *lexicalization*, is the ability to select and retrieve the most appropriate word-form of a given concept. Theories of speech production agree on two fundamental points: (i) semantic, syntactic, and lexical form information constitute independent levels of

representation, and (ii) these levels of representation are probably accessed sequentially in the course of language production. The dominant view is that lexical access involves at least two distinct stages of processing. The first stage involves the selection of a semantically and syntactically specified lexical representation or *lemma*; the second stage involves the selection of its corresponding lexical-phonological representation or *lexeme (Caramazza, 1997).*

Perhaps the best evidence that lexical access proceeds by separable steps comes from the tip-of-the-tongue (TOT) phenomenon, a failure in word retrieval accompanied by a partial recall of the word and the sensation that the full retrieval is imminent. In a TOT state [11] unimpaired young adults primarily produce phonologically-related words rather than semantically-related; moreover, they are often able to provide several phonological information about the target word such as the initial letter or phoneme (Brown, 1991). In the context of the two-stage model of lexical access, this behaviour highly suggests that the lemma is successfully activated by semantic information but the phonological representation fails or it is only partially completed. In other words, TOT states might reflect the failure to retrieve a lexeme in the context of successful retrieval of its lemma (Astell and Harley, 1996, Caramazza, 1997). However, with increasing age, TOT becomes more frequent and subjects are less able to provide phonological information about the target word. The less efficient word-retrieval mechanism in older adult compared to young subjects suggests that other phenomenon, aside the failure to access the lexeme, could be present, such as failure at the concept level or at retrieval of the lemma (Astell and Harley, 1996). This seems to be the case in the AD patients. Indeed, Astell and colleagues induced TOT states in healthy elderly and AD patients and found semantically related items and little phonological information in both groups, but this behaviour was more pronounced in the AD group, which, in addition, could not provide information about the target word (Astell and Harley, 1996). Examining the relationship between the target and non-target words produced in terms of their syntactic category, frequency, and imageability, they proposed that the retrieval deficit in AD lies between the semantic and lexical level. The failure to activate the correct lemma could be the result of the weakening of the connections between semantic representations and lemmas.

Although the precise anatomical location underpinning lexicalization is still under investigation, recent researches are pointing to the posterior portion of the MTG in the conceptually driven selection of lemma from the mental lexicon (Maess et al.,

[11] TOT states can be induced experimentally by presenting subjects with definitions of unfrequently words.

2002, Schnur et al., 2009). Thus, the functional disconnections reported in our study confirm previous results focused on TOT states in AD patients. Specifically, our results, in a task-unbiased fashion, support the notion that the word-finding difficulty in mild AD is due to an impaired access to the mental lexicon from the concept level.

The Planum Temporale. We reported also a pathology-induced increase in FC with the pMTG cluster in the left planum temporale (Figure 3.16B), region belonging to the Wernicke's territory. The left planum temporale has been implicated in phonological memory, as an auditory–motor interface with an important role in speech perception and production (Buchsbaum and D'Esposito, 2008). A recent lesion analysis study, has shown the left planum temporale, along with other posterior perisylvian regions, to be involved in phonological retrieval (Pillay et al., 2014), that is, in the selection of the lexema. In this context, the increase in FC is suggestive of a compensatory mechanism to overcome the impaired access to the mental lexicon from the semantic path (i.e., impaired access to the lemma). This increase might explain the better performance in phonemic fluency compared to category fluency in AD patients (Henry and Crawford, 2004).

Conclusion. We showed that mild AD patients exhibit the disruption of a key region of the language-semantic network, suggestive of an impairment at the lexical-semantic level. To our knowledge, this is the first study specifically focused on the functional connectivity of language-semantic network in mild AD. Our results showed that the ability of patients to manipulate semantic knowledge is altered due to a dissolution of the semantic control network, primarily originated from a break down in the pMTG functional circuitry, a vital system for language comprehension and production. Our results support the view that mild AD patients have an impaired access to the mental lexicon from the concept level, possibly accompanied by an enhanced access from the phonological level.

CHAPTER 4

Physiological modulations of LFFs

The intrinsic activity of the brain is mirrored in the spontaneous BOLD LFFs even when the brain is not specifically in the resting condition. When the brain is processing a sensory stimulation or engaged in a cognitive task LFFs are present on the top of the task-related BOLD response. It is possible to separate the latter component from the spontaneous LFFs by acquiring fMRI data during steady-state performance of a task. In practice, the task is performed constantly and consistently over the course of time in which the images are acquired. In this manner, few seconds after the onset of the stimulus, the BOLD signal reaches a steady level that is maintained for the entire experimental acquisition[12]; the variance on the top of the steady BOLD level, namely the spontaneous LFFs, can be studied in the exact same fashion as in resting-state data[13]. In the present chapter we sought to answer to two

[12] Attenuation is expected, but can be easily overcome by means of polynomial regressions or appropriate filters.
[13] The resting-state condition is indeed a steady state.

questions regarding the intrinsic activity of the brain when it is focusing on the external world.

First, we aimed to identify the basic features of LFFs when transiting from a condition of rest to a condition of activity. From several cues in literature modulations in connectivity and amplitude patterns are expected, however, at what spatial and temporal scale these happen is largely unknown.

In the second study, we sought to investigate how the intrinsic brain's activity under a visual stimulation task is modulated by the attention level. Indeed, it has been proven that visuospatial attention modulates the task-related BOLD response in retinotopical matched areas, however, it remains the issue of how the brain responds to attentional modulation at the network level.

Steady-state modulations of LFFs

Considerable efforts have been devoted to the characterization of stationary task–related changes of brain networks, however the spatiotemporal properties of task-induced LFFs are still to be clarified. Certainly, the intrinsic brain activity, mirrored in the spontaneous BOLD LFFs, plays an essential role in shaping the task-evoked activity. Indeed, spontaneous LFFs have been shown to influence behaviour (Hampson et al., 2006, Fox et al., 2007), as well as to contribute to variability in task-evoked responses (Fox et al., 2006b). Nonetheless, the brain's functional network architecture seems to conserve its topology across different kinds of evoked activity (Smith et al., 2009), albeit specific network alterations have been reported, revealing task-specific modulations (Cole et al., 2014). Task-induced modulations involve both the amplitude and the connectivity of LFF patterns. Strength of functional connectivity has shown modulations both in task-negative (i.e., DMN) and task-positive network (Fransson, 2006, Vatansever et al., 2015), while significant differences in the amplitude of LFFs have been reported in the visual network comparing open- and closed-eye resting-state conditions (Yang et al., 2007).

Inside this framework, several issues remain to be clarified. First, it is still unclear whether functional connectivity modulations concern both short- and long-range connections, among which networks and whether they are accompanied by modulations in the oscillation amplitude. Secondly, nothing is known about the temporal scale of task-induced modulations. Two possibility can be conceived. The task can affect network activity simultaneously with the task-evoked response in the activated regions; alternatively, the effect might happen at a slower temporal scale,

indicating that task-evoked response and network modulations are possibly epiphenomenon.

In the following study, we sought to investigate such open questions. Starting from the notion that the topology of resting-state network is not significantly altered among different steady-state conditions, we parcelled the brain in 7 networks of synchronized resting-state activity (Yeo et al., 2011) seeking to disclose how spontaneous brain activity is dynamically and spatially influenced by task execution. We compared two steady-state conditions: (i) an open-eye resting state and (ii) a steady-state working memory task. To allow the study of the dynamic of LFF modulations, instead of acquiring the two steady conditions (rest and task) in two separate sessions, we adopted a non-conventional block design paradigm. Namely, rest and task were alternated in the same run, but the duration of each epoch (i.e., condition) largely exceed the common time adopted in task-based fMRI (around 30 seconds). Each condition was acquired for 5 minutes, yielding sufficient time points to extract the low-frequency (< 0.1 Hz) fluctuations and to filter out any task-evoked response.

Methods

SAMPLE AND PARADIGM. Ten healthy right handed subjects (mean age = 30 ± 5 years) were scanned in a 3T Siemens Allegra system. Functional data were collected by using a 2D gradient echo planar sequence (TR/TE = 2100/30 ms, Flip Angle= 70 °, 3 x3 x 2.5 mm^3 voxels), covering the whole brain with 33 slices, with 1.25 mm skip, parallel to the anterior/posterior commissure plane. Sagittal, T1 weighted structural data were acquired at high resolution (TR/TE = 2000/4.38 ms, Flip Angle = 8 °, 1.33 x 1.33 x 1 mm^3).

Functional MRI experimental paradigm consisted in five epochs, continuously acquired, lasting 5 minutes each. These epochs were alternated in resting state and task (rest-task-rest-task-rest). During rest participants laid in the scanner with open eyes; during task they were presented by a continuous n-back auditory working memory test that divided each TR in 500 ms of stimuli appearance and 1600 ms of response time. Stimulation consisted in pseudo-random repetition of three vowels (A, E, O), that participants had to compare in n-lag trials. In each session, task epochs involved two levels of difficulty, one low load (n = 1, 1-back task) and one high load (n = 2, 2-back task), presented with inverted order. To improve statistics two functional runs, with inverted task order, were acquired for each subject. Sessions and epochs were labelled as in Figure 4.1.

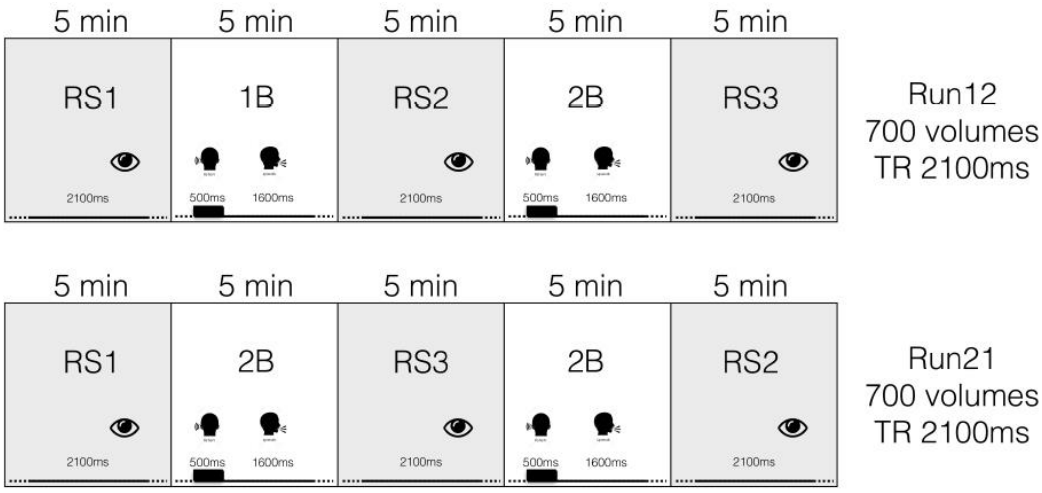

Figure 4.1 Experimental paradigm. Interleaved resting state/task execution conditions repeated in two sessions (Run12, Run21). Tasks had two levels of cognitive load, every TR corresponded to the pronunciation of a vowel and the subject was requested to remember and spell the vowel of the previous (1B) or two times back (2B) volume. The order of 1B and 2B tasks was mixed between sessions, sessions order was random among subjects.

Subjects were trained 30 minutes outside the scanner before their first experimental session, to ensure a clear understanding of the task, eventually performance scores were larger than 75%. All participants gave informed consent in accordance with S. Lucia Foundation Institutional Review Board.

PREPROCESSING. Functional and structural MRI data were preprocessed using CONN 15.b: functional connectivity toolbox (Whitfield-Gabrieli and Nieto-Castanon, 2012; http://www.nitrc.org/projects/conn) and EASYREST. For each subject, the first four volumes of the EPI time series were discarded to allow for signal and scanner stabilization. Realignment and slice-time correction were implemented to compensate for head movements and slice-dependent time shifts, respectively. Additionally, to reduce the movement-related residual variance induced by the susceptibility-by-movements interaction effect, the unwarp algorithm was applied as well (Andersson et al., 2001). Then, functional volumes were spatially normalized into Montreal Neurological Institute (MNI) coordinates (voxel size: 2x2x2 mm^3) using as source image the EPI mean volume obtained from the realignment step. Normalized images were smoothed applying an 8x8x8 mm^3 full width at half maximum (FWHM) Gaussian Kernel. Separately, the T1 weighted high resolution volume was segmented and normalized to MNI space to obtain Grey Matter (GM), White Matter (WM) and Cerebral Spinal Fluid (CSF) tissue probability maps.

Additional preprocessing steps were applied to the smoothed functional data for mitigating the effect of spurious sources of variance. These included a despiking and an 0.008-0.09 Hz band-pass temporal filter applied simultaneously to the

regression out, via a general linear model (GLM), of the following confounds: (1) a linear trend; (2) the six parameters of realignment and their first derivatives; (3) the first five eigenvectors of the PCA decomposition of the EPI time series separately averaged over WM and CSF, following the aCompCor noise removal approach (Behzadi et al., 2007); (4) the outliers volumes detected using the Artifact Detection Tools (ART: www.nitrc.org/projects/artifact_detect/).

To avoid detection of spurious effects, the entire following analysis was restrained to GM mask obtained thresholding at 40% the average subjects' GM probability map (EASYREST; brainmask method "soft"). The cerebellum was excluded from the analysis due to the limited field of view of the EPI sequence.

TEMPORAL SUBDIVISION. In the following processing and analysis, we sectioned each scan session in 5 epochs consisting of 140 volumes each. To avoid effect of ordering and fatigue we averaged similar steady-state conditions across the two scan sessions, obtaining eventually a sole session composed of: RS_1 – 1B – RS_2 – 2B – RS_3.

A finer temporal subdivision was also adopted to investigate the temporal scale at which modulations, due to the transition between different steady-state conditions, happen. We divided each of the five epochs in five finer intervals of 28 volumes (1 minute). Five is the largest number of intervals within an epoch that allowed us to maintain a reasonable number of time points, preserving all frequency components of interest (i.e., 0.008-0.09 Hz).

REGIONS OF INTEREST. Brain regions of interest (ROIs) were functionally disentangled in seven not overlapping networks using the atlas compiled by Yeo and colleagues (Yeo et al., 2011). Brain networks were classified as Visual (VIS), Somatomotor (SM), Dorsal Attention (DA), Ventral Attention (VA), Limbic System (LIMB), Frontoparietal Control (FP) and Default Mode Network (DMN).

FUNCTIONAL CONNECTIVITY ASSESSMENT. Task-induced modulations in steady-state functional connectivity among the selected networks were assessed at two different spatial scales. First, seed-to-voxel (StV, see page 34) connectivity were implemented to assess the between- and within-network behaviour, using as reference time course the average BOLD series of each network. Secondly, we assessed the local (i.e., at the voxel level) synchronization inside each network computing ReHo (see see page 42), that, differently from the StV metric, accounts only for short-range connections. Both the within-network StV and ReHo are measures of internal synchronization of a given network, however, the spatial scale at which the synchronization is computed can deeply influence the results. Indeed,

the average behaviour inside the network can partially be disentangled from what happens in its sub components.

OSCILLATION AMPLITUDE ASSESSMENT. Assessment of the oscillation amplitude in steady-state epochs was achieved computing fractional ALFF (fALFF), a normalized version of ALFF (Zang et al., 2007) that has been suggested to be less prone to physiological noise (Zou et al., 2008). See page 30 for details on computational method.

STATISTICAL ANALYSIS. Between steady-state conditions (rest and tasks) comparison for each measure (connectivity or amplitude assessments) was performed via two–sample, two–tailed paired t–tests utilizing functionalities embedded in EASYREST.

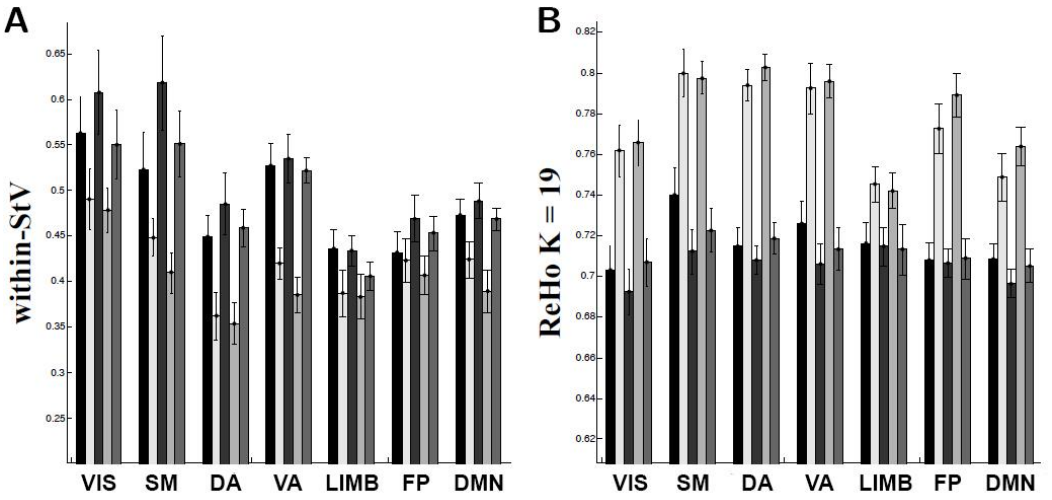

Figure 4.2 Task-induced modulations in within-network functional connectivity. A) Within-network StV connectivity for each studied network. Dark grey-scaled tones index RS1, RS2, RS3 from the darker down, light gray-scaled tones index 1B, 2B from the lighter up. StV depends on the condition significantly ($p < 0:001$), being higher during resting state than task execution. **B**) Within-network ReHo for each studied network. ReHo depends on the condition significantly ($p < 0:001$), with the opposite trend respect within-network StV, being lower during resting state than task execution.

Results

Task induced adjustments in brain's intrinsic activity detectable towards changes in connectivity strength and in oscillation amplitude.

Within-network connectivity changes induced by the stimulation were dependent on the spatial scale at which the synchronization was assessed. Task induced significant decrease ($p < 0.001$) in the within-network StV connectivity for several networks: VIS, SM, DA, VA and DMN (Figure 4.2A). Contrarily, we found an opposite trend for the within-network ReHo, namely significant ($p < 0.001$) larger ReHo values

during task execution than during resting periods (Figure 4.2B). This latter effect was reported for every studied network.

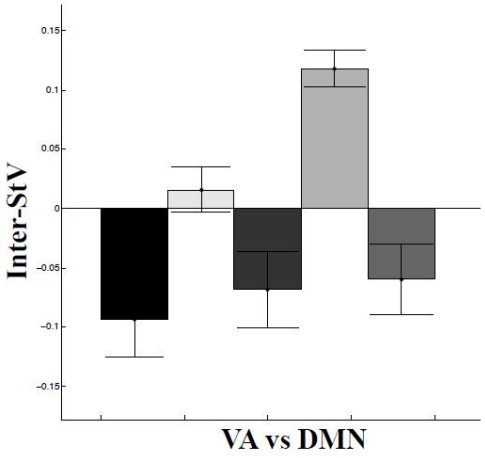

Figure 4.3 Task-induced modulations in between-network functional connectivity. StV connectivity between VA and DMN significantly differs among conditions ($p < 0.001$). Dark grey-scaled tones index RS1, RS2, RS3 from the darker down, light gray-scaled tones index 1B, 2B from the lighter up.

While the within-network connectivity changes interested almost the whole brain, no between-network change reached statistical threshold ($p > 0.05$), with the only exception of the couple VA and DMN. These two networks showed enhanced functional connectivity during task periods (Figure 4.3).

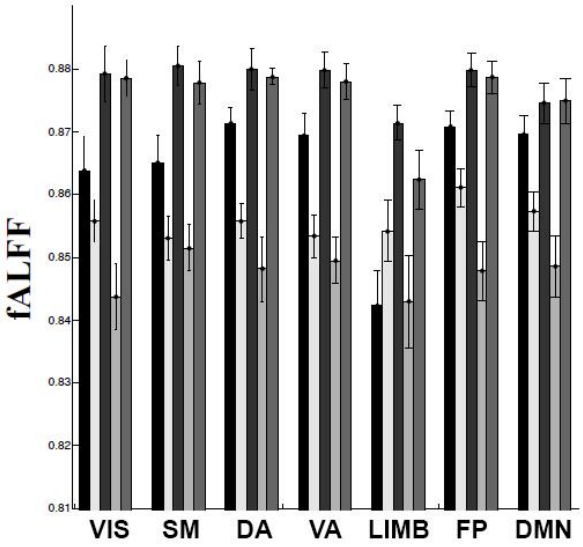

Figure 4.4 Task-induced modulations in fALFF. Within-network averaged fALFF values for each studied network. Dark grey-scaled tones index RS1, RS2, RS3 from the darker down, light gray-scaled tones index 1B, 2B . FALFF shows a significant ($p< 0:001$) decrease during task states.

Considering the oscillation amplitude of LFFs, the task induced a remarkable whole brain reduction in fALFF values ($p < 0.001$, FIGURE 4.4).

To assess the temporal scale at which the modulation in connectivity happens, we reconsidered the above analysis within the finer temporal subdivision. Since we had

previously noticed that task-induced modulations involved almost every studied network, we examined the transient dynamic considering the whole brain as a single network. We found a drop of StV connectivity in the first minute of task execution and a bump in the first minute following resting state (Figure 4.5A). In Figure 4.5B it is better explained through the derivative of the StV connectivity at the every sub-interval of each steady-state condition. The derivative in the first interval is negative during task execution, positive during rest and zero after the state has become stationary. The derivative at the transition significantly differs from zero (1B: $p < 0.001$; 2B: $p < 0.023$; $RS_{2/3}$ $p < 0.0002$).

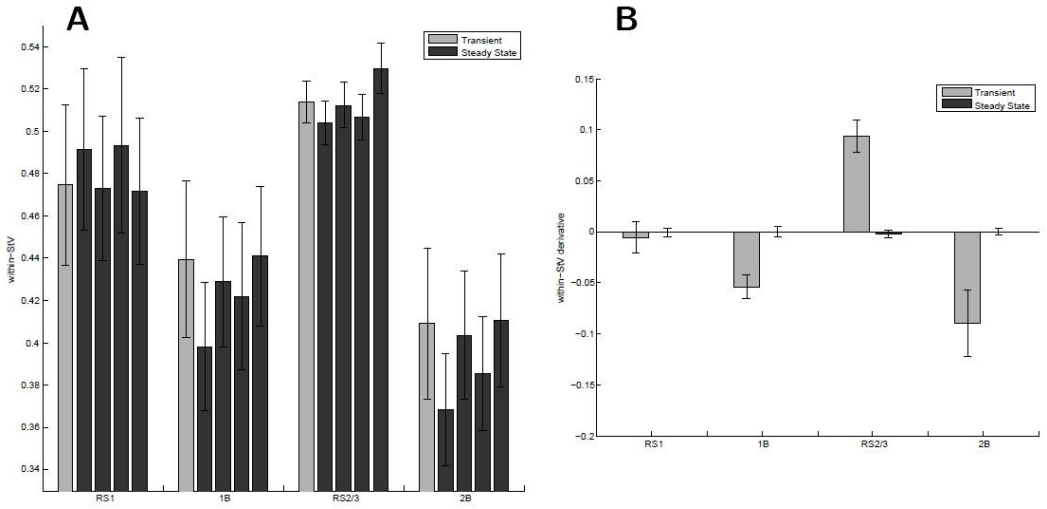

Figure 4.5 Finer temporal subdivison of within-network StV connectivity. A) Within-network StV connectivity is reported for the whole-brain network, divided in 25 intervals, light and dark grey bars distinguish transient and steady state intervals. **B**) Derivatives of the within–netowork StV connectivity for transient and steady-state intervals. RS2 and RS3 have been united because of the similarity of their behaviour.

Discussion

The multi-parametric approach adopted to study task-induced modulations of spontaneous BOLD LFFs revealed a complex pattern of adjustments following task execution. Synchronization and amplitude based proprieties of spontaneous LFFs are remarkably altered when the brain is focusing on the external world; an effect that is not enclosed in a specific network, but involves a great portion of the cerebral cortex.

When occupied in accomplishing a task, networks involved in sensory (VIS, SM), motor (SM), attention (DA, VA) and default mode (DMN) regulate their within-network connectivity. During task execution the internal synchronization of each network is partially lost, as indicated by the decrease in the within-network StV connectivity. However, the task-induced loss of correlation is due to a within-network

specialization, as indicated by the increase in ReHo. Namely, during task execution network subcomponents increase their local (i.e., first neighbour voxels) connectivity in a region-dependent fashion that produces a reshape of the internal functional structure of the network.

While the reported task-induced decrease in within-network connectivity might result in a slight redefinition of network boundaries (a possibility that we are not able to test in our a priori network approach), the overall network topology seems to be a stable feature of the brain, a notion that is in agreement with previous findings (Cole et al., 2014). In fact, different steady-state conditions did not influence the between-network StV connectivity, with the only exception of the connection between VA and DMN. This outcome is in agreement with previous research reporting enhanced correlations between DMN and task-positive network (Fransson, 2006, Vatansever et al., 2015).

The within-network specialization was accompanied by a reduction of the amplitude of LFFs (i.e., fALFF) during task execution. Since the amplitude of LFFs has shown to be correlated with metabolic rate of glucose consumption (Tomasi et al., 2013), is thought to reflect the local activity of the brain. Our results highly suggest that (i) processes sustaining the spontaneous brain's intrinsic activity during rest state are more energy demanding than those subserving the intrinsic activity during task execution[14]; (ii) the former processes are possible suspended or reduced in the task condition. Unfortunately, more precise conclusions can hardly been made since the processes that take place during resting-state conditions are still largely unknown, although some have suggested they can be involved in memory consolidation (Albert et al., 2009).

Finally, we were interested in the time scale at which such modulations happen. The long acquisition time of our experiment allowed us to achieve a reasonable good temporal resolution (1 minute), especially considering the intrinsic slow temporal scale of spontaneous BOLD LFFs. Our results showed a "fast" dynamic, with the transition effect lying within the first minute of the following steady condition. In particular, we observed a sudden decrement of within–network StV connectivity at the transition from rest to task state, followed by a stabilization of the measure. This result support the notion that modulation of LFFs happens at similar temporal scale with the task-evoked response in the activated regions.

[14] The reader should keep in mind that we are considering only the brain's intrinsic activity. Indeed, task-evoked response is known to produce a localized (in task-responding regions) increase in energy demand.

Conclusion. Cognitive engagement causes a complex pattern of modulations of both connectivity strength and spectral content of spontaneous brain activity. In particular, the working memory task induces a local synchronization inside networks that is not spatially homogenous, resulting in an overall decrease of network internal average connection. Similarly, the amplitude of the low frequency fluctuations decreases during the cognitive load. Such modulations happen with a fast dynamic, within the first minute of the incoming condition.

Visuospatial attention affects brain network organization

The human brain constantly receives more visual stimuli than what it can simultaneously process. The cognitive ability defined as visual attention allows us to select the most behaviorally relevant stimuli for processing and control over behavior while ignoring distractions. Visuospatial attention filters incoming sensory inputs basing on location, providing a competitive advantage to stimuli presented in the selected spatial area (Brefczynski and DeYoe, 1999, Gandhi et al., 1999, Somers et al., 1999, Kastner and Ungerleider, 2000, 2001, Jack et al., 2006, Bouvier and Engel, 2011).

Neural Network Underpinning Attention. The brain function of attention depends on large and distributed neural networks consisting of subcortical structures and cortical areas subdivided into anatomically and functionally distinct ventral and dorsal components (Corbetta and Shulman, 2002, Szczepanski et al., 2013) interconnected by frontoparietal long-range pathways (Thiebaut de Schotten et al., 2011, Bartolomeo et al., 2012). The dorsal attention network (DA) is made of intraparietal sulcus, superior parietal lobule, frontal eye field and supplementary eye field, whereas the anterior cingulated cortex, the temporoparietal junction and the inferior parietal lobule are included in the ventral attention network (VA; Luck et al., 1997, Hillyard et al., 1998, Kastner et al., 1998, Kastner et al., 1999). Broadly speaking, the DA plays a top-down control over incoming stimuli for volitional spatial or feature orienting, whereas the VA is considered important for detecting unexpected but behaviorally relevant events towards which attention needs to be triggered (Vossel et al., 2014). The middle frontal gyrus is considered to be a site of convergence of both VA and DA, a circuit-breaker reorienting attention from an endogenous oriented to an exogenous oriented task (Fox et al., 2006a, Corbetta et al., 2008, Japee et al., 2015). Although a common knowledge on these networks has been reached, their specific roles for attentional processes, their functional organization and interaction need to be further investigated.

ATTENTION AFFECTS BRAIN NETWORKS. Besides strongly affecting the processing of visual inputs (Luck et al., 1997, Kastner et al., 1999, Ress et al., 2000) with a retinotopically specific modulation in visual cortical areas (Gandhi et al., 1999, Somers et al., 1999), visual spatial attention also affects brain networks (Spadone et al., 2015). Previous studies suggest that visual attention affects FC, increasing the connectivity between frontal and parietal regions (Szczepanski et al., 2013), parietal and occipital regions (Greenberg et al., 2012), attention and visual networks (Spadone et al., 2015), as well as high- and low- level visual regions (Al-Aidroos et al., 2012, Bray et al., 2015). Yet, attentional modulations of networks are still poorly understood.

Among task states, attention is thought to preserve the structure of brain networks while affecting between-network connectivity (Golland et al., 2008). During an attentional task, respect to rest, some brain areas, the so-called network "hubs", show differential connectivity to a specific network, e.g. the posterior middle frontal gyrus, superior and inferior parietal lobule shift from the DMN to the DA, whereas the temporoparietal junction, areas in the cingulated and anterior insula shift from the DA to the DMN (Bray et al., 2015). A set of flexible regions can be identified near the DA, DMN and in the borders of the visual network (VIS), showing stronger connectivity with different networks depending on task, and thus mediating communication among different networks. In addition, the salience network, which can be identified in the dorsal anterior cingulated area and the anterior insula (Menon and Uddin, 2010, Di and Biswal, 2014), seems to play an important role in networks connectivity, activating executive networks and deactivating the DMN (Di and Biswal, 2014). The mechanisms behind these functional switching are still unknown, yet an hypothesis exists sustaining a phase synchronization of neural oscillations modulation to transiently organize large-scale networks (Miller and Buschman, 2013). Phase synchronization within task-specific networks is greater when attention is focused on an external task, whereas that within the DMN should be greater for inward oriented attention (Kirschner et al., 2012). It is likely that interactions among networks during attention tasks may be regulated via synchronized oscillations, thus synchrony could be used to change effective connectivity between areas (Kirschner et al., 2012). Recently, it has been shown that visuospatial attention induces a reorganization of connectivity within and between VIS and DA: compared to rest, the internetwork connectivity was enhanced, especially in top-down direction, while intranetwork instantaneous connectivity was reduced within VIS, but not within DA, suggesting that ongoing activity in DA is a needed prerequisite for attention (Spadone et al., 2015). In our study, we expanded

these results and we further characterized the modulations of visuospatial attention on whole brain networks.

Lateralization of Attention Function. The brain cognitive function of attention is commonly considered to be lateralized, with the right hemisphere specialized for attention. Support comes from studies on patients suffering from spatial neglect after lesions in the right hemisphere (Mesulam, 1981, Corbetta et al., 1993, Vallar, 1998, Gitelman et al., 1999, Heilman et al., 2000), 'pseudoneglect' results on healthy subjects (Jewell and McCourt, 2000) and structural analyses (Koch et al., 2011, Thiebaut de Schotten et al., 2011, Szczepanski et al., 2013). However, the neurophysiological substrates of this asymmetrical distribution are still largely unknown, it is still not clear which specific aspects of attention are lateralized and which of the hemisphere is indeed specialized in particular attentional functions due to equivocal results in functional imaging studies (Corbetta and Shulman, 2002, 2011). Previous neuroimaging findings from both task-state and resting-state studies support a strong lateralization of the VA to the right hemisphere (Corbetta et al., 1993, Nobre et al., 1997, Fox et al., 2006a, Corbetta and Shulman, 2011, Markett et al., 2014), yet the DA is still considered to be bilaterally distributed. The spatial deficits observed in neglect studies are closely related to the functional role of the DA, supporting Heilman's hemispatial theory, according to which the right hemisphere is dominant for spatial attention, mediating attention shifts to both hemispheres, whereas the left hemisphere exclusively mediates attention shifts to the contralateral hemisphere (Heilman and Van Den Abell, 1980). On the other hand, inconsistent results from neuroimaging studies seem to support Kinsbourne's opponent processor model, depicting each hemisphere as responsible for attention biases to the contralateral hemifield in an interhemispheric competition scenario (Kinsbourne, 1977). Impairments in functions of the dorsal system might be caused by disruptions of interactions between the DA and the damaged VA during neglect (Duecker et al., 2013, Chechlacz et al., 2015, Wang et al., 2015). Further investigations on the functional differences within the DA, and functional interactions between dorsal and ventral systems are needed.

The Aim of the Study. In this study, we investigated the modulations of attention on the whole brain networks during a continuous visuospatial attention task. We specifically designed a lateralized covert[15] attention task to assess the rightward asymmetry of the dorsal attention network across the hemispheres during a simple checkerboard visual stimulation. A functional localizer was included to activate cortical areas involved in visual processing and obtain subject specific visual

[15] Covert orienting is the act to mentally shifting one's focus without moving one's eyes.

networks, separating lateralized networks as a function of the stimulation side during a unilateral visual stimulation. Whole brain networks were obtained from a resting-state acquisition. Finally, two steady-state runs of covert attention task during bilateral visual stimulation were included, differentiating for the side of attention, to asses asymmetric attentional modulations on brain networks. Using the effect of the side of attention and the effect of the hemisphere as different main factors in a flexible factorial design, we formally tested the hypothesis that the asymmetry in brain activation during the spatial attention task is caused by an asymmetric control of spatial attention. We also assessed the effects of the interaction among these factors, namely what we call the effect of the *coherence* of the attention spot with the hemisphere (attention to the left/right hemifield in relation to the right/left hemisphere), due to the retinotopically specific properties of attentional modulations. Whereas previous imaging studies testing for hemispheric asymmetries in DA during spatial selective attention found little evidence of right hemisphere dominance (Corbetta and Shulman, 2011, Vossel et al., 2014) on healthy subjects, we found attentional asymmetric effects on dorsal areas and on between-network connectivity modulation.

Methods

SUBJECTS. Fifteen healthy subjects (mean age ± SD = 25 ± 6, 5 females) gave informed written consent to participate in this study, according to the Helsinki declaration and to European Union regulations. Of these, one was excluded because he did not complete the task, and 4 were not included in the analysis due to image quality or behavioral performances issues. All participants had normal or corrected-to-normal vision, and all except two were right handed. Exclusion criteria included any known vascular and neurological disease. The study was carried out following a protocol approved by the local Ethics Committee and in accordance with the Declaration of Helsinki.

EXPERIMENTAL PARADIGM. The study included three different functional acquisitions: functional localizer, steady-state (i.e., sustained stimulation) and resting-state scans.

VISUAL STIMULATION. The visual stimulus consisted of a circle-shaped (3° of radius) white-black rotating (2 cycles/s) checkerboard positioned either alternatively (during functional localizer) or simultaneously (during steady-state scans) in the left and right hemifield at 4° of horizontal decentering, with a uniform grey background. The checkerboards changed rotation direction with period ranging uniformly between 1 and 3 s. During bilateral stimulation, the checkerboards changed

direction independently. Stimulations were delivered during functional scans using a digital light processing projector located outside the MR scanner room and projecting the stimulus on a screen positioned on the magnet bore. The subject viewed the stimulus projected behind him via a mirror fixed to the head coil. A 4-button box was also provided to the subject in order to perform tasks.

Functional Localizer. The unilateral stimulation condition is included in the block-designed paradigm used during the functional localizer, and alternated for both hemifields to a condition of rest to obtain lateralized subject specific areas of visual response to the chosen stimuli. To keep fixation, attention and arousal, the centre of the screen was identified by a white cross rotating by 45° with a random period ranging uniformly between 1.5 and 4.5 s. Subjects were asked to press a button whenever the cross rotated. Stimulation cycle consisted in 3 epochs of 30 seconds each: right hemifield checkerboard, left hemifield checkerboard, and rest (i.e., central cross only). The whole run consisted of four cycles, for a total of 12 epochs and 6 min duration.

Steady-State Acquisition. Rotating checkerboards were presented simultaneously and continuously in each hemifield during the steady-state runs to elicit a uniform response in visual areas, differentiating only for the side of attention. The spatial attention task consisted in detecting changes in rotation direction of one of the two checkerboard, while ignoring changes in the other one. A white arrow (1° degree size) at the centre of the screen identified the fixation point. The subjects were asked to keep fixation on the central arrow and maintain the attention to the checkerboard indicated by the arrow (that did not change orientation during the run), without shifting the gaze (covert spatial orienting). Subjects were instructed to press the button for every change in rotation direction of the cued checkerboard. Two steady-state runs were performed by each subject, with cued attention either to the left or to the right checkerboard. The order of the two sessions was randomized between subjects. Each run had a duration of 12.4 min.

Resting-State Acquisition. The resting-state run was performed between the two different steady-state runs, with a duration of 12.4 min. The subjects were required to keep eyes closed and relax without falling asleep.

Subject Behavior. The subject's gaze was monitored during the functional runs through an eye-tracking system (Applied Science Laboratories, model 504) equipped with remote pan/tilt optic infrared module and a video camera that was custom-adapted for use in the scanner. Calibration was performed for each subject. All signal traces were linearly interpolated and smoothed (after an up-sampling to 1 kHz) by a boxcar filter (width ±25 ms). To correct for motion shifts, motion parameters

from the corresponding fMRI series were regressed out from signal timecourses. Peristimulus gaze position average (800 ms-wide) was computed to evaluate systematic gaze shifts.

Subject's performance during the steady state task was assessed by means of response time and error rate recording. Subject's responses were considered valid if falling inside a 700 ms window after stimulus onset.

IMAGE ACQUISITION. All images were acquired on a 3T MRI Scanner (Siemens Magnetom Allegra) equipped with a standard birdcage coil. T1-weighted anatomical images were acquired as reference using a Magnetization-Prepared Rapid Acquisition Gradient Echo (MPRAGE) sequence (TR = 2150 ms, TE = 2.48 ms, TI = 1000 ms, Flip Angle = 8˚, voxel size = 1x1x1 mm^3, FOV = 256x160 mm^2). Functional images were acquired with a Gradient Echo-Echo Planar Imaging (GE-EPI) sequence, which was different for the functional localizer (TR = 2000 ms, TE = 30 ms, Flip Angle = 80˚, voxel size = 3x3x3.75 mm^3, FOV = 192x192 mm^2) and the steady-state or resting-state runs (TR = 3100 ms, TE1/TE2/TE3 = 16, 39, 63 ms, Flip Angle = 85˚, voxel size = 3x3x3.75 mm^3, FOV = 192x192 mm^2). Multiecho acquisition was chosen for network-related acquisition to improve sensitivity and minimize the effects of physiological noise (Kundu et al., 2012, Kundu et al., 2013). Parallel imaging and partial k-space sampling were avoided by leveraging the high gradient performances (rise time 100 μs to reach a maximum amplitude of 40 mT/m).

IMAGE PREPROCESSING. Processing steps included pipelines, functions and programs from the packages SPM8 (Wellcome Trust Centre for Neuroimaging, London, UK), FSL and EASYREST.

Steady state and resting state scans were corrected for physiological noise, according to the RETROICOR method (Glover et al., 2000). Global signal regression was not performed to avoid possible spurious negative correlations (Murphy et al., 2009).

All functional volumes were realigned to correct for head movements (SPM). Single echo data were realigned to the average image. For multiecho scans, the echoes acquired at each time point were provisionally averaged, realignment was estimated as per single echo images and the relevant parameters were applied separately to each echo time series. Echoes were finally averaged with an optimized voxel-by-voxel weighting scheme (Posse et al., 1999), after estimation of voxel T2* from the data (custom Matlab routine).

Volumes were corrected for slice acquisition time and coregistered to each participant's MPRAGE anatomical scan (SPM). Anatomical images were segmented

into grey matter, white matter and cerebrospinal fluid, and the resulting parameters were used to normalize images to the standardized MNI space (SPM). Smoothing (6x6x6mm^3 Gaussian Kernel) was applied to the functional scans (with SPM), and finally steady-state data were band-filtered (0.008-0.09 Hz) (AFNI).

Analysis: Functional Localizer Data. Lateralized visual ROIs were obtained from the functional localizer, to be later exploited as seeds in the analysis of steady-state functional data.

The BOLD signal during the task period was analysed with the general linear model (GLM) by modelling the functional response to the unilateral stimulation condition voxel-by-voxel as the convolution of the standard hemodynamic response function with the stimulation paradigm. The functional region responding to the localizer task was identified by a two-tailed, one-sample *t*-test for each stimulus condition (SPM). Two subject-specific ROIs in the most activated area were defined, one for each stimulus condition, i.e., for each stimulated hemifield. Each ROI was built by growing a sphere around the peak t-voxel, until it included 33 voxels, with the constraint of including only voxels activated at the threshold of $p < 0.001$ (custom Matlab routine).

Analysis: Resting-State Data. A multi-session independent component analysis (ICA) was run in the time domain on resting state data using the Melodic FSL Toolbox (Beckmann and Smith, 2004), and a hierarchical clustering on the resulting components was carried out using FSLNets and dual regression (Beckmann et al., 2009). Frontoparietal network (FP), ventral occipital network (VOCC), saliency network, posterior parietal network (PPC), visual network (VIS) and default-mode network (DMN) were identified among ICA components and divided for hemisphere to be later exploited as seeds in the analysis of steady-state functional data.

Analysis: Steady-State Data. Modulations in LFFs induced by covert attention were studied at two different spatial scales: 1) network-to-voxel and 2) network-to-network analysis.

Network-to-Voxel. Analysis. A seed-to-voxel correlation analysis was performed on steady-state data using EASYREST. Subject-specific visual ROIs and the networks derived by ICA were used to obtain subject-specific networks for each attentional condition (left or right). Results were reported in Fisher's z and then converted into z-score.

The asymmetric effect of attention was tested through a factorial design, whose model was made of 2 factors (hemisphere and side of attention), 2 levels each (left and right), and the interaction effects of the coherence of attention. Attention was

defined as coherent when it is oriented towards the hemifield contralateral to the ROI selected as seed to obtain brain networks, and incoherent when ipsilaterally oriented. Resulting maps were corrected for multiple comparisons based on clustering. The actual clustering parameters, corresponding to a given cluster level p-value, was estimated by the AFNI program AlphaSim.

NETWORK-TO-NETWORK. ANALYSIS. Whole cortex average network to network connectivity analysis was performed using a different parcellation approach. Resting state runs in MNI space were functionally parcelled with a 2 level approach into 200 ROIs, (100 for each hemisphere), according to a criterion of similarity between voxel time courses (Craddock et al., 2012). The resulting ROIs where then classifieds according to a maximum overlap criterion into one of 7 standard networks, namely VIS, somatomotor (SM), DA, ventral attention (VA), limbic (LIM), FP, and DMN (Yeo et al., 2011). Connectivity between each couple of ROIs was evaluated as Pearson correlation between couples of timeseries obtained by averaging the timeseries of each voxel within the ROI, and finally connectivity between couples of networks was calculated averaging the z- transformed correlation coefficients corresponding to connectivity between ROIs belonging to the relevant couple of networks. This two-step approach is intermediate between averaging the connectivity between each couple of voxels or averaging the timecourses within the whole networks and then calculating the correlation, and is expected to preserve the homogeneous properties of each ROIs (Craddock et al., 2012).

Results

PERFORMANCE. As expected, covert attention affected target discrimination accuracy leading to a group-average accuracy level around 90% for both condition (Figure 4.6 Group-level behavioral data in the steady-state conditions. A) Group-level accuracy in detecting the motion of the attended (valid) and not attended (invalid) target (i.e., checkerboard). As expected, accuracy level for the invalid target was consistent with the chance level (35%). B) Group-level response delay in detecting the motion of the attended target. No attention direction effect (i.e., leftward or rightward) was reported for motion detection of the valid target, neither in the accuracy nor in the response delay measure (paired t-test, left vs right $t = 1.07$ $p = 0.31$ and $t = 0.40$ $p = 0.70$, respectively).Figure 4.6). Direction of attention, leftwards or rightwards, did not affect the accuracy level nor the response delay (paired t-tests; $t = 1.07$ $p = 0.311$ and $t = 0.40$ $p = 0.697$, respectively).

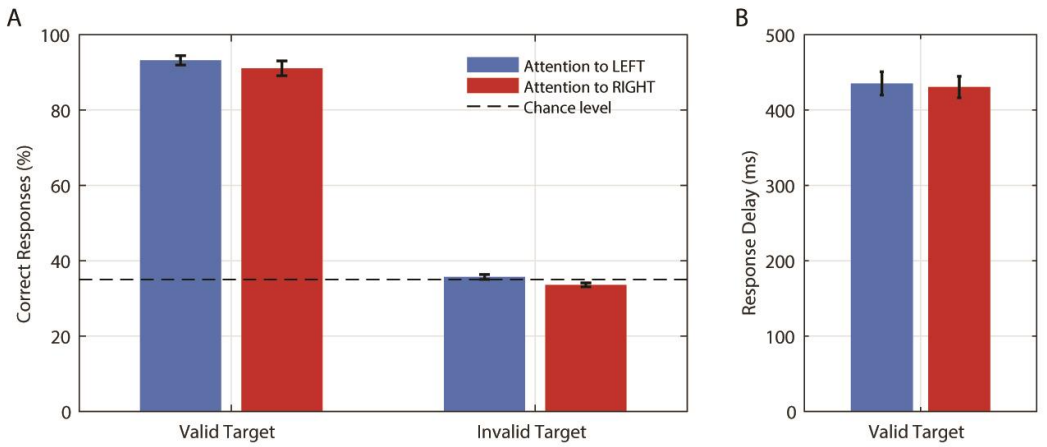

Figure 4.6 Group-level behavioral data in the steady-state conditions. A) Group-level accuracy in detecting the motion of the attended (valid) and not attended (invalid) target (i.e., checkerboard). As expected, accuracy level for the invalid target was consistent with the chance level (35%). **B**) Group-level response delay in detecting the motion of the attended target. No attention direction effect (i.e., leftward or rightward) was reported for motion detection of the valid target, neither in the accuracy nor in the response delay measure (paired t-test, left vs right $t = 1.07$ $p = 0.31$ and $t = 0.40$ $p = 0.70$, respectively).

The possibility of any significant modulation on attentional level due to the prolonged acquisition time (12.4 min each run) was ruled out by analysis of behavioral data during sub intervals of time (Figure 4.7).

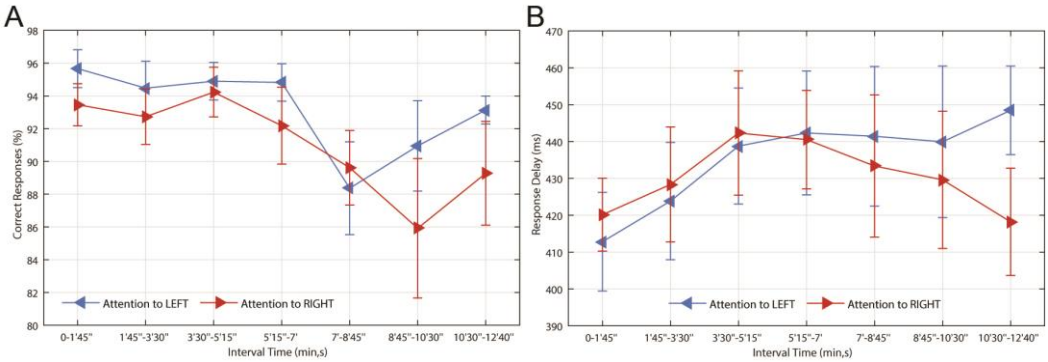

Figure 4.7 Group-level behavioral data in the steady-state conditions with a finer temporal resolution. Relevant behavioral data were recomputed dividing the whole acquisition (12.4 min) in 7 temporal intervals. **A**) Group-level accuracies and **B**) response delays in detecting the motion of the attended target. No significant time-induced modulation in behavioral data was found (ANOVA, Accuracy: attention to left $F = 2.11$, $p = 0.064$; attention to right $F = 1.32$, $p = 0.262$; Response Delay: attention to left $F = 0.57$, $p = 0.749$; attention to right $F = 0.34$ $p = 0.910$).

Eye movement analysis confirmed that subjects were able to maintain the gaze on the central fixation arrow (Figure 4.8). Peristimulus averages plot of eye fixation point shows a consistent eye position, not significantly affected by the target onset (i.e, the change in rotation direction of the attended checkerboard).

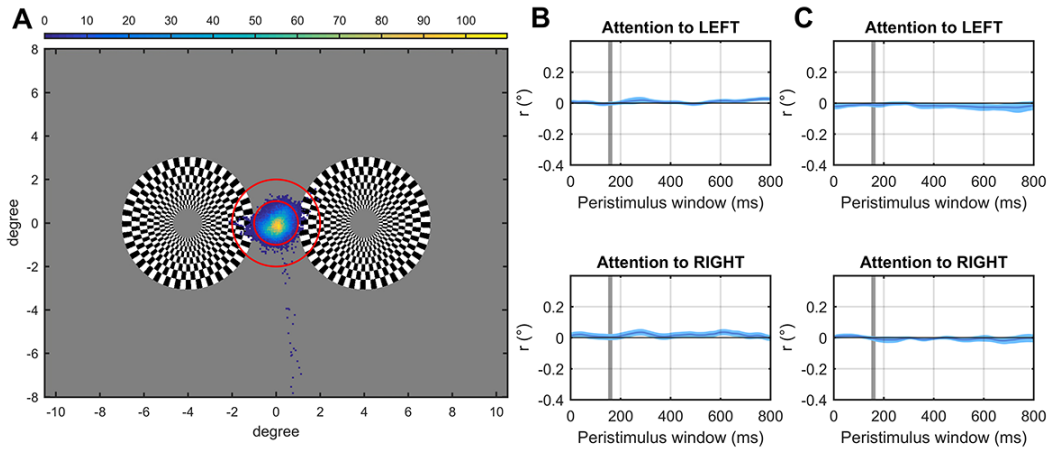

Figure 4.8 Eye movements recording. **A**) Eye positions overlapped onto the visual stimulation for one representative subject during the covert attention to the left checkerboard. Red circles mark points which distance from the central fixation arrow (not visible) is less than one or two visual degrees. Almost all points fell into the first circle. **B**) Eye movements, expressed as the distance from the central arrow, during the peri-stimulus window for one representative subject and **C**) the average across subjects. The vertical grey line marks the onset of rotation-direction change of the attended checkerboard.

NETWORK-TO-VOXEL: EFFECT OF SIDE OF ATTENTION. We found a positive effect of leftward respect to rightward oriented attention in the network derived from PPC seed. The effect is evident in high-level right visual areas (Figure 4.9), showing that connectivity of right visual areas to PPC is enhanced while subjects attend to the left hemifield.

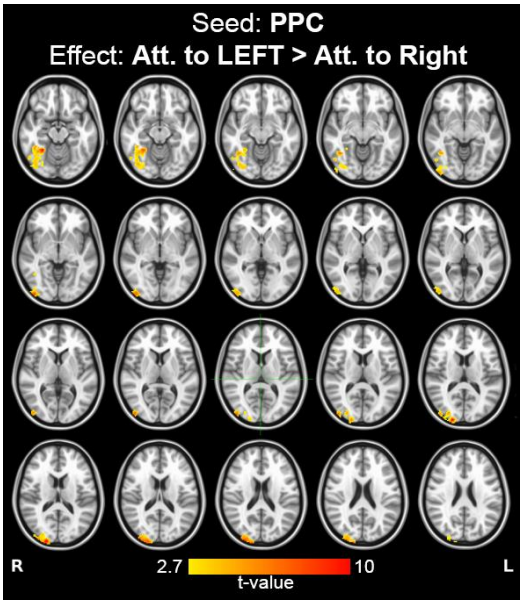

Figure 4.9 Network-to-voxel effect of attention side. Seed was placed in the PPC network derived from ICA analysis. Right superior visual areas enhance their connectivity to the PPC when attention is directed to the left hemifield.

EFFECT OF COHERENCE. An interaction effect of stimulation coherence was apparent in brain areas specifically involved in visual attention processing. Voxelwise analysis showed increased correlation with VIS (as identified by ICA) during coherent compared to incoherent attention in the bilateral superior parietal lobule, right inferior parietal lobule, right anterior-intraparietal sulcus and right middle frontal gyrus (Figure 4.10A). These results support a right lateralization of the attention control in brain areas belonging to the dorsal attention network.

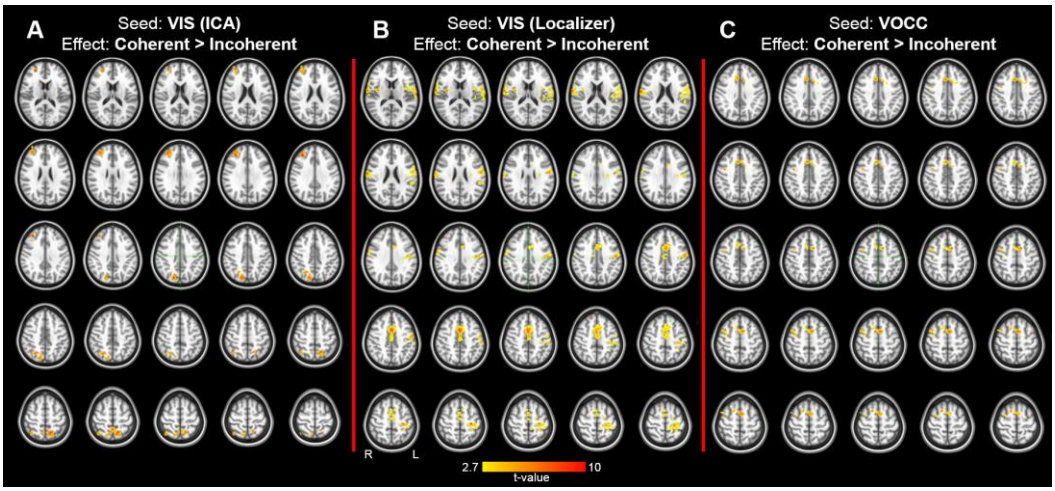

Figure 4.10 Network-to-voxel effect of coherence. Seed in **A**) visual network derived from ica anaylysis, **B**) visual network derived from functional localizer analysis, **C**) VOCC (derived from ICA). Clusters of significant effect (p <0.05 corrected) identify areas which connection with the seed is higher in the coherent condition compared to incoherent condition.

Analogous results were obtained using subject's specific visual ROIs from functional localizer. Visual areas retinotopically matched to the attentional stimulus showed increased correlation during coherent than incoherent attention with the anterior cingulate gyrus, paracingulate, bilateral inferior parietal lobule and left visual areas V2, V3 and V4 (Figure 4.10B). Finally, an effect of the coherence of attention with VOCC (ICA based) was evident in the frontal eye field, the right superior and middle frontal gyrus (Figure 4.10C).

NETWORK-TO-NETWORK. During resting state the brain showed the well-known pattern of self-organization of low frequency oscillation in patterns that strictly followed the boundaries of the networks identified by Yeo and colleagues (Yeo et al., 2011). Strikingly high and uniform internal correlations were found in all networks, and especially within VIS, SM and LIMB. DMN was characterized by the know bipartition into an anterior and a posterior area. A complex pattern of between-networks correlations was also observed. (Figure 4.11).

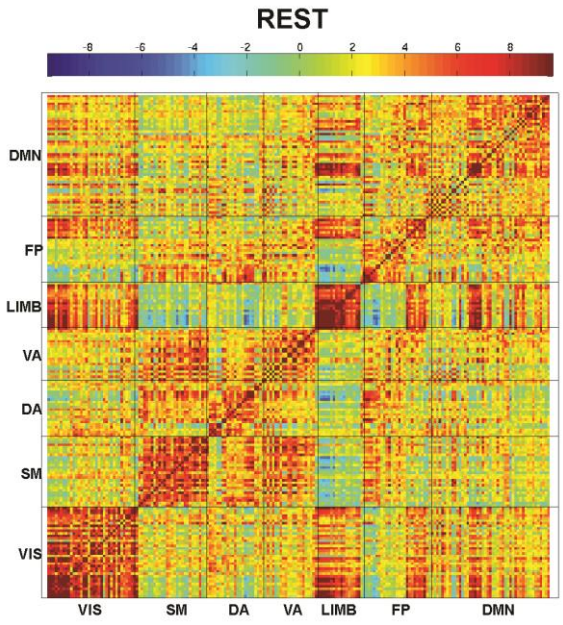

Figure 4.11 ROI based functional connectivity of the whole brain during resting state. ROIs are classified within networks and then ordered from posterior to anterior within each network, according to their center of mass. Note the apparent subdivision of DMN in 2 areas, one (smaller) posterior and one (larger) anterior, each strongly correlated within itself. A similar bipartition was observed within the fronto-parietal network, where the internal subdivision was reflected also in different patterns of correlation between networks: the frontal section was indeed more correlated with LIMB and VIS, while the rostral (parietal) area was more correlated with somatomotor and attentional networks.

EFFECT OF SIDE OF ATTENTION. Attention to left induced a higher whole brain connectivity compared to attention to right, in particular between VIS and attention networks. The connectivity within DMN and between DMN and the other networks was the less affected by the side of attention (Figure 4.12).

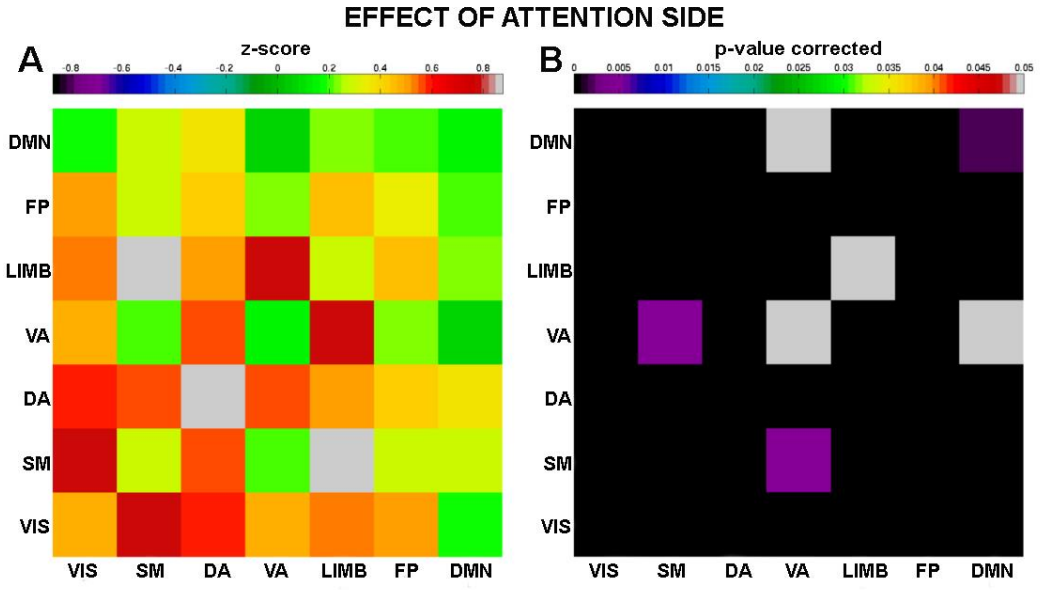

Figure 4.12 Network-to-network effect of attention side. A) Differential effect of attention to left vs attention to right, averaged in the 7 networks. B) Corresponding p-value, Bonferroni corrected. Attention to left induced a widespread increase of correlation across networks.

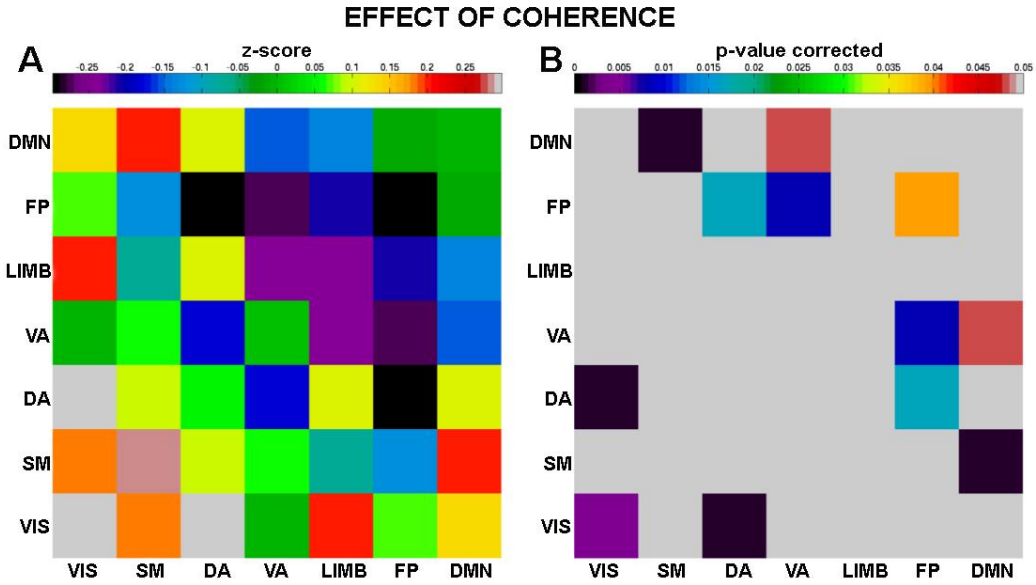

Figure 4.14 Network-to-network effect of coherence A) effect at network level of coherent attention and B) relevant p-value. The result is obtained by mixing results of both hemispheres, i.e., considering both the change of connectivity in the left hemisphere during attention to right vs attention to left, and change of connectivity in the right hemisphere during attention to left vs attention to right.

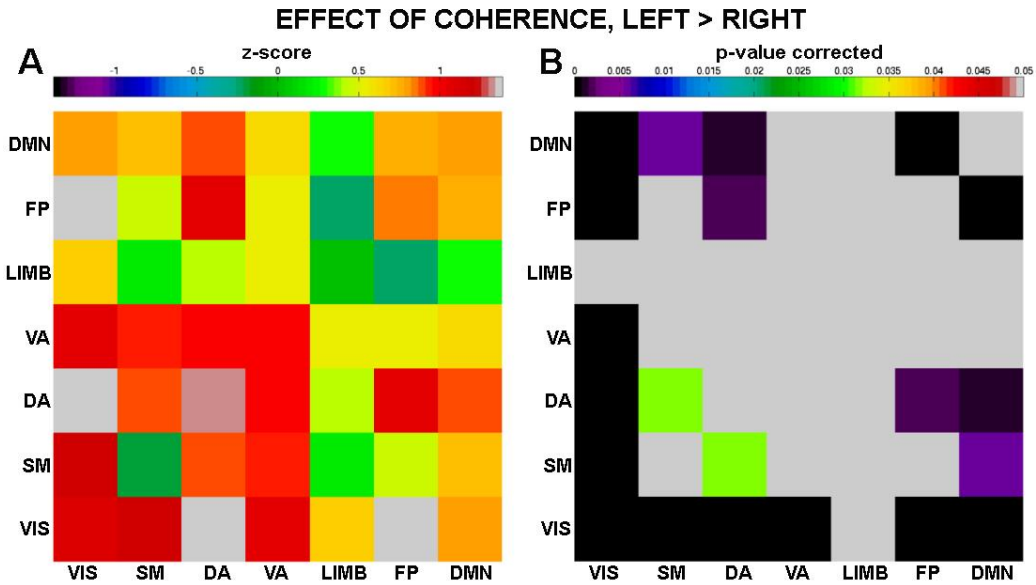

Figure 4.13 Network-to-network effect of coherence as a function of the hemishpere. Differential effect of coherent attention between left and right attention (or – equivalently- between right and left hemisphere). The panels show the differential effect between the change of connectivity induced by a coherent attention to left (in the right hemisphere) and the change in connectivity induced by coherent attention to right (in the left hemisphere). A) Average z-score and B) corrected (bonferroni) p-values.

EFFECT OF COHERENCE. Coherent attention had a more localized effect. In particular, coherence enhanced connectivity within VIS and between VIS and DA (Figure 4.14). The effect of coherent attention was markedly higher when attention was to left, i.e., when right hemisphere was involved (Figure 4.13). The positive effect of coherent attention to left was especially strong between VIS and the other networks.

Discussion

In this study we characterized the effect of stationary visuospatial attention on whole brain networks. The counterbalanced lateralized experimental design we used allowed us to disentangle the intrinsic hemispheric asymmetry of attention from the specific effects induced by coherency between lateralized networks and the stimulated hemisphere (i.e., the hemisphere contralateral to the attentional task).

Network-to-voxel based analysis suggested an asymmetric effect of lateralized attention at least on the PPC network, with right secondary visual areas more connected with PPC during visuospatial attention to left, indicating a lateral asymmetry of the attentional control (Figure 4.9). The effect was confirmed by network-to-network based analysis showing an overall enhancement of within and between network connectivity during attention to left compared to attention to right. The effect was especially strong in attentional and visual networks, while was less pronounced in DMN (Figure 4.12).

Connectivity during coherent visuospatial attention was enhanced, as expected, within the visual network, where retinotopic matching of visuospatial attention to stimulated areas is known to elicit a coherent, strong enhancement of BOLD response (Hougaard et al., 2015). Our results, however, highlighted also an increase of connectivity between dorsal attention and visual networks contralateral to the stimulated hemisphere (Figure 4.10), extending previous results (Spadone et al., 2015) with the direct evidence that the enhanced connectivity during visuospatial attention is an intrinsic, lateralized feature, sustained in time and governed by retinotopic matching of attention to visual target. Our findings on the effect of attentional coherence not only support an effect of attention on brain networks, but also strongly support a hemispheric asymmetry of attentional modulation. Specifically, the asymmetry is evident in dorsal network areas involved in the attentional control. A functional asymmetry in the control of spatial attention is still under debate. Evidence from both neuropsychological and anatomical studies argue in favour of right hemispheric dominance for visuospatial attention, reporting an impaired attentional control in patients with lesions in right frontoparietal areas and a larger tract in the right hemisphere respectively (Mesulam, 1981, Corbetta et al., 1993, Vallar, 1998, Gitelman et al., 1999, Heilman et al., 2000, Koch et al., 2011,

Thiebaut de Schotten et al., 2011, Bartolomeo et al., 2012, Szczepanski et al., 2013, Caeyenberghs and Leemans, 2014). Although there is evidence for such asymmetries in the ventral attention system, functional imaging studies thus far have failed to consistently reveal lateralization of attentional processes within the dorsal frontoparietal network, whose core nodes are recognized to be the frontal eye field and the interaparietal sulcus.

These results were broadly confirmed by ROI based connectivity that clearly showed a lateralized pattern of connectivity increase when attention is coherently directed (albeit intrinsically unable to identify specific regions where coherent attention effect was asymmetric). Indeed, while coherent attention (irrespectively of the hemisphere) increased connectivity between dorsal attention network and visual and frontoparietal networks (Figure 4.14), coherent attention to left (in the right hemisphere) had a stronger effect of coherent attention to right (in the left hemisphere) in a set of lateralized networks, including almost all networks with VIS and, among others, between frontoparietal and dorsal attention networks (Figure 4.13).

Our results clearly indicate an asymmetric effect of spatial attention in dorsal frontoparietal brain areas (Figure 4.10). Recent research has clearly demonstrated that dorsal frontoparietal areas can causally modulate the activity of visual areas. The higher correlation found between frontoparietal and occipital networks when attention was coherent confirms a strong effect of attention on internetwork cooperation to keep performances.

CONCLUSIONS. In this work we examined the effect of visual spatial attention on brain networks. We obtained results, including within-network and between-network metrics, consistently pointing towards a functional asymmetry of mechanisms related to visual attention at network level, in a fashion that involves a large volume of the brain. In particular, we investigated the sensory visual network, the cognitive attention network and the default mode network and observed that right-hemispheric brain areas in the attentional networks show enhanced connectivity for coherent rather than incoherent attention. Thus, our results clearly demonstrate that attentional asymmetric effects can be tracked at network level by functional MRI, supporting and extending previous findings in favour of a right hemispheric dominance of the visuospatial attention control in a cohort of healthy subjects.

CHAPTER 5

Conclusions

The aim of the present work was to provide more insights into the spontaneous BOLD LFFs that characterize the brain. Our findings showed that the intrinsic brain's activity is modulated under a wide range of conditions, including different physiological behavioural states – such as sustained working memory and visuospatial attention tasks - and in neurodegenerative dementia. The induced modulations are characterized by complex adjustments detectable towards different metrics.

First, given the complexity of extracting relevant information from an intrinsic noisy BOLD signal, we extensively optimized processing and analysis methods. Such efforts led to development of EASYREST, an automatized matlab "pipeline" for studying spontaneous BOLD fluctuations. As it happened in our laboratory, we believe that other groups would greatly benefit from the simplicity and efficiency of such tool. Indeed, aside from the obvious advantage of an optimized and advanced analytic tool, an automatized processing can reduce inadvertent mistakes especially in cumbersome data.

Once established the methodological tools, we next aimed to answer to several open questions regarding the spontaneous activity of the brain. First, a very essential question was whether and how the brain relates the two classes of information that can be extracted from LFFs, the functional connectivity and the oscillation amplitude. Our results obtained in a cohort of healthy elderly showed a positive linear coupling in brain areas known to belong from the most globally connected regions. The physiological relevance of the coupling was supported by the disruption of the relation by neurodegenerative dementia, even in its prodromic stage. Although further investigations in other population groups, such as young and adult healthy people, are required to endorse the physiological origin of the coupling, this outcome demonstrated the critical role of the oscillation amplitude in sustaining the synchronization among brain regions.

Much work still need to be done to clarify the mechanism behind such coupling. First, further research needs to address the contribution of spiking and synaptic activity at the origin of spontaneous BOLD LFFs. This is a crucial point in understanding why the increased local activity results in an increase in global connection. In addition, the voxel composition can influence the interpretation, indeed, it can be conceived as composed of a single processing unit or of multiple parallel computing units working independently. Although with the fMRI we have shown the existence of a physiological coupling between the two facets of spontaneous BOLD LFFs, the sole technique cannot solve the complex puzzle behind the phenomenon, multimodal approach, such as a combination of fMRI and direct electrophysiological recordings, is required.

Among the outcomes of this study we collected evidence supporting the notion that the Alzheimer's disease is primarily a disconnection syndrome. We took advantage of this notion and looked at the connectivity alterations underpinning the commonly reported semantic deficits. Our results pointed to the left posterior middle temporal region, a crucial area for language comprehension and production. It is important to stress that this finding concerns an alteration in the intrinsic brain's functional architecture, differently from previous studies it is not biased by stimulus type or attention level. Additional research can possibly clarify whether the affected area is a primary target of the pathology or undergoes a lack of upstream feed-forward connections. For this purpose, more insights can be obtained combining functional and structural connectivity, the latter by means of diffusion tensor imaging, another non-invasive MRI-based technique; or by assessing the cortical integrity of the region through voxel-based morphometry.

How spontaneous BOLD LFFs are modulated during the continuous performance of a task is an intriguing question for understanding the brain's functionality. Our findings indicated that the brain remarkably reshapes its functional architecture adjusting its internal connections and the relative oscillation amplitude when focused on the external world. The completely different behaviour in the two states suggests that processes happening at rest are reduced or even suspended during task execution. In fact, the reduction of oscillation amplitude suggests a reduction in energy consumption of LFFs during sustained stimulation.

Considering that BOLD signals reflect both the vascular and the metabolic response to brain's activity, direct assessment of cerebral metabolic oxygen consumption ($CMRO_2$) is required to further support our findings. While absolute quantification of $CMRO_2$ by means of MR techniques can hardly be achieved, fractional $CMRO_2$ changes can be easily obtained combining BOLD acquisitions and perfusion measures during hypercapnia conditions. Thus, comparing different cognitive states is possible to assess the task-induced variation in the brain's metabolic activity. Of course, the experimental paradigm must be carefully designed to allow the separation of the intrinsic brain activity from the task-evoked response, which it is already known to produce an increase in local energy consumption.

From the inspection of relevant networks, we also reported an asymmetric effect of visuospatial attention, something that was suggested by lesions studies but that task-based fMRI failed to detect. On the whole, our findings obtained during sustained stimulations clearly showed two important facts. First, the brain responds to external stimuli not only activating specialized brain regions, as highlighted by task-based fMRI, but also reshaping its intrinsic activity at the network level. Thus, the concept of functional brain mapping should be slight reconsidered. Indeed, task-based fMRI, although extremely useful to locate high specialized areas, cannot detect the entire "functional activation" that might involve several brain networks, or possibly the entire cortex. Second, the counterpart of this fact is that the brain's ongoing activity is not a stable feature, but depends on the type of steady state used during data acquisition. Therefore, an exhaustive picture of such phenomenon cannot be achieved by looking exclusively at the resting brain. The intrinsic activity of the brain when it is focusing on the external world is an important part of this complex conundrum and cannot be overlooked.

Overall, in the present work we demonstrated the great potentiality embedded in the spontaneous BOLD LFFs. Through a non-invasive measure, simply acquiring specific MR images, we can access to the most energetic demanding component of the brain activity, a fundamental window into the mechanisms behind cognition.

Surely, the technique presents some limitations, first of all the fact that is an indirect measure of the intrinsic brain activity. It is clear that the potentialities of spontaneous BOLD LFFs can be fully exploited only in a multimodal framework, as we plan to do in future developments following the indications suggested from this work. Nonetheless, the sole resting/steady-state fMRI techniques has proved to be a sophisticated tool for studying modulatory mechanisms induced by pathological and physiological conditions.

Publications

Full Papers

M. DiNuzzo, D. Mascali, B. Maraviglia, L. Serra, M. Bozzali, F. Giove. Decreased parietal but increased frontal amplitude of low-frequency fluctuations of blood oxygenationcoexists with the widespread loss of functional connectivity in Alzheimer's disease. *Biophysics and Bioengineering Letters* 01/2014; 7(2).

D. Mascali, M. DiNuzzo, M. Moraschi, M. Fratini, T. Gili, G. Garreffa, B. Maraviglia,L. Serra, M. Bozzali, F. Giove. Intrinsic Patterns of Coupling between Correlation and Amplitude of Low-Frequency fMRI Fluctuations Are Disrupted in Degenerative Dementia Mainly due to Functional Disconnectio. *PLoS One* 10.4 (2015).

M. DiNuzzo, D. Mascali, M. Moraschi, G. Bussu, B. Maraviglia, S. Mangia, F. Giove. Spatiotemporal information encoding associated with blood-oxygenation level dependent signal in resting and stimulated human primary visual cortex. *Scientific Reports* (Under revision)

D. Mascali, M. DiNuzzo, B. Maraviglia, L. Serra, M. Bozzali, F. Giove. Breakdown of the semantic network in mild Alzheimer's disease revealed by resting-state fMRI. *Journal of Alzheimer's disease* (Submitted)

G. Bussu, D. Mascali, M. DiNuzzo, S. Mangia, E. Macaluso, B. Maraviglia, F. Giove. Global reorganization of brain networks during visuospatial attention. *Human Brain Mapping* (Submitted)

S. Tommasin, D. Mascali, T. Gili, B. Maraviglia, F. Giove. Slow dynamic of resting-state recovery. *Neuroimage* (Submitted)

Abstracts and Posters

M. DiNuzzo, D. Mascali, M. Moraschi, M. Fratini, T. Gili, G. Garreffa, B. Maraviglia, F. Giove. Shannon entropy method applied to fMRI data series during evoked and resting state activity. *Proc Intl Soc Mag Reson Med*, Volume 22, 4133

M. DiNuzzo, D. Mascali, M. Moraschi, M. Fratini, T. Gili, G. Garreffa, B. Maraviglia, L. Serra, M. Bozzali, F. Giove. Rethinking correlation in the brain: a resting-state fMRI study on the progression of cognitive decline. *Proc Intl Soc Mag Reson Med*, Volume 22, 3051

D. Mascali, M. DiNuzzo, M. Moraschi, M. Fratini, T. Gili, B. Maraviglia, F. Giove. Relationship between spectral amplitude of fMRI slow fluctuations and functional connectivity in dementia. *International School on Magnetic Resonance and Brain Function (2014)*

Acknowledgments

It is a pleasure to thank the many people who made this thesis work possible. First, I want to acknowledge prof. Bruno Maraviglia, for having introduced me to his stimulating laboratory, my advisor and mentor prof. Federico Giove, for having taken me under his guidance, and the director of the PhD course, prof. Alfredo Colosimo, for his appealing approach to biophysical problems.

I am particularly grateful to the other people who collaborated with me during this PhD course. They are Dr. Mauro Di Nuzzo, Dr. Silvia Tommasin, Dr. Marta Moraschi and Dr. Michela Fratini at Enrico Fermi Center of Rome; Dr. Tommaso Gili, Dr. Laura Serra and Dr. Marco Bozzali at Santa Lucia Foundation of Rome; Dr. Alessandra Caporale, Dr. Giogia Bussu, Ilaria Suprano and Matteo Ippoliti at Department of Physics of Sapienza, University of Rome.

References

Ahmed S, Arnold R, Thompson SA, Graham KS, Hodges JR (2008) Naming of objects, faces and buildings in mild cognitive impairment. Cortex 44:746-752.

Al-Aidroos N, Said CP, Turk-Browne NB (2012) Top-down attention switches coupling between low-level and high-level areas of human visual cortex. Proc Natl Acad Sci U S A 109:14675-14680.

Albert NB, Robertson EM, Miall RC (2009) The resting human brain and motor learning. Current Biology 19:1023-1027.

Alzheimer A, Stelzmann RA, Schnitzlein HN, Murtagh FR (1995) An English translation of Alzheimer's 1907 paper, "Uber eine eigenartige Erkankung der Hirnrinde". Clin Anat 8:429-431.

Andersson JL, Hutton C, Ashburner J, Turner R, Friston K (2001) Modeling geometric deformations in EPI time series. Neuroimage 13:903-919.

Appell J, Kertesz A, Fisman M (1982) A study of language functioning in Alzheimer patients. Brain Lang 17:73-91.

Ashburner J, Friston KJ (2001) Why voxel-based morphometry should be used. Neuroimage 14:1238-1243.

Ashburner J, Friston KJ (2005) Unified segmentation. Neuroimage 26:839-851.

Association As (2014) 2014 Alzheimer's disease facts and figures. Alzheimers Dement 10:e47-e92.

Astell AJ, Harley TA (1996) Tip-of-the-tongue states and lexical access in dementia. Brain Lang 54:196-215.

Auer DP (2008) Spontaneous low-frequency blood oxygenation level-dependent fluctuations and functional connectivity analysis of the 'resting' brain. Magn Reson Imaging 26:1055-1064.

Auriacombe S, Lechevallier N, Amieva H, Harston S, Raoux N, Dartigues J-F (2006) A longitudinal study of quantitative and qualitative features of category verbal fluency in incident Alzheimer's disease subjects: results from the PAQUID study. Dement Geriatr Cogn Disord 21:260-266.

Baldo JV, Schwartz S, Wilkins D, Dronkers NF (2006) Role of frontal versus temporal cortex in verbal fluency as revealed by voxel-based lesion symptom mapping. J Int Neuropsychol Soc 12:896-900.

Baria AT, Baliki MN, Parrish T, Apkarian AV (2011) Anatomical and functional assemblies of brain BOLD oscillations. J Neurosci 31:7910-7919.

Barkhof F, Haller S, Rombouts SARB (2014) Resting-state functional MR imaging: a new window to the brain. Radiology 272:29-49.

Barth M ME (1997) Proton NMR relaxation times of human blood samples at 1.5 T and implications for functional MRI. Cell Mol Biol (Noisy-le-grand) 43:783-791.

Bartolomeo P, Thiebaut de Schotten M, Chica AB (2012) Brain networks of visuospatial attention and their disruption in visual neglect. Front Hum Neurosci 6:110-110.

Bayles KA, Tomoeda CK, Cruz RF, Mahendra N (2000) Communication abilities of individuals with late-stage Alzheimer disease. Alzheimer Dis Assoc Disord 14:176-181.

Bayles KA, Tomoeda CK, Kaszniak AW, Trosset MW (1991) Alzheimer's disease effects on semantic memory: loss of structure or impaired processing? J Cogn Neurosci 3:166-182.

Beckmann CF, Mackay CE, Filippini N, Smith SM (2009) Group comparison of resting-state FMRI data using multi-subject ICA and dual regression. Neuroimage 47:S148-S148.

Beckmann CF, Smith SM (2004) Probabilistic independent component analysis for functional magnetic resonance imaging. IEEE Trans Med Imaging 23:137-152.

Behzadi Y, Restom K, Liau J, Liu TT (2007) A component based noise correction method (CompCor) for BOLD and perfusion based fMRI. Neuroimage 37:90-101.

Berger H (1929) Über das elektrenkephalogramm des menschen. European Archives of Psychiatry and Clinical Neuroscience 87:527-570.

Binder JR, Desai RH, Graves WW, Conant LL (2009) Where is the semantic system? A critical review and meta-analysis of 120 functional neuroimaging studies. Cereb Cortex 19:2767-2796.

Birn RM, Cornejo MD, Molloy EK, Patriat R, Meier TB, Kirk GR, Nair VA, Meyerand ME, Prabhakaran V (2014) The influence of physiological noise correction on test-retest reliability of resting-state functional connectivity. Brain Connect 4:511-522.

Birn RM, Diamond JB, Smith MA, Bandettini PA (2006) Separating respiratory-variation-related fluctuations from neuronal-activity-related fluctuations in fMRI. Neuroimage 31:1536-1548.

Birn RM, Murphy K, Bandettini PA (2008) The effect of respiration variations on independent component analysis results of resting state functional connectivity. Hum Brain Mapp 29:740-750.

Biswal B, Yetkin FZ, Haughton VM, Hyde JS (1995) Functional connectivity in the motor cortex of resting human brain using echo-planar MRI. Magn Reson Med 34:537-541.

Biswal BB, Kannurpatti SS, Rypma B (2007) Hemodynamic scaling of fMRI-BOLD signal: validation of low-frequency spectral amplitude as a scalability factor. Magn Reson Imaging 25:1358-1369.

Bouvier SE, Engel SA (2011) Delayed effects of attention in visual cortex as measured with fMRI. Neuroimage 57:1177-1183.

Boxerman JL, Bandettini PA, Kwong KK, Baker JR, Davis TL, Rosen BR, Weisskoff RM (1995) The intravascular contribution to fMRI signal change: Monte Carlo modeling and diffusion-weighted studies in vivo. Magn Reson Med 34:4-10.

Bray S, Arnold AEGF, Levy RM, Iaria G (2015) Spatial and temporal functional connectivity changes between resting and attentive states. Hum Brain Mapp 36:549-565.

Brefczynski JA, DeYoe EA (1999) A physiological correlate of the 'spotlight' of visual attention. Nat Neurosci 2:370-374.

Brier MR, Thomas JB, Snyder AZ, Benzinger TL, Zhang D, Raichle ME, Holtzman DM, Morris JC, Ances BM (2012) Loss of intranetwork and internetwork resting state functional connections with Alzheimer's disease progression. J Neurosci 32:8890-8899.

Brown AS (1991) A review of the tip-of-the-tongue experience. Psychol Bull 109:204-223.

Buchsbaum BR, D'Esposito M (2008) The search for the phonological store: from loop to convolution. J Cogn Neurosci 20:762-778.

Buckner RL, Sepulcre J, Talukdar T, Krienen FM, Liu H, Hedden T, Andrews-Hanna JR, Sperling RA, Johnson KA (2009) Cortical hubs revealed by intrinsic functional connectivity: mapping, assessment of stability, and relation to Alzheimer's disease. J Neurosci 29:1860-1873.

Buxton Rb FLR (1997) A model for the coupling between cerebral blood flow and oxygen metabolism during neural stimulation. J Cereb Blood Flow Metab 17:64-72.

Buzsáki G, Draguhn A (2004) Neuronal oscillations in cortical networks. Science 304:1926-1929.

Caeyenberghs K, Leemans A (2014) Hemispheric lateralization of topological organization in structural brain networks. Hum Brain Mapp 35:4944-4957.

Caramazza A (1997) How many levels of processing are there in lexical access? Cognitive neuropsychology 14:177-208.

Cauda F, D'Agata F, Sacco K, Duca S, Geminiani G, Vercelli A (2011) Functional connectivity of the insula in the resting brain. Neuroimage 55:8-23.

Cerhan JH, Ivnik RJ, Smith GE, Tangalos EC, Petersen RC, Boeve BF (2002) Diagnostic utility of letter fluency, category fluency, and fluency difference scores in Alzheimer's disease. Clin Neuropsychol 16:35-42.

Chang C, Cunningham JP, Glover GH (2009) Influence of heart rate on the BOLD signal: the cardiac response function. Neuroimage 44:857-869.

Chechlacz M, Gillebert CR, Vangkilde SA, Petersen A, Humphreys GW (2015) Structural Variability within Frontoparietal Networks and Individual Differences in Attentional Functions: An Approach Using the Theory of Visual Attention. J Neurosci 35:10647-10658.

Christoff K, Gordon AM, Smallwood J, Smith R, Schooler JW (2009) Experience sampling during fMRI reveals default network and executive system contributions to mind wandering. Proc Natl Acad Sci U S A 106:8719-8724.

Clark LJ, Gatz M, Zheng L, Chen Y-L, McCleary C, Mack WJ (2009) Longitudinal verbal fluency in normal aging, preclinical, and prevalent Alzheimer's disease. Am J Alzheimers Dis Other Demen 24:461-468.

Cole MW, Bassett DS, Power JD, Braver TS, Petersen SE (2014) Intrinsic and task-evoked network architectures of the human brain. Neuron 83:238-251.

Cole MW, Pathak S, Schneider W (2010) Identifying the brain's most globally connected regions. Neuroimage 49:3132-3148.

Corbett F, Jefferies E, Burns A, Ralph MAL (2012) Unpicking the semantic impairment in Alzheimer's disease: qualitative changes with disease severity. Behav Neurol 25:23-34.

Corbetta M, Miezin FM, Shulman GL, Petersen SE (1993) A PET study of visuospatial attention. J Neurosci 13:1202-1226.

Corbetta M, Patel G, Shulman GL (2008) The reorienting system of the human brain: from environment to theory of mind. Neuron 58:306-324.

Corbetta M, Shulman GL (2002) Control of goal-directed and stimulus-driven attention in the brain. Nat Rev Neurosci 3:201-215.

Corbetta M, Shulman GL (2011) Spatial neglect and attention networks. Annu Rev Neurosci 34:569-599.

Cordes D, Haughton VM, Arfanakis K, Carew JD, Turski PA, Moritz CH, Quigley MA, Meyerand ME (2001) Frequencies contributing to functional connectivity in the cerebral cortex in "resting-state" data. AJNR Am J Neuroradiol 22:1326-1333.

Cox RW (1996) AFNI: software for analysis and visualization of functional magnetic resonance neuroimages. Comput Biomed Res 29:162-173.

Craddock RC, James GA, Holtzheimer rPE, Hu XP, Mayberg HS (2012) A whole brain fMRI atlas generated via spatially constrained spectral clustering. Hum Brain Mapp 33:1914-1928.

Critchley M (1984) And all the daughters of musick shall be brought low. Language function in the elderly. Arch Neurol 41:1135-1139.

Cummings JL, Benson F, Hill MA, Read S (1985) Aphasia in dementia of the Alzheimer type. Neurology 35:394-397.

Damasio AR (1989) Time-locked multiregional retroactivation: A systems-level proposal for the neural substrates of recall and recognition. Cognition 33:25-62.

Damasio H, Tranel D, Grabowski T, Adolphs R, Damasio A (2004) Neural systems behind word and concept retrieval. Cognition 92:179-229.

Damoiseaux JS, Rombouts SARB, Barkhof F, Scheltens P, Stam CJ, Smith SM, Beckmann CF (2006) Consistent resting-state networks across healthy subjects. Proc Natl Acad Sci U S A 103:13848-13853.

Deichmann R, Schwarzbauer C, Turner R (2004) Optimisation of the 3D MDEFT sequence for anatomical brain imaging: technical implications at 1.5 and 3 T. Neuroimage 21:757-767.

den Dunnen WFA, Brouwer WH, Bijlard E, Kamphuis J, van Linschoten K, Eggens-Meijer E, Holstege G (2008) No disease in the brain of a 115-year-old woman. Neurobiol Aging 29:1127-1132.

Desikan RS, Ségonne F, Fischl B, Quinn BT, Dickerson BC, Blacker D, Buckner RL, Dale AM, Maguire RP, Hyman BT, Albert MS, Killiany RJ (2006) An automated

labeling system for subdividing the human cerebral cortex on MRI scans into gyral based regions of interest. Neuroimage 31:968-980.

Di Martino A, Scheres A, Margulies DS, Kelly AMC, Uddin LQ, Shehzad Z, Biswal B, Walters JR, Castellanos FX, Milham MP (2008) Functional connectivity of human striatum: a resting state FMRI study. Cereb Cortex 18:2735-2747.

Di X, Biswal BB (2014) Modulatory interactions between the default mode network and task positive networks in resting-state. PeerJ 2:e367-e367.

Di X, Kannurpatti SS, Rypma B, Biswal BB (2013a) Calibrating BOLD fMRI activations with neurovascular and anatomical constraints. Cereb Cortex 23:255-263.

Di X, Kim EH, Huang CC, Tsai SJ, Lin CP, Biswal BB (2013b) The influence of the amplitude of low-frequency fluctuations on resting-state functional connectivity. Front Hum Neurosci 7:118.

DiNuzzo M, Gili T, Maraviglia B, Giove F (2011) Modeling the contribution of neuron-astrocyte cross talk to slow blood oxygenation level-dependent signal oscillations. J Neurophysiol 106:3010-3018.

Dronkers NF, Wilkins DP, Van Valin JRD, Redfern BB, Jaeger JJ (2004) Lesion analysis of the brain areas involved in language comprehension. Cognition 92:145-177.

Duecker F, Formisano E, Sack AT (2013) Hemispheric differences in the voluntary control of spatial attention: direct evidence for a right-hemispheric dominance within frontal cortex. J Cogn Neurosci 25:1332-1342.

Duong A, Whitehead V, Hanratty K, Chertkow H (2006) The nature of lexico-semantic processing deficits in mild cognitive impairment. Neuropsychologia 44:1928-1935.

Farrell MT, Zahodne LB, Stern Y, Dorrejo J, Yeung P, Cosentino S (2014) Subjective word-finding difficulty reduces engagement in social leisure activities in Alzheimer's disease. J Am Geriatr Soc 62:1056-1063.

Fisel CR, Ackerman JL, Buxton RB, Garrido L, Belliveau JW, Rosen BR, Brady TJ (1991) MR contrast due to microscopically heterogeneous magnetic susceptibility: numerical simulations and applications to cerebral physiology. Magnetic Resonance in Medicine 17:336-347.

Flicker C, Ferris SH, Reisberg B (1991) Mild cognitive impairment in the elderly: predictors of dementia. Neurology 41:1006-1009.

Fox MD, Corbetta M, Snyder AZ, Vincent JL, Raichle ME (2006a) Spontaneous neuronal activity distinguishes human dorsal and ventral attention systems. Proc Natl Acad Sci U S A 103:10046-10051.

Fox MD, Raichle ME (2007) Spontameous fluctuations in brain activity observed with functional magnetic resonance imaging. Nature Reviews Neurosciences 8:700-711.

Fox MD, Snyder AZ, Vincent JL, Raichle ME (2007) Intrinsic fluctuations within cortical systems account for intertrial variability in human behavior. Neuron 56:171-184.

Fox MD, Snyder AZ, Zacks JM, Raichle ME (2006b) Coherent spontaneous activity accounts for trial-to-trial variability in human evoked brain responses. Nat Neurosci 9:23-25.

Fox Pt RME (1986) Focal physiological uncoupling of cerebral blood flow and oxidative metabolism during somatosensory stimulation in human subjects. Proc Natl Acad Sci USA 83:1140-1144.

Fransson P (2006) How default is the default mode of brain function? Further evidence from intrinsic BOLD signal fluctuations. Neuropsychologia 44:2836-2845.

Friston KJ, Frith CD, Liddle PF, Frackowiak RS (1993) Functional connectivity: the principal-component analysis of large (PET) data sets. J Cereb Blood Flow Metab 13:5-14.

Fukunaga M, Horovitz SG, de Zwart JA, van Gelderen P, Balkin TJ, Braun AR, Duyn JH (2008) Metabolic origin of BOLD signal fluctuations in the absence of stimuli. J Cereb Blood Flow Metab 28:1377-1387.

Fukunaga M, Horovitz SG, van Gelderen P, de Zwart JA, Jansma JM, Ikonomidou VN, Chu R, Deckers RHR, Leopold DA, Duyn JH (2006) Large-amplitude, spatially correlated fluctuations in BOLD fMRI signals during extended rest and early sleep stages. Magn Reson Imaging 24:979-992.

Gandhi SP, Heeger DJ, Boynton GM (1999) Spatial attention affects brain activity in human primary visual cortex. Proc Natl Acad Sci U S A 96:3314-3319.

Garrard P, Lambon Ralph MA, Patterson K, Pratt KH, Hodges JR (2005) Semantic feature knowledge and picture naming in dementia of Alzheimer's type: a new approach. Brain Lang 93:79-94.

Gilden DL, Thornton T, Mallon MW (1995) 1/f noise in human cognition. Science 267:1837-1839.

Gili T, Cercignani M, Serra L, Perri R, Giove F, Maraviglia B, Caltagirone C, Bozzali M (2011) Regional brain atrophy and functional disconnection across Alzheimer's disease evolution. J Neurol Neurosurg Psychiatry 82:58-66.

Gitelman DR, Nobre AC, Parrish TB, LaBar KS, Kim YH, Meyer JR, Mesulam M (1999) A large-scale distributed network for covert spatial attention: further anatomical delineation based on stringent behavioural and cognitive controls. Brain 122 (Pt 6):1093-1106.

Glover GH, Li TQ, Ress D (2000) Image-based method for retrospective correction of physiological motion effects in fMRI: RETROICOR. Magn Reson Med 44:162-167.

Golland Y, Golland P, Bentin S, Malach R (2008) Data-driven clustering reveals a fundamental subdivision of the human cortex into two global systems. Neuropsychologia 46:540-553.

Greenberg AS, Verstynen T, Chiu Y-C, Yantis S, Schneider W, Behrmann M (2012) Visuotopic cortical connectivity underlying attention revealed with white-matter tractography. J Neurosci 32:2773-2782.

Greicius MD, Kiviniemi V, Tervonen O, Vainionpää V, Alahuhta S, Reiss AL, Menon V (2008) Persistent default-mode network connectivity during light sedation. Hum Brain Mapp 29:839-847.

Greicius MD, Srivastava G, Reiss AL, Menon V (2004) Default-mode network activity distinguishes Alzheimer's disease from healthy aging: evidence from functional MRI. Proc Natl Acad Sci U S A 101:4637-4642.

Hagmann P, Cammoun L, Gigandet X, Meuli R, Honey CJ, Wedeen VJ, Sporns O (2008) Mapping the structural core of human cerebral cortex. PLoS Biol 6:e159.

Hallquist MN, Hwang K, Luna B (2013) The nuisance of nuisance regression: spectral misspecification in a common approach to resting-state fMRI preprocessing reintroduces noise and obscures functional connectivity. Neuroimage 82:208-225.

Hampson M, Driesen NR, Skudlarski P, Gore JC, Constable RT (2006) Brain connectivity related to working memory performance. J Neurosci 26:13338-13343.

Han Y, Lui S, Kuang W, Lang Q, Zou L, Jia J (2012) Anatomical and functional deficits in patients with amnestic mild cognitive impairment. PLoS One 7:e28664.

Han Y, Wang J, Zhao Z, Min B, Lu J, Li K, He Y, Jia J (2011) Frequency-dependent changes in the amplitude of low-frequency fluctuations in amnestic mild cognitive impairment: a resting-state fMRI study. Neuroimage 55:287-295.

Harasty JA, Halliday GM, Kril JJ, Code C (1999) Specific temporoparietal gyral atrophy reflects the pattern of language dissolution in Alzheimer's disease. Brain 122 (Pt 4):675-686.

He BJ, Snyder AZ, Zempel JM, Smyth MD, Raichle ME (2008) Electrophysiological correlates of the brain's intrinsic large-scale functional architecture. Proc Natl Acad Sci U S A 105:16039-16044.

He Y, Wang L, Zang Y, Tian L, Zhang X, Li K, Jiang T (2007) Regional coherence changes in the early stages of Alzheimer's disease: a combined structural and resting-state functional MRI study. Neuroimage 35:488-500.

Heilman KM, Valenstein E, Watson RT (2000) Neglect and related disorders. Semin Neurol 20:463-470.

Heilman KM, Van Den Abell T (1980) Right hemisphere dominance for attention: the mechanism underlying hemispheric asymmetries of inattention (neglect). Neurology 30:327-330.

Henry JD, Crawford JR (2004) A meta-analytic review of verbal fluency performance following focal cortical lesions. Neuropsychology 18:284-295.

Henry JD, Crawford JR, Phillips LH (2004) Verbal fluency performance in dementia of the Alzheimer's type: a meta-analysis. Neuropsychologia 42:1212-1222.

Hillyard SA, Vogel EK, Luck SJ (1998) Sensory gain control (amplification) as a mechanism of selective attention: electrophysiological and neuroimaging evidence. Philos Trans R Soc Lond B Biol Sci 353:1257-1270.

Hiltunen T, Kantola J, Elseoud AA, Lepola P, Suominen K, Starck T, Nikkinen J, Remes J, Tervonen O, Palva S, Kiviniemi V, Palva JM (2014) Infra-slow EEG fluctuations are correlated with resting-state network dynamics in fMRI. J Neurosci 34:356-362.

Hodges JR, Salmon DP, Butters N (1992) Semantic memory impairment in Alzheimer's disease: failure of access or degraded knowledge? Neuropsychologia 30:301-314.

Hoge Rd AJGBCGRMSPGB (1999) Linear couplig between cerebral blood flow and oxygen consumption in activated human cortex. Proc Natl Acad Sci USA 96:9403-9408.

Hougaard A, Jensen BH, Amin FM, Rostrup E, Hoffmann MB, Ashina M (2015) Cerebral Asymmetry of fMRI-BOLD Responses to Visual Stimulation. PLoS One 10:e0126477-e0126477.

Indefrey P (2011) The spatial and temporal signatures of word production components: a critical update. Front Psychol 2:255-255.

Indefrey P, Levelt WJM (2000) The neural correlates of language production. In: The new cognitive neurosciences; 2nd ed, pp 845-865: MIT Press.

Indefrey P, Levelt WJM (2004) The spatial and temporal signatures of word production components. Cognition 92:101-144.

Jack AI, Shulman GL, Snyder AZ, McAvoy M, Corbetta M (2006) Separate modulations of human V1 associated with spatial attention and task structure. Neuron 51:135-147.

Japee S, Holiday K, Satyshur MD, Mukai I, Ungerleider LG (2015) A role of right middle frontal gyrus in reorienting of attention: a case study. Front Syst Neurosci 9:23-23.

Jefferies E (2013) The neural basis of semantic cognition: converging evidence from neuropsychology, neuroimaging and TMS. Cortex 49:611-625.

Jefferies E, Ralph MAL (2006) Semantic impairment in stroke aphasia versus semantic dementia: a case-series comparison. Brain 129:2132-2147.

Jewell G, McCourt ME (2000) Pseudoneglect: a review and meta-analysis of performance factors in line bisection tasks. Neuropsychologia 38:93-110.

Johnston JM, Vaishnavi SN, Smyth MD, Zhang D, He BJ, Zempel JM, Shimony JS, Snyder AZ, Raichle ME (2008) Loss of resting interhemispheric functional connectivity after complete section of the corpus callosum. J Neurosci 28:6453-6458.

Kannurpatti SS, Biswal BB (2008) Detection and scaling of task-induced fMRI-BOLD response using resting state fluctuations. Neuroimage 40:1567-1574.

Kastner S, De Weerd P, Desimone R, Ungerleider LG (1998) Mechanisms of directed attention in the human extrastriate cortex as revealed by functional MRI. Science 282:108-111.

Kastner S, Pinsk MA, De Weerd P, Desimone R, Ungerleider LG (1999) Increased activity in human visual cortex during directed attention in the absence of visual stimulation. Neuron 22:751-761.

Kastner S, Ungerleider LG (2000) Mechanisms of visual attention in the human cortex. Annu Rev Neurosci 23:315-341.

Kastner S, Ungerleider LG (2001) The neural basis of biased competition in human visual cortex. Neuropsychologia 39:1263-1276.

Kempler D (1995) Language changes in dementia of the Alzheimer type. Dementia and communication: Research and clinical implications 98-114.

Kempler D, Van Lancker D, Read S (1988) Proverb and idiom comprehension in Alzheimer disease. Alzheimer Dis Assoc Disord 2:38-49.

Kendall MG, Smith BB (1939) The problem of m rankings. The annals of mathematical statistics 10:275-287.

Kinsbourne M (1977) Hemi-neglect and hemisphere rivalry. Adv Neurol 18:41-49.

Kirschner A, Kam JWY, Handy TC, Ward LM (2012) Differential synchronization in default and task-specific networks of the human brain. Front Hum Neurosci 6:139-139.

Kirshner HS (2012) Primary progressive aphasia and Alzheimer's disease: brief history, recent evidence. Curr Neurol Neurosci Rep 12:709-714.

Kirshner HS, Webb WG, Kelly MP (1984) The naming disorder of dementia. Neuropsychologia 22:23-30.

Kiviniemi V, Kantola J-H, Jauhiainen J, Hyvärinen A, Tervonen O (2003) Independent component analysis of nondeterministic fMRI signal sources. Neuroimage 19:253-260.

Koch G, Cercignani M, Bonnì S, Giacobbe V, Bucchi G, Versace V, Caltagirone C, Bozzali M (2011) Asymmetry of parietal interhemispheric connections in humans. J Neurosci 31:8967-8975.

Krieger-Redwood K, Jefferies E (2014) TMS interferes with lexical-semantic retrieval in left inferior frontal gyrus and posterior middle temporal gyrus: Evidence from cyclical picture naming. Neuropsychologia 64C:24-32.

Küblböck M, Woletz M, Höflich A, Sladky R, Kranz GS, Hoffmann A, Lanzenberger R, Windischberger C (2014) Stability of low-frequency fluctuation amplitudes in prolonged resting-state fMRI. Neuroimage 103C:249-257.

Kundu P, Brenowitz ND, Voon V, Worbe Y, Vértes PE, Inati SJ, Saad ZS, Bandettini PA, Bullmore ET (2013) Integrated strategy for improving functional connectivity mapping using multiecho fMRI. Proc Natl Acad Sci U S A 110:16187-16192.

Kundu P, Inati SJ, Evans JW, Luh W-M, Bandettini PA (2012) Differentiating BOLD and non-BOLD signals in fMRI time series using multi-echo EPI. Neuroimage 60:1759-1770.

Laufs H, Krakow K, Sterzer P, Eger E, Beyerle A, Salek-Haddadi A, Kleinschmidt A (2003) Electroencephalographic signatures of attentional and cognitive default modes in spontaneous brain activity fluctuations at rest. Proc Natl Acad Sci U S A 100:11053-11058.

Lauritzen M (2001) Relationship of spikes, synaptic activity, and local changes of cerebral blood flow. J Cereb Blood Flow Metab 21:1367-1383.

Leopold DA, Logothetis NK (2003) Spatial patterns of spontaneous local field activity in the monkey visual cortex. Rev Neurosci 14:195-205.

Leopold DA, Maier A (2012) Ongoing physiological processes in the cerebral cortex. Neuroimage 62:2190-2200.

Liang P, Xiang J, Liang H, Qi Z, Li K, Initiative AsDN (2014) Altered Amplitude of Low-frequency Fluctuations in Early and Late Mild Cognitive Impairment and Alzheimer's Disease. Curr Alzheimer Res 11:389-398.

Liang X, Wang J, Yan C, Shu N, Xu K, Gong G, He Y (2012) Effects of different correlation metrics and preprocessing factors on small-world brain functional networks: a resting-state functional MRI study. PLoS One 7:e32766-e32766.

Lin C-Y, Chen T-B, Lin K-N, Yeh Y-C, Chen W-T, Wang K-S, Wang P-N (2014) Confrontation naming errors in Alzheimer's disease. Dement Geriatr Cogn Disord 37:86-94.

Lippert MT, Steudel T, Ohl F, Logothetis NK, Kayser C (2010) Coupling of neural activity and fMRI-BOLD in the motion area MT. Magn Reson Imaging 28:1087-1094.

Liu C, Tian X (2014) A data-driven method to reduce the impact of region size on degree metrics in voxel-wise functional brain networks. Front Neurol 5:199-199.

Liu D, Yan C, Ren J, Yao L, Kiviniemi VJ, Zang Y (2010) Using coherence to measure regional homogeneity of resting-state FMRI signal. Front Syst Neurosci 4:24-24.

Liu X, Wang S, Zhang X, Wang Z, Tian X, He Y (2014a) Abnormal amplitude of low-frequency fluctuations of intrinsic brain activity in Alzheimer's disease. J Alzheimers Dis 40:387-397.

Liu X, Wang S, Zhang X, Wang Z, Tian X, He Y (2014b) Abnormal Amplitude of Low-Frequency Fluctuations of Intrinsic Brain Activity in Alzheimer's Disease. J Alzheimers Dis.

Logothetis NK (2002) The neural basis of the blood-oxygen-level-dependent functional magnetic resonance imaging signal. Philos Trans R Soc Lond B Biol Sci 357:1003-1037.

Logothetis NK (2008) What we can do and what we cannot do with fMRI. Nature 453:869-878.

Logothetis NK, Pauls J, Augath M, Trinath T, Oeltermann A (2001) Neurophysiological investigation of the basis of the fMRI signal. Nature 412:150-157.

Long X-Y, Zuo X-N, Kiviniemi V, Yang Y, Zou Q-H, Zhu C-Z, Jiang T-Z, Yang H, Gong Q-Y, Wang L, Li K-C, Xie S, Zang Y-F (2008) Default mode network as revealed with multiple methods for resting-state functional MRI analysis. J Neurosci Methods 171:349-355.

Lu H, Zuo Y, Gu H, Waltz JA, Zhan W, Scholl CA, Rea W, Yang Y, Stein EA (2007) Synchronized delta oscillations correlate with the resting-state functional MRI signal. Proc Natl Acad Sci U S A 104:18265-18269.

Lüchinger R, Michels L, Martin E, Brandeis D (2012) Brain state regulation during normal development: Intrinsic activity fluctuations in simultaneous EEG-fMRI. Neuroimage 60:1426-1439.

Luck SJ, Chelazzi L, Hillyard SA, Desimone R (1997) Neural mechanisms of spatial selective attention in areas V1, V2, and V4 of macaque visual cortex. J Neurophysiol 77:24-42.

Lue L-F, Kuo Y-M, Roher AE, Brachova L, Shen Y, Sue L, Beach T, Kurth JH, Rydel RE, Rogers J (1999) Soluble amyloid $ peptide concentration as a predictor of synaptic change in Alzheimer's disease. The American journal of pathology 155:853-862.

Maess B, Friederici AD, Damian M, Meyer AS, Levelt WJM (2002) Semantic category interference in overt picture naming: sharpening current density localization by PCA. J Cogn Neurosci 14:455-462.

Markett S, Reuter M, Montag C, Voigt G, Lachmann B, Rudorf S, Elger CE, Weber B (2014) Assessing the function of the fronto-parietal attention network: insights from resting-state fMRI and the attentional network test. Hum Brain Mapp 35:1700-1709.

Martin A (2007) The representation of object concepts in the brain. Annu Rev Psychol 58:25-45.

Martuzzi R, Ramani R, Qiu M, Shen X, Papademetris X, Constable RT (2011) A whole-brain voxel based measure of intrinsic connectivity contrast reveals local changes in tissue connectivity with anesthetic without a priori assumptions on thresholds or regions of interest. Neuroimage 58:1044-1050.

McKhann G, Drachman D, Folstein M, Katzman R, Price D, Stadlan EM (1984) Clinical diagnosis of Alzheimer's disease: report of the NINCDS-ADRDA Work Group under the auspices of Department of Health and Human Services Task Force on Alzheimer's Disease. Neurology 34:939-944.

Menon V, Uddin LQ (2010) Saliency, switching, attention and control: a network model of insula function. Brain Struct Funct 214:655-667.

Mesulam MM (1981) A cortical network for directed attention and unilateral neglect. Ann Neurol 10:309-325.

Mickes L, Wixted JT, Fennema-Notestine C, Galasko D, Bondi MW, Thal LJ, Salmon DP (2007) Progressive impairment on neuropsychological tasks in a longitudinal study of preclinical Alzheimer's disease. Neuropsychology 21:696-705.

Miezin FM, Maccotta L, Ollinger JM, Petersen SE, Buckner RL (2000) Characterizing the hemodynamic response: effects of presentation rate, sampling procedure, and the possibility of ordering brain activity based on relative timing. Neuroimage 11:735-759.

Miller EK, Buschman TJ (2013) Cortical circuits for the control of attention. Curr Opin Neurobiol 23:216-222.

Monk CS, Peltier SJ, Wiggins JL, Weng S-J, Carrasco M, Risi S, Lord C (2009) Abnormalities of intrinsic functional connectivity in autism spectrum disorders. Neuroimage 47:764-772.

Monsch AU, Bondi MW, Butters N, Salmon DP, Katzman R, Thal LJ (1992) Comparisons of verbal fluency tasks in the detection of dementia of the Alzheimer type. Arch Neurol 49:1253-1258.

Murphy K, Birn RM, Bandettini PA (2013) Resting-state fMRI confounds and cleanup. Neuroimage 80:349-359.

Murphy K, Birn RM, Handwerker DA, Jones TB, Bandettini PA (2009) The impact of global signal regression on resting state correlations: are anti-correlated networks introduced? Neuroimage 44:893-905.

Nebes RD, Halligan EM (1996) Sentence context influences the interpretation of word meaning by Alzheimer patients. Brain Lang 54:233-245.

Nicholas M, Obler LK, Albert ML, Helm-Estabrooks N (1985) Empty speech in Alzheimer's disease and fluent aphasia. J Speech Hear Res 28:405-410.

Nir Y, Mukamel R, Dinstein I, Privman E, Harel M, Fisch L, Gelbard-Sagiv H, Kipervasser S, Andelman F, Neufeld MY, Kramer U, Arieli A, Fried I, Malach R (2008) Interhemispheric correlations of slow spontaneous neuronal fluctuations revealed in human sensory cortex. Nat Neurosci 11:1100-1108.

Nobre AC, Sebestyen GN, Gitelman DR, Mesulam MM, Frackowiak RS, Frith CD (1997) Functional localization of the system for visuospatial attention using positron emission tomography. Brain 120 (Pt 3):515-533.

Noonan KA, Jefferies E, Corbett F, Lambon Ralph MA (2010) Elucidating the nature of deregulated semantic cognition in semantic aphasia: evidence for the roles of prefrontal and temporo-parietal cortices. J Cogn Neurosci 22:1597-1613.

Noonan KA, Jefferies E, Visser M, Lambon Ralph MA (2013) Going beyond inferior prefrontal involvement in semantic control: evidence for the additional contribution of dorsal angular gyrus and posterior middle temporal cortex. J Cogn Neurosci 25:1824-1850.

Nudo RJ, Masterton RB (1986) Stimulation-induced [14C]2-deoxyglucose labeling of synaptic activity in the central auditory system. J Comp Neurol 245:553-565.

Ogawa S, Menon RS, Tank DW, Kim SG, Merkle H, Ellermann JM, Ugurbil K (1993a) Functional brain mapping by blood oxygenation level-dependent contrast magnetic resonance imaging. A comparison of signal characteristics with a biophysical model. Biophys J 64:803-812.

Ogawa S, Menon RS, Tank DW, Kim SG, Merkle H, Ellermann JM, Ugurbil K (1993b) Functional brain mapping by blood oxygenation level-dependent contrast

magnetic resonance imaging. A comparison of signal characteristics with a biophysical model. Biophysical journal 64:803-803.

Paakki J-J, Rahko J, Long X, Moilanen I, Tervonen O, Nikkinen J, Starck T, Remes J, Hurtig T, Haapsamo H, Jussila K, Kuusikko-Gauffin S, Mattila M-L, Zang Y, Kiviniemi V (2010) Alterations in regional homogeneity of resting-state brain activity in autism spectrum disorders. Brain Res 1321:169-179.

Parasuraman R, Haxby JV (1993) Attention and brain function in Alzheimer's disease: A review. Neuropsychology 7:242-242.

Patterson K, Nestor PJ, Rogers TT (2007) Where do you know what you know? The representation of semantic knowledge in the human brain. Nat Rev Neurosci 8:976-987.

Pauling L, Coryell CD (1936) The magnetic properties and structure of hemoglobin, oxyhemoglobin and carbonmonoxyhemoglobin. Proceedings of the National Academy of Sciences of the United States of America 22:210-210.

Penttonen M, Buzsáki G (2003) Natural logarithmic relationship between brain oscillators. Thalamus & Related Systems 2:145-152.

Petersen RC (2011) Clinical practice. Mild cognitive impairment. N Engl J Med 364:2227-2234.

Petersen RC, Smith GE, Waring SC, Ivnik RJ, Kokmen E, Tangelos EG (1997) Aging, memory, and mild cognitive impairment. Int Psychogeriatr 9 Suppl 1:65-69.

Petersen RC, Stevens JC, Ganguli M, Tangalos EG, Cummings JL, DeKosky ST (2001) Practice parameter: early detection of dementia: mild cognitive impairment (an evidence-based review). Report of the Quality Standards Subcommittee of the American Academy of Neurology. Neurology 56:1133-1142.

Pillay SB, Stengel BC, Humphries C, Book DS, Binder JR (2014) Cerebral localization of impaired phonological retrieval during rhyme judgment. Ann Neurol 76:738-746.

Posse S, Wiese S, Gembris D, Mathiak K, Kessler C, Grosse-Ruyken ML, Elghahwagi B, Richards T, Dager SR, Kiselev VG (1999) Enhancement of BOLD-contrast sensitivity by single-shot multi-echo functional MR imaging. Magn Reson Med 42:87-97.

Putcha D, Brickhouse M, O'Keefe K, Sullivan C, Rentz D, Marshall G, Dickerson B, Sperling R (2011) Hippocampal hyperactivation associated with cortical thinning in Alzheimer's disease signature regions in non-demented elderly adults. J Neurosci 31:17680-17688.

Qiu C, Kivipelto M, von Strauss E (2009) Epidemiology of Alzheimer's disease: occurrence, determinants, and strategies toward intervention. Dialogues Clin Neurosci 11:111-128.

Querfurth HW, LaFerla FM (2010) Alzheimer's disease. N Engl J Med 362:329-344.

Raichle ME (2006) The brain's dark energy. SCIENCE-NEW YORK THEN WASHINGTON- 314:1249-1249.

Raichle ME (2010) Two views of brain function. Trends Cogn Sci 14:180-190.

Raichle ME (2011) The restless brain. Brain Connect 1:3-12.

Raichle ME, MacLeod AM, Snyder AZ, Powers WJ, Gusnard DA, Shulmanweb GL (2001) A default mode of brain function. Proc Natl Acad Sci U S A 98:676-682.

Reisberg B, Ferris SH, de Leon MJ, Crook T (1982) The Global Deterioration Scale for assessment of primary degenerative dementia. Am J Psychiatry 139:1136-1139.

Ress D, Backus BT, Heeger DJ (2000) Activity in primary visual cortex predicts performance in a visual detection task. Nat Neurosci 3:940-945.

Rohrer D, Salmon DP, Wixted JT, Paulsen JS (1999) The disparate effects of Alzheimer's disease and Huntington's disease on semantic memory. Neuropsychology 13:381-388.

Ross SM (2003) Peirce's criterion for the elimination of suspect experimental data. Journal of Engineering Technology 20:38-41.

Saad ZS, Ropella KM, Cox RW, DeYoe EA (2001) Analysis and use of FMRI response delays. Hum Brain Mapp 13:74-93.

Santacruz K, Lewis J, Spires T, Paulson J, Kotilinek L, Ingelsson M, Guimaraes A, DeTure M, Ramsden M, McGowan E, others (2005) Tau suppression in a neurodegenerative mouse model improves memory function. Science 309:476-481.

Scheeringa R, Bastiaansen MCM, Petersson KM, Oostenveld R, Norris DG, Hagoort P (2008) Frontal theta EEG activity correlates negatively with the default mode network in resting state. Int J Psychophysiol 67:242-251.

Scheinost D, Benjamin J, Lacadie CM, Vohr B, Schneider KC, Ment LR, Papademetris X, Constable RT (2012) The intrinsic connectivity distribution: a novel contrast measure reflecting voxel level functional connectivity. Neuroimage 62:1510-1519.

Schnur TT, Schwartz MF, Kimberg DY, Hirshorn E, Coslett HB, Thompson-Schill SL (2009) Localizing interference during naming: convergent neuroimaging and neuropsychological evidence for the function of Broca's area. Proc Natl Acad Sci U S A 106:322-327.

Schölvinck ML, Maier A, Ye FQ, Duyn JH, Leopold DA (2010) Neural basis of global resting-state fMRI activity. Proc Natl Acad Sci U S A 107:10238-10243.

Serra L, Giulietti G, Cercignani M, Spanò B, Torso M, Castelli D, Perri R, Fadda L, Marra C, Caltagirone C (2013) Mild cognitive impairment: same identity for different entities. Journal of Alzheimer's Disease 33:1157-1165.

Shmuel A, Leopold DA (2008) Neuronal correlates of spontaneous fluctuations in fMRI signals in monkey visual cortex: Implications for functional connectivity at rest. Hum Brain Mapp 29:751-761.

Smith SM, Fox PT, Miller KL, Glahn DC, Fox PM, Mackay CE, Filippini N, Watkins KE, Toro R, Laird AR, Beckmann CF (2009) Correspondence of the brain's functional architecture during activation and rest. Proc Natl Acad Sci U S A 106:13040-13045.

Smith SM, Matthews PM, Jezzard P (2001) Functional MRI: an introduction to methods: Oxford University Press.

Somers DC, Dale AM, Seiffert AE, Tootell RB (1999) Functional MRI reveals spatially specific attentional modulation in human primary visual cortex. Proc Natl Acad Sci U S A 96:1663-1668.

Song X, Zhang Y, Liu Y (2014) Frequency specificity of regional homogeneity in the resting-state human brain. PLoS One 9:e86818.

Sorg C, Riedl V, Mühlau M, Calhoun VD, Eichele T, Läer L, Drzezga A, Förstl H, Kurz A, Zimmer C, Wohlschläger AM (2007) Selective changes of resting-state

networks in individuals at risk for Alzheimer's disease. Proc Natl Acad Sci U S A 104:18760-18765.

Spadone S, Della Penna S, Sestieri C, Betti V, Tosoni A, Perrucci MG, Romani GL, Corbetta M (2015) Dynamic reorganization of human resting-state networks during visuospatial attention. Proc Natl Acad Sci U S A 112:8112-8117.

Sun FT, Miller LM, D'Esposito M (2004) Measuring interregional functional connectivity using coherence and partial coherence analyses of fMRI data. Neuroimage 21:647-658.

Sun FT, Miller LM, D'Esposito M (2005) Measuring temporal dynamics of functional networks using phase spectrum of fMRI data. Neuroimage 28:227-237.

Szczepanski SM, Pinsk MA, Douglas MM, Kastner S, Saalmann YB (2013) Functional and structural architecture of the human dorsal frontoparietal attention network. Proc Natl Acad Sci U S A 110:15806-15811.

Taler V, Phillips NA (2008) Language performance in Alzheimer's disease and mild cognitive impairment: a comparative review. J Clin Exp Neuropsychol 30:501-556.

Tessitore A, Esposito F, Vitale C, Santangelo G, Amboni M, Russo A, Corbo D, Cirillo G, Barone P, Tedeschi G (2012) Default-mode network connectivity in cognitively unimpaired patients with Parkinson disease. Neurology 79:2226-2232.

Thiebaut de Schotten M, Dell'Acqua F, Forkel SJ, Simmons A, Vergani F, Murphy DGM, Catani M (2011) A lateralized brain network for visuospatial attention. Nat Neurosci 14:1245-1246.

Thulborn Kr WJCMPMRGK (1982) Oxygenation dependence of the transverse relaxation time of water protons in whole blood at high field. Biochem Biophys Acta 714:265-270.

Tofts P (2005) Quantitative MRI of the Brain: Measuring Changes Caused by Disease: Wiley.

Tomasi D, Wang G-J, Volkow ND (2013) Energetic cost of brain functional connectivity. Proc Natl Acad Sci U S A 110:13642-13647.

Tulving E (1987) Multiple memory systems and consciousness. Human neurobiology 6:67-80.

Turken U, Dronkers NF (2011) The neural architecture of the language comprehension network: converging evidence from lesion and connectivity analyses. Front Syst Neurosci 5:1-1.

Vallar G (1998) Spatial hemineglect in humans. Trends Cogn Sci 2:87-97.

van den Heuvel MP, Pol HEH (2010) Exploring the brain network: a review on resting-state fMRI functional connectivity. Eur Neuropsychopharmacol 20:519-534.

van den Heuvel MP, Sporns O, Collin G, Scheewe T, Mandl RCW, Cahn W, Goñi J, Hulshoff Pol HE, Kahn RS (2013) Abnormal rich club organization and functional brain dynamics in schizophrenia. JAMA Psychiatry 70:783-792.

Vargas C, López-Jaramillo C, Vieta E (2013) A systematic literature review of resting state network--functional MRI in bipolar disorder. J Affect Disord 150:727-735.

Vatansever D, Menon DK, Manktelow AE, Sahakian BJ, Stamatakis EA (2015) Default mode network connectivity during task execution. Neuroimage 122:96-104.

Vincent JL, Patel GH, Fox MD, Snyder AZ, Baker JT, Van Essen DC, Zempel JM, Snyder LH, Corbetta M, Raichle ME (2007) Intrinsic functional architecture in the anaesthetized monkey brain. Nature 447:83-86.

Viswanathan A, Freeman RD (2007) Neurometabolic coupling in cerebral cortex reflects synaptic more than spiking activity. Nat Neurosci 10:1308-1312.

Vossel S, Geng JJ, Fink GR (2014) Dorsal and ventral attention systems: distinct neural circuits but collaborative roles. Neuroscientist 20:150-159.

Wang J, Tian Y, Wang M, Cao L, Wu H, Zhang Y, Wang K, Jiang T (2015) A lateralized top-down network for visuospatial attention and neglect. Brain Imaging Behav.

Wang K, Liang M, Wang L, Tian L, Zhang X, Li K, Jiang T (2007) Altered functional connectivity in early Alzheimer's disease: a resting-state fMRI study. Hum Brain Mapp 28:967-978.

Wang L, Zang Y, He Y, Liang M, Zhang X, Tian L, Wu T, Jiang T, Li K (2006) Changes in hippocampal connectivity in the early stages of Alzheimer's disease: evidence from resting state fMRI. Neuroimage 31:496-504.

Wang Z, Yan C, Zhao C, Qi Z, Zhou W, Lu J, He Y, Li K (2011) Spatial patterns of intrinsic brain activity in mild cognitive impairment and Alzheimer's disease: a resting-state functional MRI study. Hum Brain Mapp 32:1720-1740.

Wee C-Y, Yap P-T, Denny K, Browndyke JN, Potter GG, Welsh-Bohmer KA, Wang L, Shen D (2012) Resting-state multi-spectrum functional connectivity networks for identification of MCI patients. PLoS One 7:e37828-e37828.

Wei L, Duan X, Zheng C, Wang S, Gao Q, Zhang Z, Lu G, Chen H (2014) Specific frequency bands of amplitude low-frequency oscillation encodes personality. Hum Brain Mapp 35:331-339.

Weissenbacher A, Kasess C, Gerstl F, Lanzenberger R, Moser E, Windischberger C (2009) Correlations and anticorrelations in resting-state functional connectivity MRI: a quantitative comparison of preprocessing strategies. Neuroimage 47:1408-1416.

Welch PD (1967) The use of fast Fourier transform for the estimation of power spectra: A method based on time averaging over short, modified periodograms. IEEE Transactions on audio and electroacoustics 15:70-73.

Whitfield-Gabrieli S, Nieto-Castanon A (2012) Conn: a functional connectivity toolbox for correlated and anticorrelated brain networks. Brain Connect 2:125-141.

Whitney C, Jefferies E, Kircher T (2011a) Heterogeneity of the left temporal lobe in semantic representation and control: priming multiple versus single meanings of ambiguous words. Cerebral Cortex 21:831-844.

Whitney C, Kirk M, O'Sullivan J, Lambon Ralph MA, Jefferies E (2011b) The neural organization of semantic control: TMS evidence for a distributed network in left inferior frontal and posterior middle temporal gyrus. Cereb Cortex 21:1066-1075.

Wiener N (1949) Extrapolation, interpolation, and smoothing of stationary time series: MIT press Cambridge, MA.

Winblad B, Palmer K, Kivipelto M, Jelic V, Fratiglioni L, Wahlund LO, Nordberg A, Bäckman L, Albert M, Almkvist O, Arai H, Basun H, Blennow K, de Leon M, DeCarli C, Erkinjuntti T, Giacobini E, Graff C, Hardy J, Jack C, Jorm A, Ritchie K, van Duijn C, Visser P, Petersen RC (2004) Mild cognitive impairment--

beyond controversies, towards a consensus: report of the International Working Group on Mild Cognitive Impairment. J Intern Med 256:240-246.

Wise RG, Ide K, Poulin MJ, Tracey I (2004) Resting fluctuations in arterial carbon dioxide induce significant low frequency variations in BOLD signal. Neuroimage 21:1652-1664.

Wu T, Long X, Zang Y, Wang L, Hallett M, Li K, Chan P (2009) Regional homogeneity changes in patients with Parkinson's disease. Hum Brain Mapp 30:1502-1510.

Xi Q, hu Zhao X, jun Wang P, hao Guo Q, gan Yan C, He Y (2012) Functional MRI study of mild Alzheimer's disease using amplitude of low frequency fluctuation analysis. Chin Med J (Engl) 125:858-862.

Xi Q, hu Zhao X, jun Wang P, hao Guo Q, He Y (2013) Abnormal intrinsic brain activity in amnestic mild cognitive impairment revealed by amplitude of low-frequency fluctuation: a resting-state functional magnetic resonance imaging study. Chin Med J (Engl) 126:2912-2917.

Xia W, Wang S, Sun Z, Bai F, Zhou Y, Yang Y, Wang P, Huang Y, Yuan Y (2013) Altered baseline brain activity in type 2 diabetes: A resting-state fMRI study. Psychoneuroendocrinology 38:2493-2501.

Yan C, Liu D, He Y, Zou Q, Zhu C, Zuo X, Long X, Zang Y (2009) Spontaneous brain activity in the default mode network is sensitive to different resting-state conditions with limited cognitive load. PLoS One 4:e5743-e5743.

Yang H, Long X-Y, Yang Y, Yan H, Zhu C-Z, Zhou X-P, Zang Y-F, Gong Q-Y (2007) Amplitude of low frequency fluctuation within visual areas revealed by resting-state functional MRI. Neuroimage 36:144-152.

Yeo BTT, Krienen FM, Sepulcre J, Sabuncu MR, Lashkari D, Hollinshead M, Roffman JL, Smoller JW, Zöllei L, Polimeni JR, Fischl B, Liu H, Buckner RL (2011) The organization of the human cerebral cortex estimated by intrinsic functional connectivity. J Neurophysiol 106:1125-1165.

Yu R, Chien Y-L, Wang H-LS, Liu C-M, Liu C-C, Hwang T-J, Hsieh MH, Hwu H-G, Tseng W-YI (2012) Frequency-specific alternations in the amplitude of low-frequency fluctuations in schizophrenia. Hum Brain Mapp.

Yu R, Chien YL, Wang HL, Liu CM, Liu CC, Hwang TJ, Hsieh MH, Hwu HG, Tseng WY (2014) Frequency-specific alternations in the amplitude of low-frequency fluctuations in schizophrenia. Hum Brain Mapp 35:627-637.

Yuan Y, Zhang Z, Bai F, Yu H, Shi Y, Qian Y, Liu W, You J, Zhang X, Liu Z (2008) Abnormal neural activity in the patients with remitted geriatric depression: a resting-state functional magnetic resonance imaging study. J Affect Disord 111:145-152.

Zang Y-F, He Y, Zhu C-Z, Cao Q-J, Sui M-Q, Liang M, Tian L-X, Jiang T-Z, Wang Y-F (2007) Altered baseline brain activity in children with ADHD revealed by resting-state functional MRI. Brain Dev 29:83-91.

Zang Y, Jiang T, Lu Y, He Y, Tian L (2004) Regional homogeneity approach to fMRI data analysis. Neuroimage 22:394-400.

Zhang H-Y, Wang S-J, Liu B, Ma Z-L, Yang M, Zhang Z-J, Teng G-J (2010) Resting brain connectivity: changes during the progress of Alzheimer disease. Radiology 256:598-606.

Zhang J, Wei L, Hu X, Zhang Y, Zhou D, Li C, Wang X, Feng H, Yin X, Xie B, Wang J (2013) Specific frequency band of amplitude low-frequency fluctuation predicts Parkinson's disease. Behav Brain Res 252:18-23.

Zhao Z, Lu J, Jia X, Chao W, Han Y, Jia J, Li K (2014) Selective changes of resting-state brain oscillations in aMCI: an fMRI study using ALFF. Biomed Res Int 2014:920902-920902.

Zhou F, Gong H, Li F, Zhuang Y, Zang Y, Xu R, Wang Z (2013a) Altered motor network functional connectivity in amyotrophic lateral sclerosis: a resting-state functional magnetic resonance imaging study. Neuroreport 24:657-662.

Zhou G, Liu P, Wang J, Wen H, Zhu M, Zhao R, von Deneen KM, Zeng F, Liang F, Gong Q, Qin W, Tian J (2013b) Fractional amplitude of low-frequency fluctuation changes in functional dyspepsia: A resting-state fMRI study. Magn Reson Imaging 31:996-1000.

Zou Q-H, Zhu C-Z, Yang Y, Zuo X-N, Long X-Y, Cao Q-J, Wang Y-F, Zang Y-F (2008) An improved approach to detection of amplitude of low-frequency fluctuation (ALFF) for resting-state fMRI: fractional ALFF. J Neurosci Methods 172:137-141.

Zuo X-N, Martino AD, Kelly C, Shehzad ZE, Gee DG, Klein DF, Castellanos FX, Biswal BB, Milham MP (2010) The oscillating brain: complex and reliable. Neuroimage 49:1432-1445.